Improving the Performance of Discontinuous Fibre Reinforced Composites

by

Nega Biruk Fikre

Thesis submitted to the University of Nottingham for the degree of Doctor of Philosophy

July 2023

Abstract

The automotive industry is under increasing pressure to produce light weight and fuel-efficient vehicles to meet stringent global emission targets. Discontinuous carbon fibre composites with thermoset resin are being favoured in the industry due to their potential for easy automation, short cycle times, and overall cost efficiency. The complex interactions of material, process, and microstructural parameters can significantly affect the mechanical, damping, and impact properties of the composites. Thus, the aim of the current study is to study the influence of these parameters and tailor to improve the composite performance. The primary parameters studied include the size effect in the reinforcing fibres, the types of fibres used, flow-induced fibre orientation, as well as impact resistance and post impact residual properties of the composites.

A study of size effect, i.e., fibre length vs. tensile strength, in range of carbon fibre grades demonstrated that high performance (both PAN and pitch-based) fibres exhibit lower defect population, thus, lower strength reduction at longer length than intermediate grades. However, composite strength was seen to increase monotonously with fibre length up to ~50 mm, beyond which no gain was observed for all the fibre types studied. Composite stiffness exhibited increasing trend with increasing fibre stiffness while composite strength with increasing fibre strength showed greater discrepancy with prediction in composites with higher fibre-matrix modulus ratio. This is perceived to be due to high interfacial and fibre stress concentrations which act as failure initiation site, as supported by literature.

The effect of hybridization of different fibre types has been studied using jute-carbon hybrids as a novel investigation of high-performance composites with reduced carbon

footprint suitable for high volume applications. The results showed that hybrids with jute skin layers have higher tensile and damping performance due to the blocking effect of carbon layers and excellent vibration dissipation capability of natural fibres. On the other hand, as expected, higher flexural stiffness and strength were obtained when the stiffer and stronger carbon layers were used as external skin layers. The Cost-Performance Ratios (CPRs) have been used to evaluate the hybrids against their carbon and jute benchmarks.

In addition, in light of increased susceptibility to impact induced damage in automotive industry, a study has been conducted to investigate the impact behaviour and residual properties under different loading conditions. Notably, the impact response exhibited greater sensitivity to changes in composite thickness. Moreover, post impact compression loading resulted in greater strength reduction and stronger correlation between impact damage and post impact failure initiation site compared to tension loading.

Finally, experimental studies showed that longer fibre tows exhibit greater resistance to flow induced fibre alignment during compression moulding of carbon fibre Sheet Moulding Compounds (SMCs). Furthermore, a skin-core layered structure was observed, where the core maintained the initial fibre orientation relatively while high flow induced fibre orientation was seen on the surfaces. Moreover, by encouraging charge flow in the preferential alignment direction of the preform, high tensile stiffness and strength in the preferred direction were achieved (56.7 GPa and 238.9 MPa respectively) at 30% fibre volume fraction. Additionally, circular statistics parameters were employed for the interpretation of fibre orientation distributions, as a more detailed alternative to orientation tensor components.

Acknowledgements

The author would like to thank his supervisors Dr. Robert Pierce and Professor Xiaosu Yi for their invaluable guidance and support throughout the course of the study. The author would also like to thank Dr. Xiaoling Liu for the funding acquisition and members of Composites Research Group for their help around the lab.

Special appreciation goes to Professor Nick Warrior and Dr. Lee Harper for their continuous counselling and support throughout the project.

The financial support from the New Material Institute, Ningbo S&T Bureau, and Zhejiang Innovation Team scheme is greatly acknowledged.

Abbreviations

AFP	Automated Fibre Placement
ASTM	American Society for Testing and Materials
ATP	Automated Tape Placement
BiW	Body-in-White
BRAC3D	Bentley–Raycell Automated Carbon Composite Charge Deposition
CAFE	Corporate Average Fuel Economy
CAI	Compression After Impact
CFRP	Carbon Fibre Reinforced Polymer
CPR	Cost Performance Ratio
DCFP	Directed Carbon Fibre Preforming
DFC	Directed Fibre Compounding
DFP	Directed Fibre Preforming
DIC	Digital Image Correlation
DSC	Differential Scanning Calorimetry
DWCM	Dynamic Wet Compression Moulding
GMT	Glass Mat Thermoplastics
HiPerDif	High Performance-Discontinuous Fibre

HP-RTM	High Pressure Resin Transfer Moulding
INDC	Intended Nationally Determined Contribution
JMC	Jiangling Motors Corporation
MAPP	Maleic Anhydride grafted Polypropylene
MLE	Maximum Likelihood Estimation
NDC	Nationally Determined Contribution
PAN	Polyacrylonitrile
QI ADFRC Composite	Quasi-Isotropic Aligned Discontinuous Fibre Reinforced
RODFRC	Randomly Oriented Discontinuous Fibre Composites
SAE	Specific Energy Absorption
SEM	Scanning Electron Microscope
SFT	Single Fibre Testing
SMC	Sheet Moulding Compounds
SRIM	Structural Reaction Injection Moulding
SSP	Shear Stiffening Polymer
STF	Shear Thickening Fluid
TAI	Tension After Impact
VRA	Voith Roving Applicator

WCM	Wet Compression Moulding

Contents

List of Tables

List of Figures

Chapter 1. Introduction

Automotive industries are in search of alternative energy sources and energy efficient vehicles. Along with developing hybrid and electric cars, the use of lightweight materials is considered as a potential solution to overcome the challenges. Fibre reinforced composite are very attractive due to their high strength to weight ratio, corrosion resistance and part-integration benefits. On the other hand, high performance composite materials are considerably expensive, which in turn increases the cost of products along with lengthy and multi-stage manufacturing processes. Hence the challenge is further extended to finding a balance between high raw material costs with affordability of finished products. Due to varying cost and performance requirements for different applications, material development in the composite sector shall be streamed in a number of different directions. Discontinuous fibre composites materials manufactured using compression moulding and injection moulding are appealing due to reduced cycle time suitable for high volume automated production and cost effectiveness. However, the performance of these materials is far lower than continuous fibre composites, especially strength wise. There has been increased effort in optimization of various material and process parameters to increase the performance ceiling of these materials.

1.1 Lightweighting for low carbon emission

In light of the growing environmental concern, the Paris Agreement (2016), a convention held to undertake ambitious efforts to reduce global greenhouse gas emission, required all parties take effort through their nationally determined contributions (NDC)[1]. China, as the largest emitter of greenhouse gas, is considered as the important force in determining the success or failure of the cooperation.

According to the Paris climate summit, China has submitted its intended NDC (INDC) and reaffirmed its intention to reduce carbon intensity by 60-65% by the year 2030 from its 2005 level. Out of the total global emissions, the transportation sector accounts about 23% of global carbon dioxide [2]. China, being the largest automobile market in the world both in terms of demand and supply [3], [4], is working on advancement of fuel efficient automobiles to reduce the average fuel consumption of passenger cars to 5L/100 km [5]. The European Union emission control is also targeting passenger cars and light-commercial cars to reduce the average CO_2 emission by 15% by 2025 and 37.5% by 2030 from the base line year of 2021 which targeted new cars average CO_2 emission of 95g/km [6]. Similarly, corporate average fuel economy (CAFE) regulation in US required a fleet average of 54.5 mpg (23.2 km/L) by the year 2025 [7]. The total number of vehicles worldwide is also expected to rise to 3.5 billion an increase of 300% by the year 2050 due to high mobility expected [8], much of which is coming from fast-expanding Chinese market.

Beside the stringent regulation on climate change, rising fuel cost is also another challenge the automotive industry is facing and forcing to advance towards development of lightweight materials. Number of studies have indicated that for 10% weight reduction in automobile there is a resulting 6-7% fuel saving [8], [9]. Hence it comes with added opportunity for automakers to downsize other components such as engine, transmission, brakes, suspension and others and thus further compounding vehicle weight reduction. Body-in-White (BiW), car body's sheet where other components such as hoods, fenders, seats etc. are welded together, is where large weight saving can be gained by replacing with light material. It accounts for about 27% [10] of the average automobile curb weight, hence large scale penetration opportunity for lightweight materials such as aluminium and composites. Aluminium has been widely

used in automotive industries due to an already established process and lower material cost. It has been reported that for one kilograms of aluminium used to replace heavier materials like steel, has a potential to reduce up to 20kg of CO_2 in the life time of the vehicle[11]. Therefore, fibre reinforced composite materials that are lighter than aluminium results in far greater reduction in emission of greenhouse gases.

1.2 Composite materials in the automotive industry

The use of advanced fibre reinforced composite is an attractive solution for light weight automotive parts due to their high strength to weight ratio, part integration, corrosion resistance and tailorable property per requirement. Numerous researches have shown that composite materials in general are 35% lighter than aluminium and 60% lighter than steel and can result up to 10% weight saving on the overall vehicle [12]. Furthermore, optimally designed continuous carbon fibre provides even increased weight saving of up to 75% over steel, 40% over aluminium and 60% over glass fibre SMC composites [13]. Additionally, due to part consolidation, composite materials offer reduction of tooling cost by 50 – 70% compared to steel[14]. Even though they have superior mechanical property with weight saving advantage their application is largely limited to high end automotive and aerospace industry due to longer cycle time and high raw material cost.

Towards reducing the cycle time in composite manufacturing, resin matrix manufacturing companies are developing rapid curing resins. A recent announcement showed a promising result, resin which can cure in few minutes and suitable for high volume production. For instance Huntsman's fast cure solution (Araldite LY3585) [15] cures in 1-2 min and is suitable for Wet Compression Moulding (WCM) and high pressure resin transfer moulding (HP-RTM). Other companies' breakthrough include

from Dow automotive [16] (VORAFORCE: 30sec-3mins), HEXION [17] (Epikote & Epikure: 2min), CYTEC industries [18](XMTR: 3 – 5 mins) and Hexcel's discontinuous prepreg (HexPly M77: 2 mins) [19]. However, traditional composite manufacturing techniques cannot take advantage of rapid curing resin systems due to long processing time requirements. Therefore, automated cost-effective composite manufacturing process developments are considered in curtailing manufacturing cost significantly with short cycle time and increased production volume. Among these processes are Automated Fibre Placement (AFP), Automated Tape-Placement (ATP), Wet Compression Moulding (WCM), and Dynamic Wet Compression Moulding (DWCM). Fast curing resin systems along with automated manufacturing processes are promoting the advancement towards light weighting in both automotive and aerospace industries through the use of composite materials.

Glass fibre composites have been the widely used form in the automotive industry for interior applications and exterior body panels. In recent years, composite materials derived from carbon fibre and high-performance thermoset resin matrix are also gaining interest from leading automakers globally. For instance, in 2019 CSP VICTALL announced its advanced composite pickup boxes for Jiangling Motors Corporation's (JMC) new Yuhu 3 and Yuhu 5 pickup trucks, the first ever use in Chinese automotive market [20]. The new composite product uses integrated sheet moulding compound (SMC) in proprietary fully automated compounding line and is 30% lighter than a sheet metal pick up box in the same configuration, Figure 1-1. Another collaborative project between the Chinese advanced material development company Kingfa Sci. & Tech. Co. Ltd. and Germany's automotive supplier Brose Fahrzeugteile recently developed a door module carrier for the production of new Ford Focus [21], Figure 1-2 (left). The new door module was developed using continuously

reinforced material with about 35% weight saving to standard injection moulded one, without compromising the performance. The Chinese composite manufacturing company, Kangde Group, is building an Industry 4.0 smart factory for large production of carbon fibre auto parts which also marked that the Chinese carbon fibre production reaching industry 4.0 stage [22].

The US automotive company General Motors' carbon fibre composite pickup box which is the first application of its kind appeared on 2019 GMC Sierra with innovative features and offering 25% weight reduction than traditional steel bed [23]. From the European market, the collaboration between Audi and Voith Composite has recently developed a fully digital 4.0 production line for mass production of carbon fibre reinforced polymer (CFRP) rear wall for Audi A8. The new patented Voith Roving Applicator (VRA) uses fully automated preforming and Ultra-RTM resin injection with fast curing VORAFORCE epoxy resin [24]. BMW has also used CFRP monocoque cabin for its i3 EV which was also the first to use an RTM moulded monocoque in a production vehicles [25]. These recent announcements from global automakers show the industry's ongoing efforts towards light weighting through fibre reinforced composites and the future auto materials.

Figure 1-1: CSP VICTALL's composite pickup truck box [20]

Figure 1-2: Ford focus door module carrier [21]

1.3 Automated composite manufacturing

The global demand for CFRP composites material is increasing in both automotive and aerospace industries. The traditional composite manufacturing technique could not meet the projected demand of which the largest share is expected from the automotive market if not backed with high volume automated production schemes. The two widely used automated composite manufacturing techniques for prepreg layup are Automated Fibre Placement (AFP) and Automated Tape-Placement (ATP) [26]. Both techniques use pre-impregnated carbon fibre, with a main difference between the two being the width of the prepreg, and the material is heated slightly to tack the prepreg in place during layup. With ATP process, UD tapes of width 75 – 300 mm are laid up side by side to cover part geometry and is best applicable for wide and flat surfaces due to difficulty in covering complex parts with double curvatures. For such complex part geometries, AFP which utilizes narrowly slit prepregs or multiple fibre tows is efficient preforming technique relatively. Layup speed, tape temperature, feed rate and tape tension are controlled on the CNC machine. After layup, the charge is transferred to autoclave for curing process. However, these automated composite manufacturing technologies are limited in application as they require huge investment,

part complexity and cost efficiency on top of these is the throughput rate is also relatively low. The use of advanced automation and robotic techniques, and process optimizations are bringing step change in these technologies. For instance, Voith's fully digital 4.0 production line [24] utilizes highly efficient direct fibre placement technology with resin injection technique where subsequent part trimming, transport between different process units and assembly are done via robotic systems.

Other automated processes for serial production of fibre reinforced thermoplastic composites such as Wet Compression Moulding (WCM), Dynamic WCM (DWCM) are also allowing automation and short cycle time as viscous draping, resin infiltration and consolidation are achieved simultaneously. Even though cycle time of few minutes is achieved with various processes, the automotive market demand of CFRP composite still needs cost efficient production methods to cope up with the increasing demand from automakers globally. With this regard, another potential for high volume manufacturing techniques comes from the use of discontinuous fibre composites. Discontinuous fibre composites offer both process automation and cost-effective production as it does not require intermediate preforming processes such as weaving and pre-impregnation.

1.4 Discontinuous fibre composites

In discontinuous fibre composites, fibres or fibre tows are chopped and randomly distributed in polymeric matrix and transferred to compression moulding, RTM/HP-RTM or other conventional methods for curing process. The discontinuous nature of fibre/fibre tows and tendency to flow allows these materials to be moulded in more complex shapes than continuous fibre composites. Furthermore, their production can be easily automated for high volume production, providing cost effective

preforming solution for the automotive industry with reduced material waste. Their microstructural parameters (fibre length and reinforcement scale) and fibre/tow orientation can also be varied to tailor the mechanical properties for desired loading requirement. Achievable high fibre volume fraction in these material preserves good mechanical properties, especially stiffness [27], which also widens their application in automotive industry as the design requirement is mostly stiffness dominated [28].

Injection moulded short glass fibres such as glass mat thermoplastics (GMT) and sheet moulding compounds (SMC) are widely used discontinuous fibre composites for non-structural and semi-structural application in automotive industries [29] accounting for about 70% composites use by mass [30]. As most of these materials use glass fibre in polyester resin at low fibre volume fraction of approximately 20%, they are unsuitable for structural applications. In recent years, following the development of advanced manufacturing technique to process carbon fibres at higher volume fraction of more than 50%, SMC composite are showing potential for structural application in both automotive and aerospace industries. The 2003 Dodge Viper Convertible's first application of all carbon fibre SMC and tailored hybridization of carbon fibre SMC to reinforce glass fibre SMC marked a milestone in automotive industry driving the exploration for mass production of CFRP [31]. Weight reduction and stiffness improvement was achieved using a total of 8 kg carbon fibre composite on nine components. Another commercial application carbon fibre sheet moulding compound was in Mercedes-AMG E-Class vehicle for manufacturing of multifunctional spare wheel pan which resulted in 45% weight reduction in addition to improved stiffness and structural integrity during event of crush [32]. In 2015 Automobili Lamborghini used carbon fibre SMC with A-class surface finish for its Lamborghini Huracán car [33]. Advanced carbon fibre SMC called Forged Composite has also been developed

by Lamborghini in collaboration with Callaway Golf Company which was used in the inner monocoque and suspension control arm of the 'Sesto Elemento' concept car and the Diablo Octane drivers from Callaway Golf [34]. More recently, in 2017 Toyota also started to use Mitsubishi Rayon's carbon fibre SMC hatch door frame for its Toyota Prius Plug-in Hybrid or Prius PHV hybrid vehicle [35], Figure 1-3. The component was manufactured in much reduced time of 2 – 5 minutes using compression moulding process which allowed high formability into complex shapes with nearly uniform mechanical properties overcoming high variability associated with DFCs.

Figure 1-3: PHV hybrid vehicle carbon fibre SMC door frame [35]

Commercialized application of carbon fibre sheet moulded composite available include Quantum Lytex 4149 and Hexcel HexMC which uses chopped 3k carbon fibre tow and slit prepreg respectively. However the cost of these materials is still expensive for automotive application as the industry is willing to spend only $2.2 – $8.8 for 1 kg of weight saving while the aerospace is willing to spend $2200 - $4400 [36]. Hence the automotive industry is still in search of low-cost high-performance carbon fibre SMC with easy automation. Directed Carbon Fibre Preforming (DCFP) and Directed Fibre Compounding (DFC) are two low-cost automated carbon fibre preforming techniques developed at the University of Nottingham (UK) composite research group offering high volume production potential.

1.5 Directed Carbon Fibre Preforming

Directed Carbon Fibre Preforming (DCFP) is an adopted process from established Directed Fibre Preforming (DFP) in which chopped glass fibres and emulsified binder are sprayed on a tool surface eliminating intermediate fibre processing such as weaving and impregnating [37]. DCFP process is designed to improve the limitation of conventional carbon fibre fabric low production rate (<5000 ppa) to 50,000 ppa. The process typically involves four main stages; reinforcement deposition, consolidation, stabilization and extraction [38], see Figure 1-4 (left). First, a fibre chopping device mounted on a six-axis industrial robot is used for automated fibre chopping and spreading along with powdered polymeric binder on a perforated tool. A vacuum system is connected to underside of the perforated tool to hold the fibre and powdered binder in place. After deposition a second matching perforated tool is placed to consolidate the preform and control the thickness, then hot air is cycled to activate the binder. Finally, ambient temperature is pushed through to stabilize the preform followed by extraction of the preform for resin injection via RTM, structural reaction injection moulding (SRIM) or other conventional means. Although the preforming process takes under 5 minutes with a potential of 100,000 ppa, conventionally used moulding technologies such as RTM with longer cycle time limit the production rate. Industrial application by Sotira Composites implemented this process to produce only 15,000 ppa of door opening rings and boot lid surrounds for the Aston Martin DBS[28], [39].

Second generation of this preforming technology developed, also at the University of Nottingham, UK; Directed Fibre Compounding utilizes wet preforming for isothermal compression moulding [30]. It uses the same fibre chopping and spreading mechanism as DCFP and simultaneous spraying liquid epoxy matrix via resin

spray gun mounted on the same robot. Both the cones of atomized resin spray and randomly oriented chopped fibre converge on a tool surface, see Figure 1-4 (right). The charge is then B-staged where the resin partially cures to enable handling for compression moulding and cross linking occurs during curing at higher temperature. Simultaneous resin spraying eliminates intermediate resin injection phase associated with DCFP, holds the fibre in place during deposition and also ensures high fibre impregnation resulting in reduced porosity. A fibre volume fraction of 55% was achieved for both 2D and 3D net-shaped charges with less 3% material wastage.

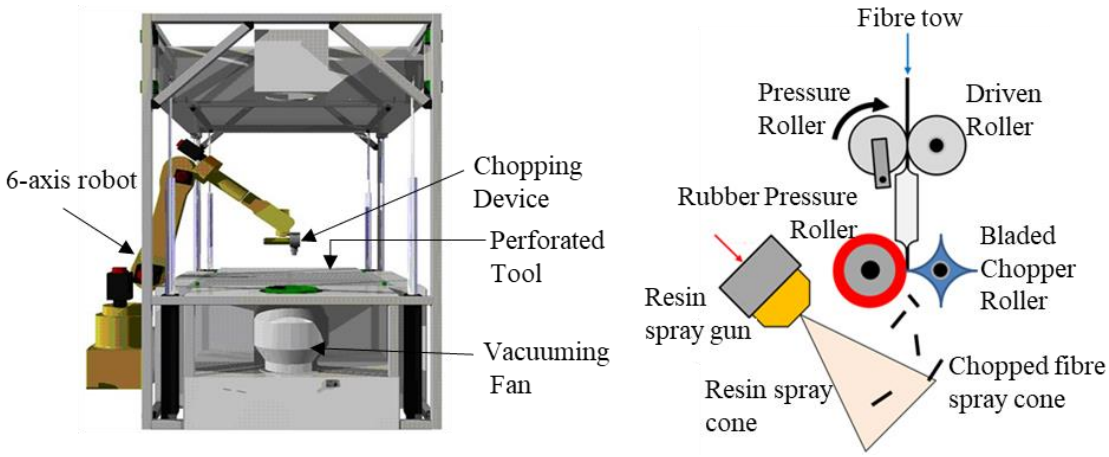

Figure 1-4: Directed Carbon Fibre Preforming (DCFP) [37] (left) and Directed Fibre Compounding (DFC) [30] processes

1.6 Theme of the work

The automation of composite materials manufacturing processes is becoming increasingly important to meet the growing demand from multitudes of industries, largely from the automotive sector. Discontinuous carbon fibre composites are becoming attractive options for high volume applications with acceptable mechanical performance and high formability into complex shaped parts in addition to easy automation potential. However, the lower mechanical performance compared with their

continuous counterparts has limited their application in demanding application. Recent advances in composite industry are aiming to decrease the cost of carbon fibres [93], creating an opportunity for high performance discontinuous fibre composites derived from high performance fibres. Furthermore, limited understanding of how different materials, microstructural and process parameters affect their mechanical performance presents a significant challenge. Hence, this work seeks to understand the effects of different material and process parameters in an effort to improve the mechanical performance of discontinuous fibre composites.

The characteristics of constituent fibre used is one of the principal parameters having significant effect on the processing, performance, and cost of the composite. As the fibre length changes, for instance, various factors such as defects, tensile strength, and load transfer mechanism changes, ultimately affecting the stiffness and strength of the composite. Hence, the current study seeks to investigate the size effect at fibre scale for a range of carbon fibre grades – to determine the fibre tensile strength as a function of fibre chopping length. Then, translate the fibre size effect to tow and composite levels, and explore the achievable composite performance from high performance aerospace grade carbon fibres.

Growing environmental concerns and high material costs are encouraging industries towards green composite materials. However, the lower mechanical performance and susceptibility to environmental damage of green composites pose a greater challenge. Hybridisation of synthetic and natural fibres has been used in conventional laminated composites with slow process times to reduce cost and environmental impact while improving natural fibre composite performance. In the current study, the opportunity of using synthetic-natural fibre hybrid SMC composite for high-volume application has also been investigated from mechanical performance and cost considerations.

As the application of carbon fibre SMC composites in the automotive industry extends to the use in external body panels, their susceptibility to impact induced damage also increases. In particular, low-velocity impact with barely visible damage can result in significant strength reduction. Hence, the characterisation of impact and post-impact residual strength under different loading condition is also of interest to determine the critically affected post-impact properties.

Furthermore, the understanding of fibre orientation development during compression moulding of discontinuous fibre composites is lacking due to the limitations of the conventional characterisation methods. This study seeks to build understanding of the effect of different processing parameters on the flow-induced fibre orientation and consequently on the mechanical performance of discontinuous carbon fibre composites.

1.7 Thesis structure

Following this introduction chapter, an extensive review of literature in the area of discontinuous fibre composites is presented in Chapter 2, exploring the effect of various microstructural, material, and processing parameters. Chapter 3 presents the tensile strength characterization of different grades of PAN- and pitch-based carbon fibres using an automated single fibre testing (SFT) to quantify practical variabilities. Furthermore, fibre geometric irregularities that give rise to tensile strength variability and the limitation of traditional SFT have also been investigated. Chapter 4 focuses on manufacturing and testing of high-performance discontinuous fibre composites using DFC-like method, to establish a relationship with fibre properties evaluated in Chapter 3. The effect of synthetic-natural fibre hybridization configuration and hybridization ratio on the cost and performance of SMC composites has been presented in Chapter 5. The impact behaviour and post-impact tensile and compressive residual strength properties of carbon fibre SMC composites have been studied in Chapter 6. In Chapter

7, an experimental investigation of the influence of charge size and geometry on flow-induced fibre orientation and mechanical performance in carbon fibre SMC composites has been studied. In the final chapter, Chapter 8, the major conclusions from the works carried out in this thesis are presented.

Chapter 2. Literature review

In light of the growing interest in discontinuous fibre composites owing to their suitability for high volume production, short cycle time, reduced production waste, and overall cost advantages, considerable research has been undertaken in different areas demonstrating further favourable characteristics. In this chapter literature review material behaviour and factors that affect the mechanical properties and processability of discontinuous fibre composites are presented.

2.1 Material behaviour

It has been reported that discontinuous fibre composites exhibit high damage tolerance behaviour in open-hole tension, compression after impact, and delamination resistance. Feraboli et al. [40] conducted a series of tests on carbon epoxy discontinuous fibre composites manufactured from UD prepreg chips with an intent of defect inspection, characterization and their effect on damage initiation and growth. Mechanical testing on coupons with manufacturing defect form their ultrasonic inspection, which are known to compromise mechanical performance in continuous fibre composites, were observed to have insignificant effect. Similar result has been reported by other researchers [41] for open hole tension test of DFC and suggested that failure initiation away from the hole should not be associated with poor specimen preparation but to the complex microstructure giving rise to high stress concentration elsewhere. However, other studies have also reported fibre length, bundle size, and notch-diameter dependent notch behaviour [37], [42], emphasizing the challenge in understanding such material performance.

Moreover, continuous fibre composites are known to have significantly lower compressive strength than their tensile strength. Interestingly enough tests on

discontinuous carbon fibre composite with various fibre strength showed very close performance in both tension and compression with (<5%) difference for range of fibre grades tested [28]. Due to fibre bridging in DFC during mode I fracture test, crack initiation load and mode I fracture toughness were also seen to increase by 37% and 27% respectively than UD interface [43]. The randomness of fibre architecture and complex interaction, number of microstructural, processing and material parameters affect the mechanical performance and failure behaviour of discontinuous fibre composites.

2.2 Microstructural parameters

2.2.1 Volume fraction

It is intuitive to assume that both the stiffness and strength of fibre reinforced composites increase with increased volume fraction of reinforcement, which has also been proved with analytical and finite element predictions. Even though achievable theoretical volume fraction is higher (>70% [44]) for continuous fibre composites, in practice it hardly exceeds 60% for discontinuous due to manufacturing difficulty. From experimental and numerical predictions for discontinuous fibre composites, a relatively linear increase in mechanical properties has been observed with an increase in fibre volume fraction [45][46][47]. But this increasing trend falls even before a volume fraction of 60 % due to high void content resulting from poor resin impregnation. For example, Luchoo et al. [48] investigated the achievable fibre volume fraction from Bentley–Raycell automated carbon composite charge deposition (BRAC3D) process. Composites with a volume fraction varying from 10% – 57% were manufactured and tested where a general linearly increasing trend with volume was seen between 33 and 54%. This 54% volume fraction was marked as practical upper limit as both stiffness

and strength reduced by 13% and 18% respectively at 57% volume fraction due to poor resin impregnation. This can be clearly seen from Figure 2-1 as void content increased significantly from 1.6% at a volume fraction of 54% to 8.6% at 57%. Harper et al. [47] also performed 2D and 3D finite element simulation and used the above mentioned set of experimental data [48] for validation. Their prediction showed good correlation with the experimental trend up to volume fraction of 54% and up to 30% difference at volume fraction of 57% due to the same reason in manufacturing, voids, and dry spots.

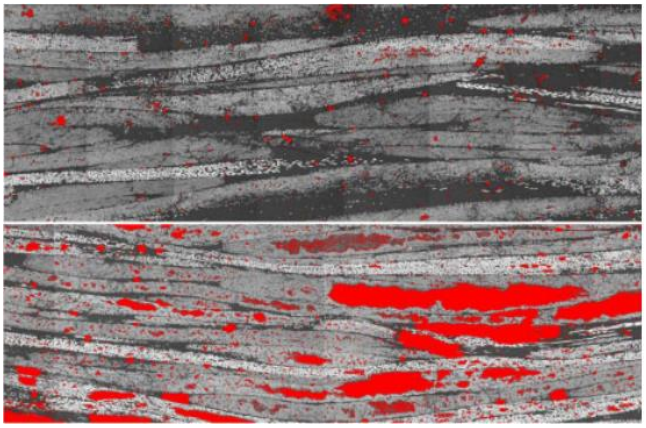

Figure 2-1: Cross-sectional optical micrographs for BRAC3D specimens at fibre volume fraction of 54% (upper) and 57% (lower) [48].

High reinforcement content also requires high compaction pressure to achieve desired preform thickness, during stage II of the DCFP process. Harper [37] studied the effect of filamentisation on preform loft in DCFP process where preform compaction pressure required was fitted with power law relationship with volume fraction. Moreover, high volume fraction preforms also require high resin injection pressure which in turn results in "fibre washing" and fibre distortion in processes like high pressure RTM or HP-RTM. Due to lower permeability issues at higher volume fraction, resin injection fails to wet-out high fibre content DCFPs. In line with this, Endruweit et al. [49], [50] performed permeability modelling and resin injection simulation of

random discontinuous fibre composite and results showed a decrease in macroscopic permeability with an increase in fibre volume fraction, as expected. Therefore, Directed Fibre Compounding likely exhibits better potential for higher volume fraction manufacturing before high void content impairs the achievable mechanical performance as simultaneous fibre and resin spray ensure high fibre impregnation and reduce in-mould resin flow minimizing risk of porosity.

2.2.2 Fibre alignment

Randomly oriented discontinuous fibre composites offer simplified design freedom due to isotropic mechanical properties in every direction. Although more than 90% stiffness retention to quasi-isotropic continuous fibre composite has been achieved, strength retention of only 59% has been attained for random discontinuous fibre composites [48]. The alignment of fibres in the loading direction has received attention from researchers as a way of improving tensile strength and achieve higher volume fraction due to more efficient fibre packing. These alignment techniques take either a dry process where fibres are aligned by pneumatic, electrical or mechanical means or a wet process where fibres are suspended in liquid/water medium and forced through converging nozzle to align fibres in flow direction [51]–[53]. The pneumatic processing method used for Glass Mat reinforced Thermoplastic (GMT) blows chopped glass fibre with powdered binder between two orientation plates onto perforated sheet during spray-up of the preform for compression moulding. Fibres from this process were widely distributed between $\pm 52^0$ and mechanical testing of moulded part showed a stiffness ratio of up 3.8 between longitudinal and transverse directions [54]. The use of an electrical field to align discontinuous fibres for improved mechanical performance has also been demonstrated using E-glass fibres [55]. Chopped fibres are continuously feed between two spaced alignment plates/electrodes with electric field and fibres get

aligned when passing through, which then fall into TEFLON release film to form a mat of fibres. Powdered resin was then sprayed and infrared heated before transferring for compression moulding. Effectiveness of this alignment was reflected from mechanical testing where up to 97% and 86% stiffness and strength improvement, respectively, was obtained from randomly orientated benchmark. Other alignment techniques suitable for high volume and high-performance fibres, i.e., carbon fibres have also been developed in recent years.

Harper et al. [56] used rectangular nozzle like mechanical alignment concentrator with converging sides with 10 mm exit slot to align carbon fibre tows from DCFP process in the desired direction. Two factors, i.e., tow size and fibre length were investigated as both affect processing cost and higher tendency of heavier fibre tow to retain position once it falls onto the tool surface. It was also reported that the fibre alignment decreases with increasing preform thickness due to the reduction in fibre holding force from the vacuum bed as the perforated screen clogged from subsequent layer. A high level of alignment (94%) was achieved for the heavier 24k fibre tow within ±10° to desired direction, thereby increasing tensile stiffness and strength by 206% (71 GPa) and 234% (444 MPa) respectively against random fibre benchmarks. Another recently developed fibre alignment technique at the University of Bristol named High Performance-Discontinuous Fibre (HiPerDif) [53] utilizes short single fibres instead of virgin tows. In this process water suspended short fibres are driven between parallel plates via peristaltic pump nozzle where momentum change of suspended fibres aligns the fibres. The fibres are then aligned on a conveyor belt and the water is drawn using vacuum suction system. Subsequently the aligned fibres are dried using infrared heating before resin impregnation. By aligning 67% of 3mm short fibres in ±3° high performance discontinuous fibre composites with tensile modulus

and strength of 115 GPa and 1509 MPa were achieved at 55% fibre volume fraction. Longana et al. [57] studied the effect of fibre architecture on mechanical performance of discontinuous fibre composites from the HiPerDif process. In their study mechanical behaviour of quasi-isotropic aligned discontinuous fibre reinforced composite (QI ADFRC) and randomly oriented (RODFRC) were investigated. The QI ADFRC showed 26% and 77% stiffness and strength enhancement respectively with improved consistency and coefficient of variation over RODFRC due to its structured fibre arrangement. Thus, fibre alignment techniques provide a means of tailoring microstructure for improved mechanical performance in the preferred direction.

2.2.3 Fibre/Tow length

A number of studies have shown that tensile strength of brittle fibres such as carbon fibre decreases with increasing length due to the increased probability of containing critical flaws, inducing local weak point [58]–[60]. This size effect or strength reduction can be described using Weibull theory[61] which was originally developed for isotropic brittle materials. Van Hattum and Bernardo [62] demonstrated Weibull effect on brittle carbon fibre, Tenax HTA 5131, and showed more than 40% strength reduction when the fibre length is increased from 5mm to 80mm. In similar work on HTA carbon fibre, Harper [37] reported a 37% filament strength reduction when the gauge length increased from 5mm to 100mm. Extension of the theory to bundle level also showed tow strength increased to its peak at 2mm which then starts to drop showing 35% reduction between gauge lengths 5 mm to 100mm.

Other experimental and analytical studies relating fibre length to mechanical performance of discontinuous fibre composites in contrary suggest that fibre length has to exceed a *critical length, L_C,* which is a function of fibre diameter. This fibre length

beyond L_C encourages tensile failure of fibres rather than shear failure of the matrix or matrix cracking. Fibre stress distribution from analytical models shows that the fibre will not reach its ultimate strength up to a length of $L_C/2$ from both ends [63], hence a fibre should be significantly longer than its critical length for maximum potential. For instance, perfectly aligned discontinuous fibre with fibre length greater than $5L_C$ can retain up to 90% strength of continuous fibre composites [63]. For tow based discontinuous fibre composites, tow critical length is much larger than filament critical length which can be predicted considering the fibre bundle as large single fibre [64]. As previous analytical predictions of tow critical length consider ideal circular cross section, Harper et al. [64] developed a more realistic analytical prediction model assuming elliptical cross section based on Kelly-Tyson's slip-theory [65]. A cross-sectional aspect ratio was established using image analysis taking the micrographs of carbon fibre tows. Different non-coinciding predictions exist for stiffness, strength and impact requirements from different analytical models [37], [65]–[68] which shows different properties have different fibre length dependency. Shorter fibre length, but higher than critical length, also offer the advantage of improved surface finish and part homogeneity in turn improved performance than longer fibre composites [64]. However, a trade-off exists as shorter fibres increase stress concentrations due to increased fibre ends and balance should be maintained.

Harper et al. [64] studied the combined effect of fibre length and natural filamentisation associated with short fibres from DCFP on tensile properties of 2D discontinuous carbon fibre composites. Stiffness was found to be insensitive to fibre length beyond critical value while tensile strength shows decreasing power law relationship with increasing length where strength improvement was attributed to improved preform coverage and less probability critical flaws at shorter lengths.

Contrary to this trend, Feraboli et al. [27] studied the length effect on tensile properties of randomly oriented carbon fibre composites from preimpregnated unidirectional tapes where all flexural, compressive, and tensile strength improved monotonically with increase in chip length or aspect ratio while stiffness was relatively indifferent. However microscopic image of the failed sampled revealed matrix dominated failure or chip pullout which suggesting that tested samples chip length is below critical length. Similar increasing trend was also seen in tensile strength of carbon fibre reinforced polybenzoxazine discontinuous composite up to certain length before it starts to decrease while compressive strength showed continuous decline[69]. Furthermore, in an effort to isolate the effect of fibre orientation from bundle aspect-ratio Masoumy et al. [70] studied the effect of fibre aspect ratio on tensile properties of aligned E-glass discontinuous fibre composites where 65 – 80% of fibre bundles were aligned within $\pm 15^{o}$. It was observed that as the aspect ratio varied from 185 to 557, stiffness retention rose to 99% of continuous fibre system while strength retention reaches a 60% plateau at aspect ratio above 400.

The influence of fibre length on the performance of discontinuous fibre composites has also been studied for dynamic properties. Jacob et al. [71] studied the effect of different microstructural parameters on performance discontinuous fibre composite Specific Energy Absorption (SAE) capacity. Although tests were limited to two discrete lengths, shorter fibre length was observed to have improved SAE capacity than longer fibre length due to increased number of stress raisers at fibre ends which in turn increase fracture initiation sites. Moreover, higher stiffness and strength properties were recorded for longer fibre lengths at two different fibre loadings. Other dynamic properties, Charpy impact strength, tensile impact and high speed impact, were reported to increase steeply for glass fibre reinforced polypropylene discontinuous fibre

composite up to 6 mm, reaching plateau at longer fibre lengths [72]. Damping properties and thermal stability of carbon fibre reinforced polypropylene composites has also been seen to improve employing longer fibre length [73].

Critical fibre length or tow length is therefore an important microstructural parameter having significant effect on the performance of discontinuous fibre composites. Depending on the material system and reinforcement level different analytical models can be employed in predicting optimum aspect ratio for improved stiffness, strength and impact properties. As true as shorter fibre length is proven to improve composite performance due to fewer critical flaws and other gains, a number of studies also showed improvement of various properties with longer fibre reinforcement. This may suggest that improvement in load transfer mechanism might have dominated fibre strength reduction associated with Weibull effect resulting in enhanced composite performance.

2.2.4 Tow size/filamentisation

Processing larger (>24k) or smaller (<12k) tow size in DCFP or DFC is not only a preference of fibre deposition rate for high volume production but also affects microstructural parameters and hence mechanical performance. Studies have shown that the performance of discontinuous fibre composites improved by utilizing smaller tow size due to enhanced areal density variation or homogeneity reducing failure initiation sites[64], [74], [75]. However, the choice has been largely driven by cost benefit of larger, commercial grade tows as smaller aerospace grade tow sizes are considerably expensive[37], [41], [76] associated with low throughput with the same precursor and processing cost as larger ones. In larger tows stress concentration at fibre ends is higher due to synchronized coplanar filaments but the number of these failure

initiation sites decrease for a given volume fraction. Utilizing larger tows also results in poorer fibre coverage due to a smaller number of bundles over a given areal mass and volume fraction. Experimental results showed that an average of 37% and 74% reduction in stiffness and strength respectively when the fibre bundle size increased from 3k to 24k for thinner parts at 30% volume fraction [41]. The effect was seen to reduce to 29% and 67% respectively for thicker parts due to improvement in fibre distribution. Jacob et al. [71] also showed a 22% reduction in both stiffness and strength while increasing tow size from 12k (150 gsm) to 48k (300 gsm) at a chopping length of 25.4 mm. The effect worsens to 20% and 60% reduction in stiffness and strength respectively when the fibre bundle length doubled due higher variability and stress concentrations. Furthermore, improved specific energy absorption (SAE) capacity was also reported for smaller tow size. Although tow size has an impact on both elastic and failure behaviours, it has been shown to have a considerable influence on strength.

Efforts have also been made to fragment or filamentisize larger cheaper tows into smaller tows using mechanical and pneumatic means [37] in order to exploit cost benefit of high filament count tows. Harper et al. [37] studied the effect of different level of induced filamentisation on mechanical performance of discontinuous fibre composites from DCFP process. In their study high velocity air was blown in the fibre landing direction to split larger tow into smaller ones, as shown in Figure 2-2. High filamentisation was achieved for 24k tow splitting into an average of 425 filaments where moulded samples showed increased stiffness and strength of 13% and 55% respectively. However, highly filamentised tows were also seen to increase preform loft to unacceptable level reducing the achievable volume fraction from 50% down to 27%. It was also reported that employing lower filament count bundles also poses a problem of reduced permeability, increasing cycle time in liquid composite moulding

technologies [38], [74] due to reduced intra-tow pore sizes as the bundle size becomes smaller. In contrary to this Endruweit et al. [77] performed a series of experiments on tow size ranging from 3k to 24k with different types of sizing and tendency of natural filamentisation. Permeability measurement from their unidirectional injection experiment showed a peak at 6k and constant reduction for increasing bundle size, showing no clear trend. It was attributed to the type of sizing agent used which was considered to affect the cohesion and packing density of filaments in the bundles. However, similar trend has been observed in another study performed by the aforementioned authors showing that macroscopic permeability to be independent of filament count but decreases with increasing superficial density [49].

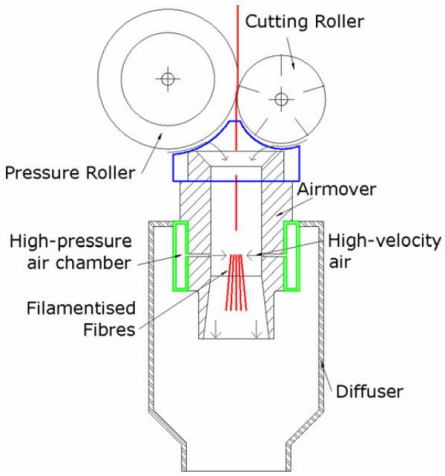

Figure 2-2: Schematic of DCFP fibre chopping apparatus with pneumatic filamentisation [37]

2.2.5 Thickness

It has been demonstrated in various studies that tow size and length are crucial for optimization of preform homogeneity which ultimately determine the composite performance. Part homogeneity is also a function of preform thickness as it gets optimized with increasing thickness. As a result, both stiffness and strength improve

with part thickness due to near uniform property and reduction of weak failure initiation sites. Since variability increases for longer and larger fibre tows, optimized preform homogeneity is attained at different levels for shorter/smaller and longer/larger tows. Kirupanantham [41] studied the effect of preform thickness on mechanical properties for various tow size and chopping lengths. As expected, larger tows size likely to result in poor homogeneity for thin parts showed larger improvements in both strength and stiffness with part thickness. An increase of 40% in strength was observed as fibre length increased from 1mm to 3mm for 24k tow while 19% improvement was seen for 6k. Further increasing of chopping length from 3mm to 10mm also showed 88% improvement for 24k and 29% for 6k tows. For the two tow sizes studied, strength and stiffness plateau were not observed for tested length ranges except stiffness results from 6k tow reaching optimized homogeneity at 3mm thickness. These results showed thicker parts result in reduced variability and improved mechanical performance more significantly in strength. Hence part thickness is an important parameter influencing preform homogeneity in discontinuous fibre composites.

2.3 Constituent material properties

2.3.1 Fibre Properties

The mechanical properties of fibre reinforced composites are dependent on a number of factors, i.e., basic mechanical properties of reinforcing fibre, fibre-matrix interface, fibre volume fraction and fibre orientation. But the extent of their effect is different on continuous and discontinuous fibre composites due to the nature of their microstructure and pertinent failure mechanisms involved. There is lack of demonstrated study to support that higher stiffness and strength fibres result in stiffer and stronger discontinuous fibre composites as it is the case in continuous. For instance, on a study

attempting to improve achievable mechanical properties from tow based discontinuous fibre composites, Xiao [28] used high strength and stiffness fibre using DCFP coupled with RTM resin application. Lower and converging composite stiffness and strength were observed for increasing fibre stiffness and strength properties which was attributed to resin dominated failure. Moreover, higher local volume fraction variability and poor resin infiltration were reported for their RTM process which did not achieve the anticipated composite properties. The converging mechanical properties of discontinuous fibre composite for an increasing stiffness and strength could result from strength reduction associated with Weibull effect. A number of studies [78], [79] confirmed that both PAN- and pitch-based high strength fibres show low Weibull modulus implying large strength scatter. Lower Weibull modulus is also associated with higher strength reduction with increasing fibre length. However, further studies are required to better understand the influence of fibre type, properties, and length on the mechanical performance of discontinuous fibre composites.

2.3.2 Fibre type/hybridization

Numerous studies have shown that multi-fibre type/hybrid composites offer superior cost saving and composite performance [80]–[82]. Studies on hybrid continuous fibre composite focus on carbon/glass fibre to achieve a balance between mechanical property and cost [83], [84]. When the brittle carbon fibre with higher stiffness and strength was hybridized with less stiff glass fibre, failure strain of the carbon fibre was observed to improve due hybrid effect. The first failure in the hybridized composite, called knee point, occurs in lower elongation fibre, interestingly at failure strain/strength greater than in pure low-elongation fibre composite [85]. Hence hybridization also serves as a way to avoid catastrophic failure and achieve pseudo-ductile failure response in composite materials. Yu et al. [85] studied the pseudo-ductile

response of intermingled highly aligned carbon/glass fibre discontinuous fibre composites. They observed good pseudo-ductility response from high modulus/E-glass than high strength/E-glass due to fragmentation of high elongation carbon fibre. Cabrera-Ríos and Castro [86] also studied the effect of ply-wise hybridization of carbon/glass fibre reinforced SMC composite on the mechanical properties and found out that the relative stacking has effect on the ultimate strength. Moreover, Xiao [28] used different high modulus and high strength carbon fibre to establish cost effectiveness of small volume of high performance with high purchase cost over larger volume of industrial grade fibres.

Hybridization of synthetic and natural fibres has also been the centre of interest of many research, to take advantage of superior mechanical performance synthetic fibres and the sustainability and other excellent properties of natural fibres such as damping. Synthetic fibres are generally more expensive, cause adverse impacts on the environment and provide excellent mechanical performance. Natural fibres, on the other hand, exhibit much lower mechanical performance relatively and are prone to environmental degradation due to poor fire retardance and moisture absorption [87], [88]. The hybridization of synthetic with natural fibres is one effective way to address these challenges while retaining the useful properties of both.

2.3.3 Fibre/matrix interface properties

Since the fibre/matrix interface is largely responsible for load transfer mechanism in discontinuous fibre reinforced composites, it directly influences the mechanical performance. Hence composites with higher interface properties result in improved mechanical performance. The two widely used methods for enhancing interface properties are fibre surface treatment by changing the surface of the fibre (sizing) and

resin modification by introducing reactive sites with higher chemical affinity towards the fibres [89]. Fibre sizing is generally used to protect fibre surface during transport and processing and also improve interfacial adhesion between the fibre and matrix. Coupling agent, a chemical generally designed as sizing agent has been used as matrix modification techniques to improve interfacial strength in fibre reinforced composites. Yang et al. [89] used silane coupling agent as matrix modification to increase interfacial adhesion in carbon fibre/epoxy composite. Evaluating the performance of carbon fibre composite with modified epoxy resin, they reported 4, 44 and 42% improvement on tensile, flexural and interlaminar shear strength respectively. Wong et al. [90] have also used maleic anhydride grafted polypropylene (MAPP) coupling agent as matrix modification to study the effect of coupling agent on recycled carbon fibre polypropylene composite from compounding and injection moulding processes. In their study, 150% tensile strength improvement was obtained with addition of 5 wt% of coupling agent which was attributed to the improvement in interfacial shear strength. Furthermore, Burn et al. [91] investigated the influence of coupling agent on the interfacial shear strength of carbon fibre and polypropylene. Their micro bond characterization showed 320% interface strength improvement with addition of 2 wt% of maleic anhydride coupling agent. The effect of maleic anhydride coupling agent on macroscale mechanical properties of long discontinuous fibre composites has also been studied by the same researcher [92] where the tensile and flexural strength showed 68% and 70% improvement. Other studies have reported that resin modification technique results in better mechanical performance than fibre surface treatment [93], [94].

However, resin modification techniques not only change the mechanical properties but also the viscosity and cure kinetics of the resin, hence influencing the processability and ultimately the composite performance. Therefore, more research is required to

better understand how fibre type, constituent properties, modification techniques influence the fibre-matrix interface behaviour and in turn the composite performance.

2.4 Processing parameters

2.4.1 Initial charge geometry

In a typical manufacturing route, chopped fibres are randomly and evenly dispersed on a resin paste, compacted and B-staged, where partial curing of the resin occurs to allow for handling of the charge before compression moulding. The in-mould flow of these compounds during compression moulding also enables forming of complex geometries with out-of-plane features such as ribs and fasteners. On the contrary, if not properly designed and controlled high in-mould flow may result in fibre orientation, local volume fraction variability, segregation and knit lines which significantly affect the mechanical performance of the material.

Initial charge coverage and shape significantly influence flow induced fibre/bundle reorientation and thereby the in-plane anisotropy of the moulded sheet. Evans et al. [30] studied the effect of initial charge coverage on the macroscopic charge flow and tensile properties along with other material and process parameters, allowing unidirectional charge flow. It was reported that in-plane anisotropy in tensile properties increased with reduced charge coverage and more pronounced in shorter fibres than longer fibres. Furthermore, higher moulding pressure and promoting charge flow were suggested as a mechanism to reduce porosity due to entrapped air. Luca et al. [95] also studied the morphology with tensile and compressive properties of carbon fibre SMC with high in-mould flow, manufactured from 20% charge coverage. Their morphological characterization showed higher tow distortion and filamentisation in the skin region, 200 μm from the top and bottom surface, due to high shear stress between the surface

and mould while the core region is relatively intact. Tensile and compressive properties were evaluated from 0^0, 45^0 and 90^0 coupons where higher values were reported for 0^0 followed by 45^0 and 90^0. The quasi-static and fatigue properties under incremental loading/unloading loop and tension-tension controlled fatigue loading of highly and randomly oriented SMC has also been investigated by Nony-Davadie et al. [96]. From the quasi-static test, it was shown that samples in 0^0 to the flow direction showed minimal stiffness degradation and ductility than 45^0 and 90^0 directions during loading/unloading cycle. Post failure SEM and radiographic characterizations revealed micro cracks failure mode at both inter-bundle and intra-bundle levels. Moreover, fatigue life evolution of both configurations also showed similar trend with ultimate stress in quasi-static test with the similar failure modes.

The other important factors to consider are shrinkage and warpage/dimensional stability in SMC composites with high in-mould flow. This dimensional instability mainly results from volumetric shrinkage of the resin and material in-homogeneity in the form of flow induced fibre orientation, curing, poor thermal lay-out and processing conditions [97]. Residual stress built up from differential curing due to temperature difference and variation of fibre orientation through the thickness could result in significant warpage in areas with lower stiffness [97], [98]. Hence fibre reinforced SMCs with low fibre content suffer more due to higher heterogeneity in fibre distribution, orientation and amplified from non-uniform distribution of temperature and pressure. Kite et al. [99] studied the effect of initial charge placement on the dimensional instability and strain concentration of carbon fibre SMCs. CF-SMC plaques were manufactured from 25% charge coverage placed at the geometric centre of the mould. Despite charge flow being encouraged in all directions, saddle shape distortion with a maximum distortion of 3.2 mm at one of the corners was observed.

This was due to higher propensity of fibre alignment towards the corner as a result of longer flow distance. Strain distribution was also seen to be affected by fibre orientation distribution due to charge flow.

2.4.2 Mould closure speed

The differential temperature profile of the initial charge due to prior thermal exposure of the bottom surface before the mould closes results in different charge viscosity in the thickness direction. This in turn result in different flow behaviour between the front and back surfaces of the moulded part [100]. Homogenizing charge temperature prior to mould closure through dwelling time and high mould closure speed have been suggested to mitigate the differential flow profile. However, it has also been reported that high mould closure speed can result in fibre-matrix separation. Alternatively, high mould closing speed and press force were used to overcome mould filling problem of SMC composites with relatively fast curing resin.

2.5 Chapter conclusions

In this chapter a review on the effect microstructural, material, and process parameters on the processability and performance of discontinuous fibre composites has been presented. Due to the complex interaction of these parameters and sometimes contrasting influence on the processability and composite performance, parameters optimization is crucially important. For instance, increasing fibre length has been shown to improve the load transfer mechanism and conversely increase material variability and strength reduction due to Weibull effect, resulting in contradicting effects on the composite performance. Similarly, the cost reduction and high deposition rate advantages from processing higher filament count tows comes with a cost of higher material variability and stress concentration at bundle ends, causing weak zones for

failure initiation. Furthermore, conflicting notch sensitivity behaviour has been reported for this class of materials. The understanding of the changes in fibre orientation during charge flow has also been limited due to the limitations in conventional analysis techniques. Thus, this study aims to improve the performance of discontinuous fibre composites through a better understanding and tailoring of different microstructural, material and process parameters.

Chapter 3. Influence of size effect on fibre properties

3.1 Introduction

As established in Section 2.2.1, the performance of discontinuous fibre-reinforced Sheet Moulding Compounds (SMCs) composites is highly dependent on the properties and geometry of the constituent fibres. Increased fibre length increases the likelihood of fibre flaws, potentially reducing composite strength but also reduces shear stresses at the fibre-matrix interface – potentially increasing strength. Thus, the performance of these materials is dependent on parameters such as the aspect ratio of the reinforcing fibre and the interfacial shear strength. A precise understanding of these microstructural parameters on the global performance of SMCs is important for efficient implementation.

In the development of high-performance, low-density SMC, carbon fibres and high-performance thermosetting resins, such as vinyl-ester or epoxy, are replacing traditional polyester-based glass fibre materials. Such carbon fibres can be derived from two precursor types: polyacrylonitrile (PAN), accounting for about 90% of carbon fibres produced, and pitch-based fibres [101], [102]. The resulting mechanical properties are governed by the type, structure and processing conditions of the precursor material. Currently, ultrahigh strength (7000 MPa) and ultrahigh modulus fibres (900 GPa) are commercially available, however research has shown that the tensile strength of these fibres experience significant scatter [103]–[105]. This scatter in carbon fibre tensile strength has been attributed to the inherent variability in the distribution of flaws resulting from either precursor treatment or handling processes. These flaws take the form of fibrillar misalignment, micropores, and surface defects of varying shape, size, and orientation. As the nature of these defects is random, statistical methods are commonly used to describe their influence on the tensile strength. One of the most

widely used statistical considerations for brittle fibres, such as carbon fibre, is the Weibull distribution [106]. This theory assumes the volume of material is constructed from small individual elements linked in series, thus the failure of the entire material is governed by the weakest link in the chain.

Weibull distribution modelling has previously been used to characterize the stochastic distribution of tensile strength for different fibre types and supports the composite strength prediction for discontinuous fibre composite materials. One observation from the literature is that the strength of brittle fibres decreases with increasing gauge length, due to the higher propensity to contain more flaws, which is referred to as a 'size effect', as outlined in Section 2.2.3. Conversely, Cox [66], and extensions of his work [65][107], showed that the stiffness, strength, and impact properties of discontinuous fibre composites increase with increasing fibre length due to greater efficiency in load transfer from an increase in surface area. Provided the fibres exceed a critical fibre length, fibre failure is experienced instead of matrix failure (in the form of fibre pull out or matrix cracking). Hence, a theoretical trade-off exists between the fibre strength reduction due to size effects and the enhancement in composite performance due to improved load transfer, which are both a function of the fibre length in discontinuous fibre composites.

Fibre manufacturers commonly report the tensile strength, modulus, and strain for their materials based on the ASTM D4018 test standard [108], which involves testing a fibre tow infused with resin. The back-calculated fibre properties are affected by the microstructural nature of the infused tow, such as volume fraction variability, the presence of defects, and the fibre-matrix interface. Crabtree et al. [109] examined how the mechanical properties from single filament carbon fibre test relate to other commonly used tow-based testing practices; testing infused tows prepared either

manually or using automated processes. Microstructural analysis of the infused tow cross-sections showed higher fibre packing and local volume fraction variabilities in the tow prepared manually. Tensile strength, modulus, and strain values obtained from the different approaches showed considerable differences. Manually infused samples had the highest properties followed by the automated infused tow, with the single filament samples having the lowest. Filaments in the infused tows failed progressively due to load sharing via the fibre/matrix interface, whereas single filaments failed catastrophically.

Information on the stochastic nature of fibres is not currently part of standard material datasheets, however there are ongoing efforts to better understand the statistical nature of fibre strength for different fibre types and grades. Naito et al. [79] evaluated the performance and failure morphology of commercially available standard, high, and ultrahigh strength/modulus fibres. The study showed that Weibull modulus decreases with an increase in tensile modulus and tensile strength, suggesting that high strength/modulus fibres exhibit greater variability in tensile strength. However, the trends are not so conclusive from other studies [78], [110], [111]. For example, fibre tensile strength (and Weibull modulus) has been shown to increase linearly on a log-log scale with decreasing gauge length [110], since longer fibres are likely to contain more critical flaws.

Despite these efforts, the stochastic nature of these materials still results in considerable variability and uncertainty in fibre strength testing. Furthermore, unsuccessful attempts to utilise high-performance carbon fibres to produce advanced discontinuous fibre moulding compounds [28] also highlights the need to characterize the size-dependent properties, i.e. strength reduction and increased scatter with increasing reinforcement length, of these fibres. Hence, the work in this chapter

investigates the tensile strength of high-strength PAN-based, and high-modulus pitch-based, carbon fibres using an automated Single Fibre Testing (SFT) process. Poor interfacial bonding, as a result of graphitic crystal alignment at the smooth and inert fibre surfaces [112], limits the achievable composite performance. Subsequently, the characterisation of fibre surface morphology can provide useful information to devise counter strategies. Moreover, anomalies in conventional single fibre testing such as fibre misalignment, pre-tensioning, and fibre diameter measurement cause significant error in characterization of fibre tensile strength [113]. Quantifying these discrepancies and their effects can help in taking reasonable correction where accurate automated SFT is not possible. The effect of surface irregularity, sample size, and fibre diameter measurement on the Weibull analysis have also been analysed, along with the surface morphology of the fibres using high resolution SEM images.

3.2 Statistical fibre strength theory

According to Weibull [106], the defect density in a volume of brittle material increases with increasing applied stress according to a specified power law [103]. The strength distribution can thus be described by means of a two-parameter Weibull model as given in Eq. (3.1).

$$P(\sigma) = 1 - \exp\left[-\left(\frac{\sigma}{\sigma_0}\right)^m\right] \qquad \text{Eq. (3.1)}$$

where σ is the applied stress, σ_0 is the characteristic stress (at which the failure probability is 63%), and m is the Weibull modulus, which is a measure of flaw distribution in the tested volume. Taking logarithms of both sides of Eq. (3.1) and rearranging gives:

$$\ln\left(\ln\left(\frac{1}{1-P_F}\right)\right) = m\ln\left(\frac{\sigma}{\sigma_0}\right) \qquad \text{Eq. (3.2)}$$

The Weibull parameters for Eq. (3.2) can thus be obtained from least square curve fitting. Another approach used for parameter estimation is Maximum Likelihood Estimation (MLE), where the parameters are estimated in order to maximize the likelihood of the model to reasonably describe the observed data. The likelihood function of the conventional two-parameter Weibull model is given in Eq. (3.3), which is preferred over least square estimation for its greater precision and lower variance [114].

$$L(\sigma; \sigma_0, m) = \frac{m}{\sigma_0}\left(\frac{\sigma}{\sigma_0}\right)^{m-1} \exp\left[-\left(\frac{\sigma}{\sigma_0}\right)^{m}\right] \qquad \text{Eq. (3.3)}$$

3.3 Experimental characterization

3.3.1 Materials

Five different types of carbon fibre have been considered, including high-strength and high-modulus PAN-based fibres and high-modulus and ultra-high-modulus pitch-based fibres. Physical and mechanical data as supplied by the manufacturers are given in Table 3-1. All fibres studied were in the ‘as received’ state, without any further modifications or treatments.

Table 3-1: Supplier physical and mechanical properties of PAN- and pitch-based fibres.

Fibre type	Precursor	Tow size (K)	Tensile strength (MPa)	Failure strain (%)	Tensile Modulus (GPa)	Filament Diameter (μm)	Density (g/cm^3)
PAN-1	PAN	12	4900	2.1	230	7	1.8
PAN-2	PAN	12	5490	1.9	294	5	1.81
PAN-3	PAN	6	4210	0.9	436	5	1.84
Pitch-1	Pitch	12	3200	0.8	420	9.5	2.06
Pitch-2	Pitch	16	3200	0.4	760	9.5	2.15

3.3.2 Specimen preparation and testing

Single fibre tensile testing commonly relies upon manual specimen preparation, involving a separate procedure for taking multiple diameter measurements to determine the mean fibre diameter [78], [79], [110].

A Dia-Stron single fibre testing instrument was used to conduct automated measurements. It performs both the measurement of the fibre diameter using a laser diffraction system mounted on a rotary device, and the subsequent uniaxial tensile testing according to the ISO 11556 test standard [115]. Fibre ends are mounted on two plastic tabs, which are arranged into a slotted cassette. The fibres are aligned with the help of a V-notch on the plastic tabs and a UV curing resin (QUINSON) to hold the fibre in place. The cassette is then mounted on the Dia-Stron instrument for the fully automated process of transferring samples, diameter measurement, and tensile testing. The diameter measurement is done by the rotary laser diffraction system at a number

of points around the perimeter of the fibre, with the resulting mean elliptical area for each individual fibre used for the tensile strength calculation. Figure 3-1 shows the different components of the test instrument.

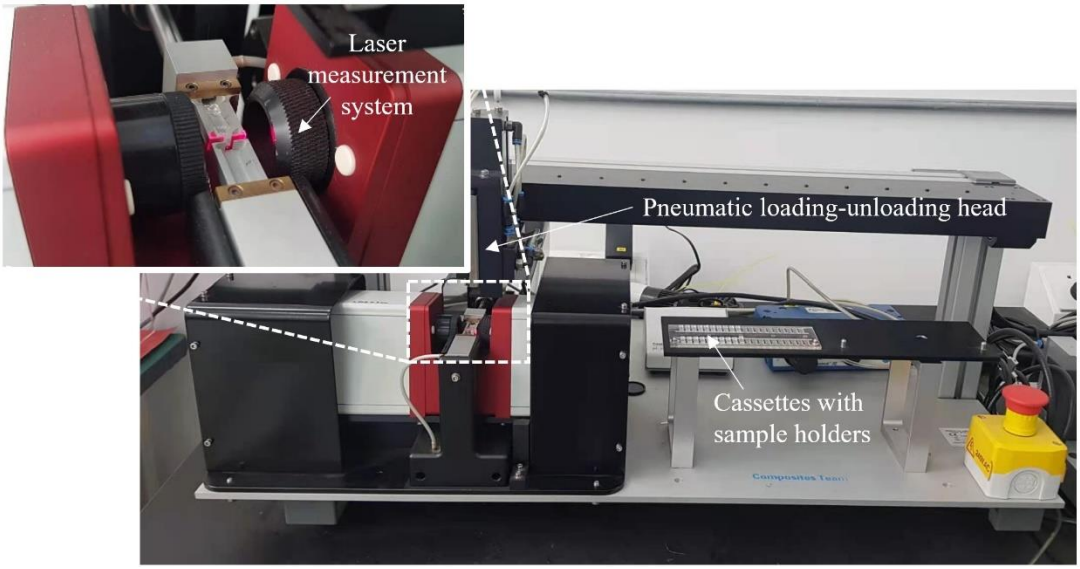

Figure 3-1: Components of a Dia-Stron automated single fibre test instrument.

The breaking force during testing was detected when the observed load dropped by more than 10%. Stress and strain values were then obtained by fitting a least squares linear regression between data points according to the test standard. The compliance of the instrument for carbon fibre testing was determined to be 0.1653 mm/N and the average strain values have been corrected accordingly, following the procedure outlined in EN11566 test standard.

3.4 Automated single fibre testing

Results from the single fibre tensile testing are presented to characterize the stochastic nature of the fibre tensile strength for each fibre type. SEM micrographs of the surface and cross-section of the fibres have also been used to evaluate the surface irregularities of the different fibres. Other relevant observations from sample preparation, diameter variability, and sample size dependence are also discussed.

3.4.1 Fibre diameter variability

Carbon fibres are typically assumed to have perfectly cylindrical structures, when in reality most fibres show some sort of surface irregularity. In previous studies, these surface irregularities were considered as surface defects from which failure may initiate and reduce the tensile strength [116]. Moreover, the surface characteristics of a fibre are reported to influence the adsorption, impregnation, and interfacial bonding [117]. Thus, in the current study, the term surface irregularity is used to refer the smoothness of a fibre surface about its circumference, affecting its wettability and interfacial bonding potential, while flaw population is used to refer failure inducing critical defects along its length. Fibre manufacturers often rely on indirect measurement techniques such as weighing (in combination with the fibre linear density), or optical microscopy. However, these methods rely on representative sampling and cannot provide an accurate measure of individual fibre diameters or cross-sectional shape without destructive analysis. Alternatively, non-destructive techniques such as vibroscopy [118] and laser diffraction [119], [120] can offer a rapid and accurate dimensional measurements of individual fibre cross-sections.

The geometric irregularity and variability were analysed using SEM images and by laser scanning the circumference of each tested fibre at between 40 and 200 points. The surface morphology of the fibres reveals significant corrugation of the PAN-2 high-strength and PAN-3 high-modulus fibre surfaces, as shown in Figure 3-2. In these fibres, micro-fibrils run along the length of the fibres creating longitudinal ridges and channels. Alternatively, the PAN-1 and both pitch-based fibres appear to have smoother surfaces. These observations are reflected quantitatively by the laser diffraction measurements of the fibre diameters. Table 3-2 shows the intra-fibre variability of the measured diameters for the different fibre types, based on the mean

and maximum relative standard deviations from individual fibres. All fibre types exhibited very low intra-fibre variability (with mean relative standard deviations less than 1%), reflective of their highly cylindrical geometries. However, the corrugated PAN-2 and PAN-3 fibres showed the greatest variability, with mean values of 0.3% and 0.7% respectively. Notably, the maximum relative standard deviation of fibre diameter measurements was as high as 9.1% for one of the PAN-3 fibres.

Table 3-2: Intra-fibre diameter variability in tested carbon fibres.

Relative SD (%)	PAN-1	PAN-2	PAN-3	Pitch-1	Pitch-2
Mean	0.2%	0.3%	0.7%	0.1%	0.1%
Maximum	0.8%	1.2%	9.1%	0.4%	0.4%

The inter-fibre diameter variability from each batch of fibres was found to be much more significant than the intra-fibre variability, as shown in Table 3-3. Higher inter-fibre variability was observed in the pitch-based fibres (8-10%) compared with the PAN-based fibres (4-7%). However, the PAN-2 and PAN-3 fibres both showed higher inter-fibre variability (6% and 7% respectively) than the PAN-1 fibres (4%). The manufacturer's data for each fibre type is also provided for comparison, with the mean measured Pitch-1 and PAN-1 fibre diameters deviating from these values by as much as 7% and 5% respectively.

Table 3-3: Inter-fibre diameter variability in tested carbon fibres.

Fibre diameter (μm)	PAN-1	PAN-2	PAN-3	Pitch-1	Pitch-2
Supplier data	7.00	5.00	5.00	10.00	10.00
Mean measured	6.64	5.14	5.07	9.34	9.56
S.D. measured (COV)	0.24 (4%)	0.32 (6%)	0.36 (7%)	0.92 (10%)	0.77 (8%)

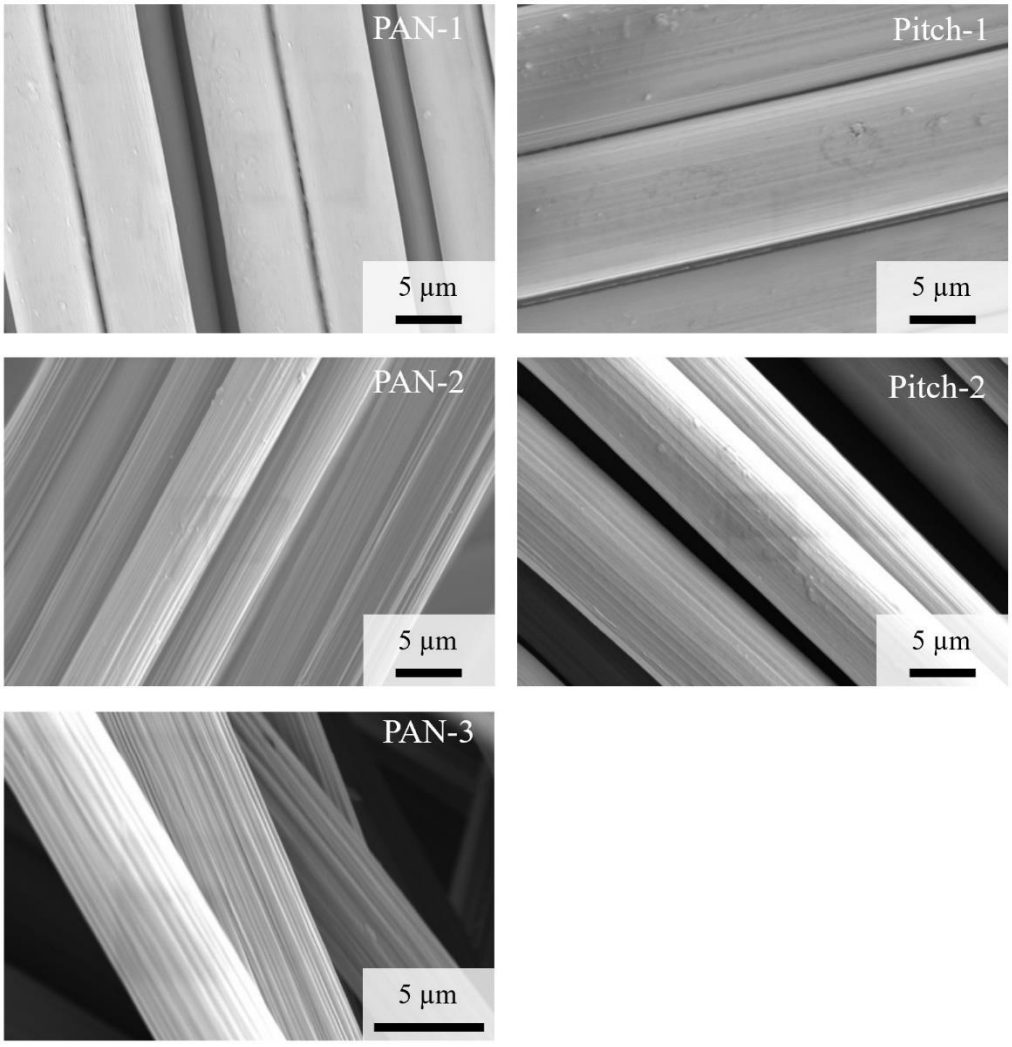

Figure 3-2: SEM images showing the surface morphology of different fibre types.

3.4.2 Observations

One of the most challenging aspects of SFT is the sample preparation, due to the scale and brittle nature of carbon fibres. The PAN-2 and PAN-3 filaments were difficult to isolate from their bundles due to their small fibre diameter (5 µm), whereas the larger diameter (10 µm) pitch-based fibres required considerable care as they were more prone to breaking prematurely due to their relatively low failure strain (~ 0.4%). In all cases, great care was taken to prevent any off-axis bending that could introduce damage.

The ISO 11566 standard recommends that a minimum of 20 successful single filament specimen tests are required in order to report fibre tensile strength with confidence. In the current study, it was noted that fibres with higher intra-fibre diameter variability (PAN-2 and PAN-3, as highlighted in Table 3-2) experienced poor Weibull curve fitting due to high strength scattering. Hence, the minimum recommended number of test samples (20) was not statistically representative for these fibres and the number was increased until the coefficient of determination (R-squared) approached 0.95. Figure 3-3 shows the Weibull plot for PAN-3 fibres for the three sample sizes (N = 20, 30, 36) indicated in Table 3-4.

According to Table 3-4, the Weibull parameter varies significantly with sample size and more noticeably for the PAN-3 fibre, which exhibits higher intra-fibre diameter variability. The Weibull modulus decreased by almost 30% when the sample size increased from 20 to 30 for the PAN-3 fibre, compared with a 7% reduction for the PAN-2 fibre across the same range. The R-squared value also increased from 0.84 to 0.94 for the PAN-3 fibre, but a less significant change was observed in the PAN-2 fibre. The scattering of tensile strength data for these particular fibres can be attributed to the observed diametric variability, since surface irregularities and such variability are commonly considered to act as failure initiators [116], [121]. The Weibull parameters were therefore determined from a statistically representative sample size with an R-squared value of ~ 0.95 for these fibres.

Table 3-4: Effect of sample size on Weibull parameters for fibres with geometrical irregularity.

Fibre type	No. of samples, N	Weibull plot parameters		
		m	σ_0	R^2
PAN-2	20	5.89	5986.48	0.9007
	30	5.50	6491.61	0.9151
	38	5.43	6515.95	0.9487
PAN-3	20	9.85	5688.71	0.8363
	30	6.96	5775.57	0.9438
	36	5.71	5752.62	0.9553

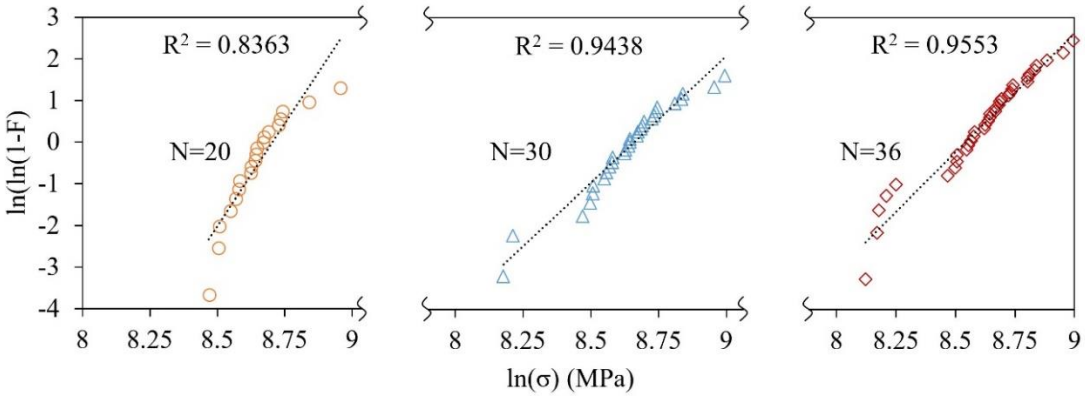

Figure 3-3: Effect of sample size on the Weibull parameters of PAN-3 fibre.

3.4.3 Weibull analysis

The Weibull parameters estimated from a linear regression of the Weibull plot and a MLE for each fibre are presented in Table 3-5 for comparison. In general, both the Weibull modulus and the characteristic stress from the MLE are higher than those from the Weibull plot, except for the Weibull modulus for the PAN-2 fibre derived from the MLE, which exhibits the opposite trend. In the most extreme cases for the PAN-2 and

Pitch-1 fibres, the discrepancy between the Weibull modulus estimates from the two approaches was as high as 19% and 17% respectively. However, for all fibres, both the characteristic and mean tensile strength estimates exhibited discrepancies of less than 6% between the two approaches.

As expected, the Weibull modulus of the PAN-1 fibre was found to be lower than that of the higher-performance PAN-2 fibre, suggesting the presence of a greater flaw population in the PAN-1 fibre for the same gauge length, which equates to a greater strength reduction for an increasing filament length. Moreover, the PAN-3 fibre showed the highest Weibull modulus indicating less scattering of the tensile strength and a smaller defect population among the tested PAN-based fibres. The lowest mean tensile strength of PAN-based fibres was observed for the PAN-1 fibre, rather than the PAN-3 fibre as expected, as shown in Table 3-1. This is potentially the result of using different test standards (single filament as opposed to infused bundle testing). As noted in previous literature [109], bundle testing can introduce inaccuracies stemming from anomalies caused during sample preparation, or irregular surface features on the fibres.

For the pitch-based fibres, the Pitch-1 Weibull modulus was lower than that of the higher-modulus Pitch-2 fibres, with the Pitch-2 fibres exhibiting less scatter in the tensile strength values. Whilst the tensile strength of these two pitch-based fibres were reported to be 3200 MPa on the manufacturer's data sheet, the mean tensile strength of the Pitch-2 fibre was seen to be 7% higher here. The results in Table 3-5 do not indicate any clear trend between Weibull modulus and tensile strength, although past literature has reported both increases [110] and decreases [78], [111] in Weibull modulus with increasing tensile modulus and strength.

Table 3-5: Comparison of Weibull parameters from conventional Weibull plot and MLE.

Fibre type	***Weibull plot***			***Maximum likelihood (MLE)***		
	m (GPa)	σ_0 (MPa)	$\bar{\sigma}$ (MPa)	m (GPa)	σ_0 (MPa)	$\bar{\sigma}$ (MPa)
PAN-1	3.11	5911.25	5287.26	3.23	6271.12	5619.58
PAN-2	5.43	6515.95	6011.15	4.55	6910.09	6310.01
PAN-3	5.71	5752.62	5322.08	5.73	6092.28	5637.33
Pitch-1	4.55	3921.47	3580.93	5.03	4132.99	3795.94
Pitch-2	5.58	4155.85	3839.83	6.68	4357.12	4065.89

3.5 Comparison against traditional SFT methods

In conventional single fibre tests, the use of paper tabs increases the chance of fibre misalignment and pre-tensioning prior to testing. This can lead to inaccuracies in the reporting of gauge length, failure strain, and elastic modulus results. Pre-tensioned filaments will result in a higher gauge length, lower failure strain, and higher modulus, while misaligned/bent filaments will result in the opposite. Inaccuracies in the axial alignment of fibre ends between the upper and lower jaws of the tensile testing machine will also introduce non-axial stretching of the fibre [113]. Furthermore, due to the practical difficulty of measuring the filament diameter for each individual fibre, traditional SFT methods commonly rely on the mean diameter of *N* samples from a separate batch of fibres for tensile strength calculations. This can introduce errors compared with methods that measure the diameter of each individual fibre being tested.

3.5.1 Calibration and error in Weibull analysis

The possibility of fibre pre-tension using an automated SFT method is low, as fibres are mounted on a standard plastic cassette, but fibre misalignment can occur depending on the gauge length and the method for sample preparation. Figure 3-4 shows a typical SFT load versus extension curve, using a straight-line fit for the modulus calculation after gauge length and strain corrections have been made. As can be seen from Table 3-6, there is a noticeable discrepancy between the intended gauge length, 4mm, and the corrected values. A maximum gauge length correction of 7% was observed in the PAN-2 and PAN-3 fibres and a correction of approximately 6% was observed in the PAN-1, Pitch-1 and Pitch-2 fibres.

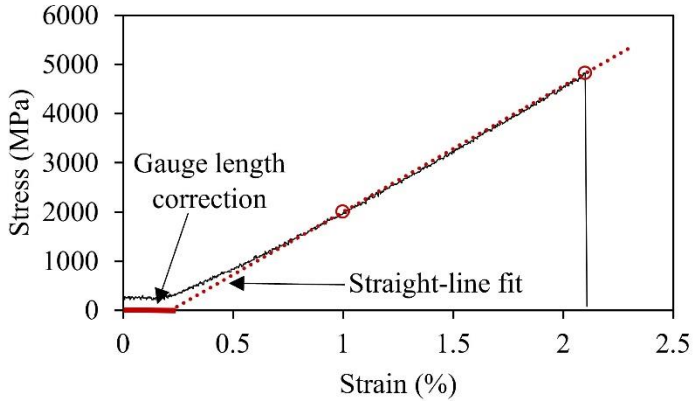

Figure 3-4: Typical gauge length correction due to de-crimping misaligned fibres.

In the current study the automated SFT facility was used to determine the diameter of each individual filament, to investigate the sensitivity of the uniaxial tensile strength to the diameter measurement, rather than using an average filament diameter taken across a batch of fibres. The individual filament diameter was calculated as the mean of the intra-fibre diameter measurements.

Table 3-6 shows the comparison of Weibull parameters obtained from the two approaches used to measure the filament diameter, along with the coefficient of

variation for the fibre area measurement and the tensile strength of the tested samples. The Weibull plots of tensile strength data from the individual and mean area approaches are also shown in Figure 3-5. In general, the use of individual or mean diameter values does not have a significant effect on the mean or characteristic stress predictions, with less than 3% deviation between the two approaches. However, the averaging of fibre diameter values can have a significant effect on the Weibull modulus calculations as these are more sensitive to the scatter of the data (reflected by the slope of the linear trends in Figure 3-5). For the PAN-based fibres, there is a larger discrepancy between the Weibull parameters determined from the mean and individual area methods for fibres with higher Weibull modulus (i.e., exhibiting lower strength scattering and higher inter-fibre diameter variability). The PAN-1 fibre for example, with the lowest Weibull modulus and lowest diameter variability, showed very consistent results between the two Weibull parameter predictions.

Table 3-6: Comparison of Weibull parameters from mean and individual area approaches.

Fibre type	Actual Gauge length (mm)	Individual area		Mean area		Difference		CV_A (%)	CV_σ (%)
		m	σ_0	m	σ_0	m	σ_0		
PAN-1	4.23	3.11	5911.25	3.11	5898.96	0%	0%	7%	36%
PAN-2	4.27	5.43	6515.95	6.38	6367.64	-18%	2%	13%	22%
PAN-3	4.27	5.71	5752.62	7.10	5588.20	-24%	3%	14%	20%
Pitch-1	4.24	4.55	3921.47	3.69	3960.73	19%	-1%	19%	24%
Pitch-2	4.22	5.58	4155.85	5.15	4140.36	8%	0%	16%	19%

However, the fibres with higher surface irregularities and sample size sensitivity, for example the PAN-3 and PAN-2 fibres, showed the highest deviation in Weibull modulus, 24% and 18% respectively. The pitch-based Pitch-1 and Pitch-2 fibres also showed a reduction in Weibull modulus between the two approaches studied.

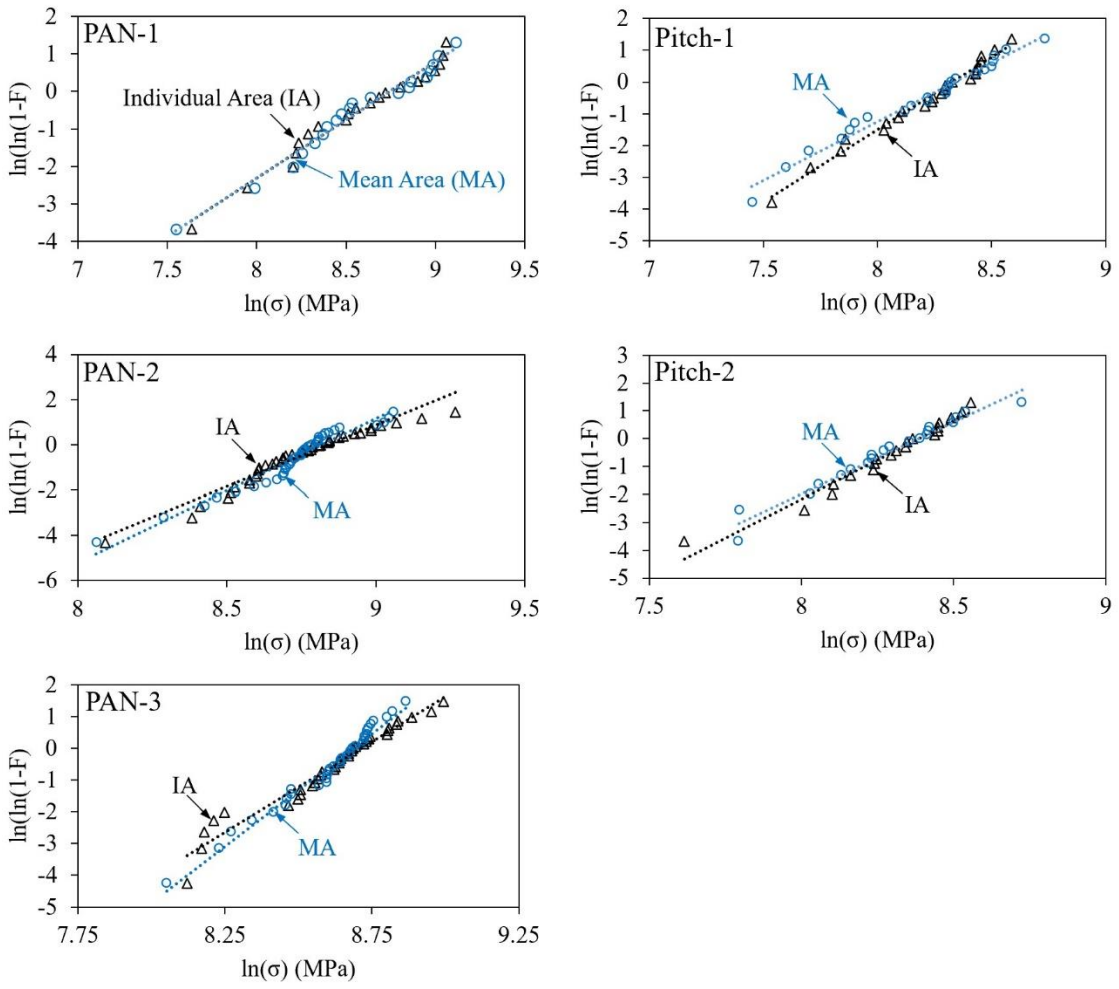

Figure 3-5: Weibull plots of tensile strength data from individual and mean area approaches.

3.6 Influence of fibre length on tensile strength

Tensile strength variation for brittle fibres, such as carbon fibre, is known to be as high as 30% [103], which is in-line with the scatter observed for discontinuous fibre composites [58], [122]. Fibre strength variability increases with increasing fibre length due to the presence of more critical flaws. Single fibre tests also showed that the

Weibull modulus decreases with increasing gauge length for both PAN- and pitch-based fibres [110]. The resulting reduction in mean tensile strength due to a higher defect population is, therefore, higher in fibres with lower Weibull modulus. Figure 3-6 shows the prediction for the mean tensile strength at longer gauge lengths, adopting the two-parameter Weibull model and the individual cross-sectional area measurements used in the current study. Fibres with the lowest Weibull modulus (PAN-1) exhibited a 26% reduction in mean tensile strength as the gauge length increased from 5 mm to 10mm, while the PAN-3 fibre showed a 15% reduction over the same range.

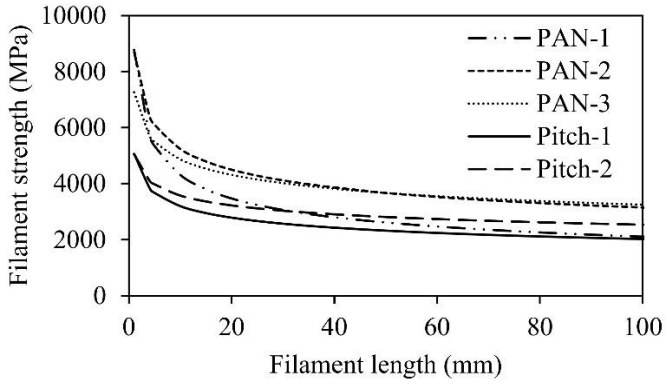

Figure 3-6: Filament strength as a function of filament length.

3.7 Chapter conclusions

In this chapter an automated single fibre testing process has been employed to characterize the tensile strength of high strength PAN-based, high modulus pitch-based and ultra-high modulus pitch-based carbon fibres. In general, high strength and high modulus fibres (PAN-2, PAN-3 and Pitch-2), regardless of precursor material, showed higher Weibull modulus values (implying a lower flaw population) relative to the lower performance PAN-1 and Pitch-1 fibres. It was also found that surface irregularities could result in uncertainties in tensile strength characterization and therefore a greater number of samples is required to yield a reliable representative strength value. Fibre

misalignment and the use of the mean cross-sectional area for determining the tensile strength were also observed to affect the Weibull parameters, resulting in corrections of up to 7% and 24% in the gauge length and Weibull modulus respectively. Hence care should be taken during the characterization of fibres with high surface irregularities, particularly during the calibration of the gauge length and the measurement of the fibre diameter. As defect population, thus fibre strength, is a function of filament length, it is crucial to link the size effect in the fibre to composite performance.

Chapter 4. Extending fibre properties to composite properties

4.1 Introduction

Carbon fibre SMCs are typically manufactured using industrial grade fibres, with fibre stiffnesses reported to be ~240 GPa and ultimate strengths of ~4900 MPa [123], [124] , yielding composite stiffnesses of approximately 35 GPa and strengths of <300 MPa at 50% fibre volume fraction [40], [48], [125]. There is little-to-no data in the literature to suggest that high modulus or even ultrahigh modulus fibres have been used in this context before, but they could potentially offer an increase in mechanical properties for higher performance applications. In spite of this potential, for the case of continuous fibre composites, high performance fibres have not been able to achieve their theoretical performances in practice due to their smooth and extremely inert surface, caused by highly aligned crystallites [112], [126], [127]. Alternative solutions of employing low surface energy resin matrices and liquid multi-walled carbon nanotubes (MWCNTs) have been suggested to improve the interfacial adhesion, and the subsequent composite performance, by improving the wettability and chemical bonding [94], [126]. However, there is also a concern that these high performance fibres may not achieve their supposed tensile properties in practice due to increased scatter and reduction at longer reinforcement lengths [110] and restricted stress transfer between the high modulus fibres and the low modulus matrix [128].

The fibre tensile strength reduction due to Weibull effect plateaus beyond certain fibre length, as illustrated in the Chapter 3. Thus, translating its effect on composite performance is more relevant and important in discontinuous fibre composites with shorter fibre length than continuous. Analytical models based on Kelly-Tyson slip theory are commonly used to study the effects of constituent materials, reinforcement

aspect ratio and other parameters on the performance of short fibre composite. The method has also been extended for multi-scale modelling of tow based discontinuous fibre composites by considering bundle of filaments as single, large diameter fibre. Different approaches have been used to compute the equivalent single fibre geometry to represent the fibre bundle and calculate and critical bundle length [38], [129]. Simplified assumptions of using tow width or circular cross section [129], [130] and more realistic, elliptical cross section have been proposed to compute the embedded tow surface area and critical bundle length. Moreover, Harper [37] used micrograph images to establish a tow cross sectional geometry to calculate tow critical length and subsequent study of Weibull effect on fibre length vs. strength relationship.

In this chapter multi-scale analytical model has been used to superimpose the stochastic fibre scale size effect and fibre bundle length/aspect ratio to study the effects on bundle and composite strength of the fibres studied in Chapter 3. Tow based discontinuous carbon fibre composites have also been manufactured from the three high performance PAN-based carbon fibres in vinyl ester resin to evaluate the achievable practical composite properties. Experimentally obtained tensile properties were then evaluated against the analytical predictions.

4.2 Analytical prediction of composite properties

4.2.1 Tensile stiffness

Most analytical stiffness models assumptions of randomly oriented discontinuous fibre composites are based on simple micromechanical unit cell model and averaging properties over all possible orientations. Cox [66] model, for instance, assumed papers as perfectly homogeneous mat of long straight thin fibres without resin material and

performed orientation averaging for elastic property predictions. Although it is not considered to be accurate enough as it does not consider the matrix contribution it is widely used for its simplicity, given in Eq. 4.1.

$$\tilde{E} = \frac{E_f v_f}{3}, \qquad \text{Eq. (4.1)}$$

Alternatively rule of mixture models with length efficiency and orientation factors have been used to account for the discontinuous nature of the fibre tows and their orientation state in the composite respectively, applied at meso- and macro-scales. The composite properties are thus calculated from tow level properties:

$$E_C = \eta_o V_f E_{tow} + E_m(1 - V_f) \qquad \text{Eq. (4.2)}$$

The widely used orientation efficiency factor is derived by Krenchel [131] where fibres are grouped, and weighted summation is performed accounting for proportion of fibres in a group and its orientation angle. For any given orientation density function efficiency factor η_o can thus be determined integrating over all possible orientations with their proportions. For perfectly random in-plane fibre orientation distribution η_o is equal to 0.375. Incorporating these orientation distribution factor with the rule of mixture can also be applied to partially oriented fibre distribution short fibre composites.

$$\eta_o = \sum_{n=1}^{\infty} a_n Cos^4\, \theta_n \qquad \text{Eq. (4.3)}$$

Where $a_n -$ Proportion of fibres

$\theta_n -$ Inclination angle of fibres

The tow properties can be calculated assuming each fibre tow is a large single cylinder embedded in a matrix material of assumed fibre volume fraction in the tow (usually

60%). Therefore, an adjusted volume fraction is used in macro-level using the relationship:

$$V_f = \frac{V_{f_{tow}}}{V_{f_{composite}}}, \quad \text{Eq. (4.4)}$$

Shear lag analysis is then used to compute the stiffness of the tows in the composite considering the fibre length efficiency factor and aspect ratio.

$$E_{tow} = V_f E_f \left(1 - \frac{\tanh(\varphi s)}{\varphi s}\right) + E_m(1 - V_f) \quad \text{Eq. (4.5)}$$

Where

$$\varphi = \sqrt{\frac{2E_m}{E_f(1 - v_m) ln \frac{1}{V_f}}}$$

The tow aspect ratio, S, can be calculated from the fibre length and equivalent tow diameter with the assumed fibre volume fraction (V_{tow}) and filament count (n):

$$S = \frac{l}{d_{tow}}, \quad \text{Eq. (4.6)}$$

Where $d_{tow} = d_f \sqrt{\frac{n}{V_{tow}}}$

4.2.2 Tensile strength

Strength prediction of discontinuous fibre composite is much more complicated than stiffness as it is significantly dependent on microstructural details and interaction between fibres or fibre tows. However, simplified approximation has been made using multi-level rule of mixture, with similar assumptions made in the above section. The longitudinal tensile strength the fibre tows is to be computed using rule of mixture

modified to include length efficiency factor of short discontinuous fibres as the resin carries the load and transfer through fibre-matrix interfacial shear stress. Hence Kelly-Tyson [65] shear lag model with plastic stress transfer has been employed to determine the longitudinal tensile strength of a tow bundle as given using a piece-wise function that is a function of critical length inequality:

$$\sigma_{tow}(l) = V_{tow}\frac{\tau l}{d} + \sigma'_m(1 - V_{tow}) \quad \text{for } l < l_{C_{filament}} \quad \text{Eq. (4.7a)}$$

$$\sigma_{tow}(l) = V_{tow}\sigma_f(l)\left(1 - \frac{l_{C_{filament}}}{2l}\right) + \sigma'_m(1 - V_{tow}) \quad \text{for } l \geq l_{C_{filament}} \quad \text{Eq. (4.7b)}$$

Where the critical filament length, $l_{C_{filament}}$, can be computed using:

$$l_{C_{filament}} = \frac{\sigma_f(l)d}{2\tau},$$

The composite strength can thus be computed from tow level properties considering the level of fibre alignment using the orientation and length efficiency factors [132]:

$$\sigma_{comp}(l) = \eta_o V_{comp}\frac{\tau l}{d} + \sigma'_m(1 - V_{comp}) \quad \text{for } l < l_{C_{tow}} \quad \text{Eq. (4.8a)}$$

$$\sigma_{comp}(l) = \eta_o V_{comp}\sigma_{tow}(l)\left(1 - \frac{l_{C_{tow}}}{2l}\right) + \sigma'_m(1 - V_{comp}) \quad \text{for } l \geq l_{C_{tow}} \quad \text{Eq. (4.8b)}$$

Where $l_{C_{tow}}$ calculated from the relationship between the interfacial shear force acting on the interface of an embedded tow and the ultimate tensile force acting on the tow, giving:

$$l_{C_{tow}} = \frac{2\sigma^*_{tow} A_{tow}}{\tau_i P_{tow}}, \tag{4.9}$$

Where

$$A_{tow} = \frac{\pi {\phi_f}^2 n}{4V_{tow}}, and \;\; P_{tow} = \pi d \sqrt{\frac{n}{V_{tow}}}$$

4.3 Materials and methods

The discontinuous fibre composites were manufactured from the three different PAN-based high performance commercial carbon fibres, i.e., PAN-1, PAN-2, and PAN-3 fibres and MgO thickenable vinyl ester (supplied by INEOS Composites). The physical properties of these fibre materials are given in Section 3.2. Although the effects of fibre diameter and tow size could not be isolated simultaneously due to the nature of these commercial fibres, tow count (12k) and fibre length (25mm) were kept constants for all three composites manufactured. The SMC charges were prepared using a fibre chopper mounted on a six-axis industrial robot, used in similar studies[28], [30], [37], that chop and randomly disperse fibre tows on a resin paste. The number of alternating layers of fibre tows and resin paste, fibre feed rate, and deposition speed were adjusted accordingly to result a flat plaque of 400x400x4 mm at a nominal fibre volume fraction of 30%. The charge was then thermally B-staged at 50 °C for 1 hour before curing in the mould.

4.4 Characterisation

4.4.1 Resin viscosity and cure kinetics

The viscosity of the resin during preforming stage is critical for the infiltration of carbon fibre tows than it would for a typical glass fibre SMCs due to smaller fibre

diameter resulting in denser fibre packing. The resin used in this study comprises four-part mix, i.e., 1.5 wt.% tert-butylperoxybenzoate hardener, 2 wt.% MgO thickening agent, 4 wt.% zinc stearate (ZnST) in-mix release agent and 100 wt.% derakane 782 vinyl ester resin. The mix viscosity was characterised using rotational rheometer (Kinexus, NETZSCH) at a shear rate range appropriate for the free-falling fibre tows on a resin paste. The measured viscosity, shown in Figure 4-1, was observed to be significantly higher than typically required for carbon fibre SMC preforming [30], [133], [134]. Hence, the powdered release agent was replaced with on mould release agent in an effort to reduce the mix viscosity. Although, significant gain was achieved, the steady viscosity of 5 Pa·s is still a concern to properly infiltrate the tows. Hence, an intermediate cold pressing step was introduced for 5 minutes at 10 MPa pressure to improve the infiltration.

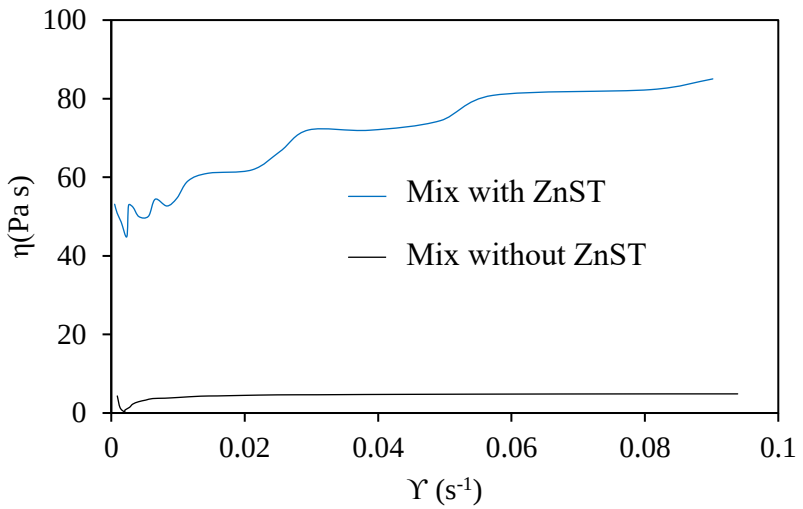

Figure 4-1: Measured viscosity of the resin with and without the (ZnST) release agent.

Moreover, the cure kinetics of the resin have also been characterised using Differential Scanning Calorimetry (DSC) with isothermal temperature scans (Q20 TA

instruments). The curing process under isothermal heating was evaluated for a temperature range of 130 – 150°C at 10°C steps. The exothermic curing process, shown in Figure 4-2, was completed in less than 3 minutes for all cases considered. As curing process can be influenced by non-uniform heating of the mould and composite part thickness, the manufactured SMC plaques were moulded at a temperature of 150°C and 10 MPa pressure for a minimum of 5 minutes to ensure complete curing.

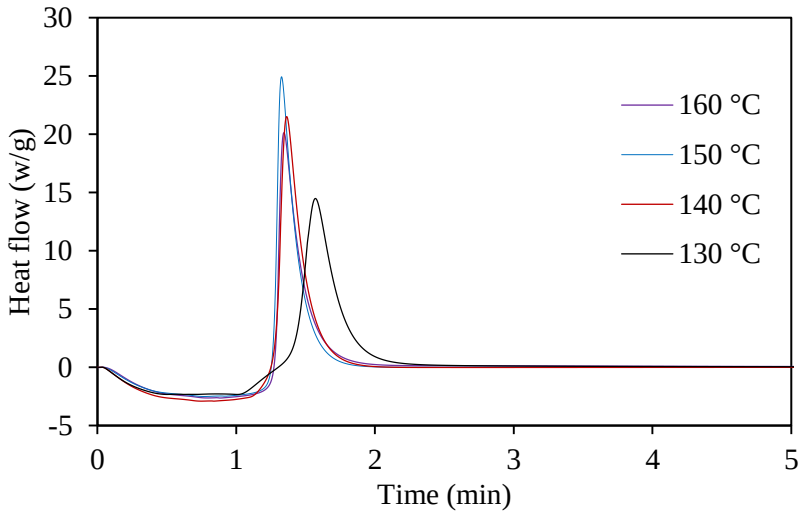

Figure 4-2: Isothermal DSC scan of the vinyl ester resin cured at different temperatures.

4.4.2 Composite quality

To evaluate the quality of the manufactured composites, optical microscopy samples were taken from similar locations of each of the composites manufactured from the three different fibres. In general, all samples showed relatively higher extent of defect in the form of voids, shrinkage cracks, resin rich areas, and out-of-plane fibre swirling, as a result of charge flow and inhomogeneous fibre distribution as can be seen from Figure 4-3. This might have resulted from poor fibre impregnation due to high resin

viscosity coupled with small fibre diameter, especially in the PAN-2 and PAN-3 fibre composites. Thus, large voids and shrinkage cracks can be seen in resin rich areas.

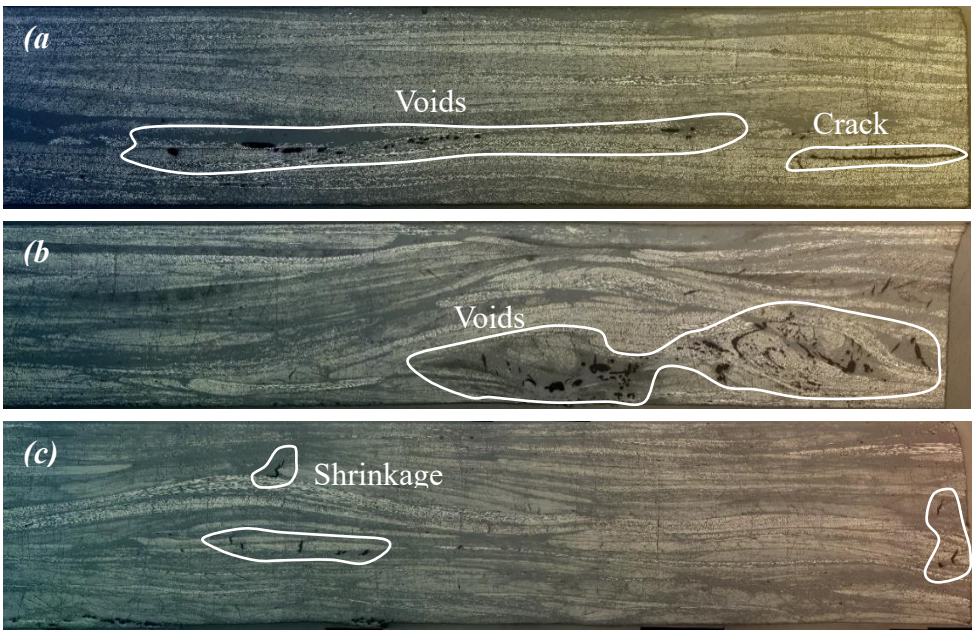

Figure 4-3: Optical microscopy characterization of composite quality of samples taken from composites of the PAN-1 (a), PAN-2 (b), and PAN-3 (c) fibres.

4.4.3 Tensile testing

To evaluate the mechanical performance of the SMC composites manufactured from the different fibres, tensile tests were performed according to ISO 527-4 testing standard, using samples taken from two orthogonal directions of the same plaques, as shown in Figure 4-4. Tensile coupons of 200 x 25 mm, with a gauge length of 100 mm, were tested under a uniaxial extension of 2 mm/min for all sample groups. An extensometer of 50 mm gauge length was used to measure applied strain up to failure.

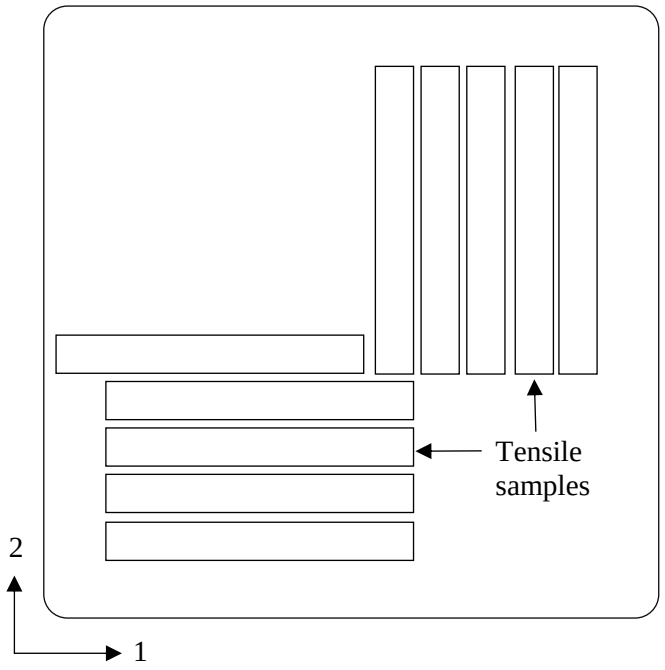

Figure 4-4: Tensile test coupons cutting plan, (all panels are 400 x 400 mm)

4.5 Results

4.5.1 Tensile stiffness

Figure 4-5 shows the composite modulus from the test and analytical prediction as function of fibre modulus. As can be expected naturally, increasing composite modulus for an increasing fibre modulus was observed from both the prediction and test results. The multi-level rule of mixture-based prediction showed a closer estimation to the test result as it accounts microstructural parameters in the estimation. Compared with the analytical prediction using the multi-level rule of mixture model, the PAN-1 fibre composite showed a very close agreement with the prediction while the PAN-2 and PAN-3 fibre composites showed 7% and 15% deviations respectively. Thus, greater deviation from prediction was observed with increasing fibre modulus. As a result, only about 50% improvement in the modulus was attained when the fibre modulus increased by more than 85% between PAN-1 (230 GPa) and PAN-3 (290 GPa) fibre composites.

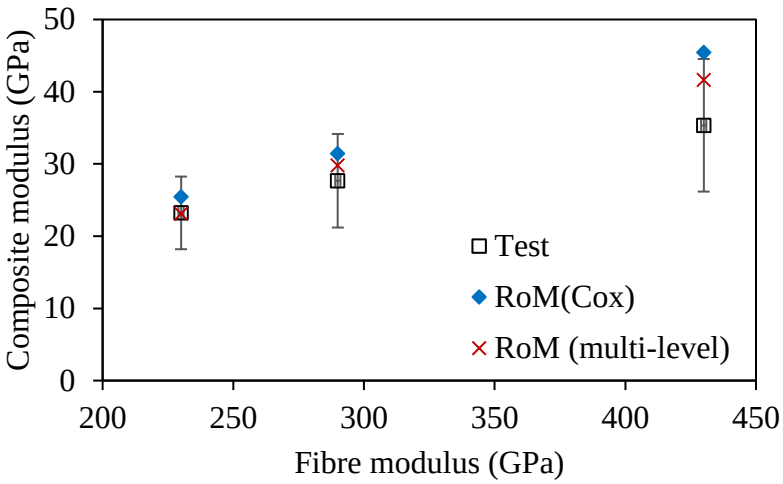

Figure 4-5: Discontinuous carbon fibre composite modulus as a function of fibre modulus.

4.5.2 Tensile strength

First, the length dependency of tow tensile strength has been estimated superimposing the effect of filament length on the fibre tensile strength demonstrated in Section 3.6 with Eq.4.7. The tow strength as a function of fibre length is given in Figure 4-6 for the five fibre fibres studied in Chapter 3. All five fibres attained a peak tow strength between 1.5 mm and 2 mm, beyond which a reduction in strength was observed due to the associated Weibull effect at fibre level. Hence, the PAN-1 fibre with the lowest Weibull modulus showed a greater decline in tow longitudinal tensile strength with increasing fibre length while the Pitch-2 with the highest Weibull modulus showed the lowest reduction.

Then the strength of tow-based discontinuous fibre composites as a function of fibre length has been estimated using equation 4.8, assuming the same tow count of 12k for all fibre types. The predicted composite strength for the fibre fibres studied is shown in Figure 4-7. The peak in composite strength has been observed at different fibre length

for the different fibre types before declining or reaching a plateau. This is due to the dependency of critical tow length given in Eq. 4.9 on the fibre strength and fibre diameter (given the same tow count and tow volume fraction for all fibre types). Thus, the PAN-1 fibre with relatively smaller fibre diameter and lower Weibull modulus reached a strength plateau at a fibre length of 50mm while the Pitch-2 fibre with larger diameter and Weibull modulus plateaued at 120 mm.

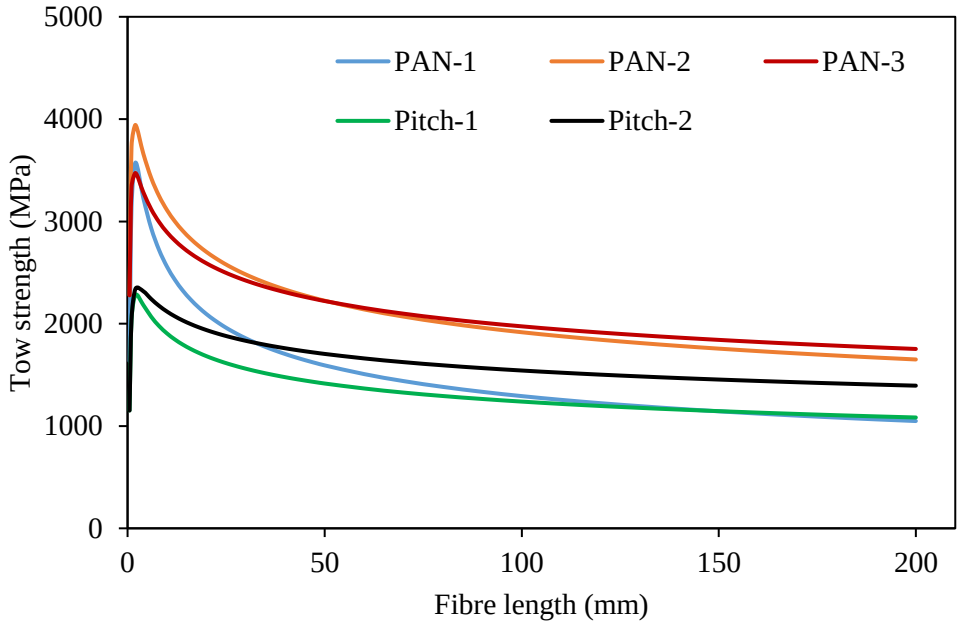

Figure 4-6: Tow longitudinal tensile strength dependency on fibre length for the five different fibres in vinyl ester resin (assumed: tow volume fraction – 60%, matrix strength – 65 MPa, matrix modulus 3.5 GPa).

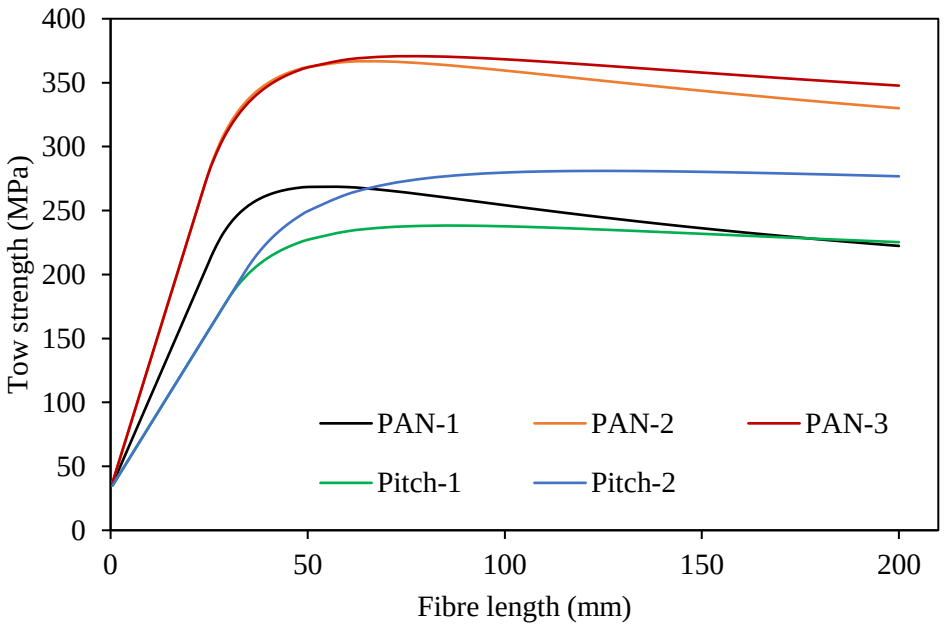

Figure 4-7: Composite tensile strength as a function of fibre length for the five different fibres in vinyl ester resin (assumed: composite volume fraction – 30%).

In Figure 4-8 the composite strength is shown for the three different fibre types tested as a function of fibre strength at 25 mm fibre length. Initially, increasing trend, i.e., 85% improvement in composite strength for 16% increase in fibre strength was observed from test results. However, for subsequent 12% increase in fibre strength, a 21% decline in composite strength has been shown between Pan-1 and PAN-2 fibres. Compared with the analytical estimation, the standard modulus and strength fibre, PAN-1, showed a 31% lower strength. However, the high strength (PAN-2) and high modulus (PAN-3) fibres showed a significant deviation of 60% and 72% respectively. One reason for relatively lower composite strength from PAN-2 and PAN-3 could be due to subpar composite quality as a result of poor resin impregnation from high viscosity resin and smaller fibre diameter. This is supported in part by the microscopic characterization in the previous section and related study [28]. Furthermore, surface morphology characterisation of these fibres from Chapter 3 showed that the PAN-3 and PAN-2 fibres showed high geometric irregularity while the PAN-1 fibre exhibited near

round smooth surface. Extremely inert surface in high performance fibres has been also illustrated to be the challenge to achieve the expected performance as it results in poor wettability and interfacial adhesion [94], [126].

Furthermore, it has been reported in the previous literature that in short fibre composites, stress concentration factor in the matrix increases rapidly with increasing fibre to matrix modulus ratio [128], [135]. This stress concentration near the fibre end act as failure initiation site causing premature failure. For instance, the finite element analysis result showed that the matrix stress concentration factor reached 20 when the fibre to matrix modulus ratio increased to 200 [128]. Accordingly, the least composite strength was observed in the high modulus PAN-3 fibre with a modulus ratio of 125 while the intermediate modulus PAN-1 fibre with a modulus ratio of 67 showed the highest composite strength.

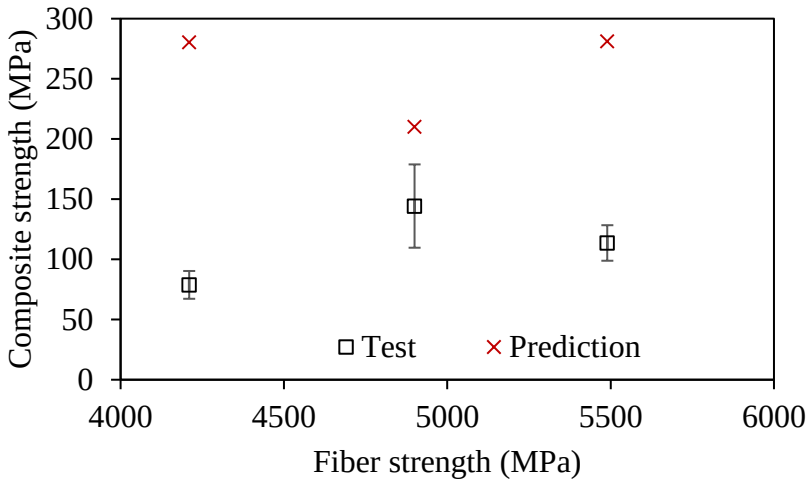

Figure 4-8: Composite strength from test result and analytical prediction as a function of fibre strength.

4.6 Chapter conclusions and future work

In this Chapter, the achievable improvement in mechanical performance of discontinuous carbon fibre composites using high performance fibres of different grades has been investigated. Although there has been a discrepancy between the analytically predicted values and experimentally obtained ones, increasing trend in composite modulus for increasing fibre modulus was observed. However, regarding the composite strength, it was observed that composites with higher fibre/matrix modulus ratio showed lower composite strength than expected. This might be due to a rapid increase in both interfacial and fibre stress concentration as fibre to matrix modulus ratio increases which act as failure initiation site, as supported by shear-lag based stress analysis in the related literatures. Furthermore, poor resin impregnation of fibre tows with smaller fibre diameter due to high resin viscosity compromised the composite quality, which may have limited the achievable composite strength.

Hence, future extension of the work focuses on employing directed fibre compounding (DFC) process with low viscosity resin for improved homogeneity and impregnation, thus, improved composite quality. Future works also consider characterisation of the fibre-matrix interface behaviour of these high-performance fibres with high geometric irregularity and devise composite performance improvement strategies.

Chapter 5. Hybridization with natural fibre

5.1 Introduction

Although the market penetration of carbon fibre reinforced SMCs has been initially driven by a desire for greater fuel efficiency and stringent environmental policies globally, there is a growing concern regarding their source and poor recyclability [136]. Furthermore, the high cost of carbon fibres is also another challenge for their wider adoption, that often limits their use to concept, high-performance, and luxury cars [137]. On the other hand, bio-based composites offer number of advantages including low cost and low density with acceptable specific stiffness and strength [81], with up to 30% weight and 20% cost reduction in vehicles when replacing steel-based designs [138]–[140]. Natural fibre composites have already seen some success for Mercedes-Benz, Ford, Toyota, and General Motors [140], [141] for the use in door and floor panels, seat backs, dashboards, sound proofing, and other interior parts. Despite their attractive benefits, issues with moisture absorption, fire retardancy [142], [143], and fibre-matrix adhesion [144] are the main inhibitors of natural fibre utilization. A wide range of studies have been performed in these areas through surface modification of the fibres [88], [145]–[148], or additives [149], [150], resulting in complicated interactions that can improve the mechanical performance. For the most part, the relatively low mechanical performance of natural fibres has also been limiting their application to non-structural applications [151]. Hence, hybridization of carbon and natural fibres is an effective way to balance cost, performance, and environmental concerns with wide range of mechanical properties by selectively controlling the hybridization parameters.

Hybridization of synthetic-synthetic, synthetic-natural and natural-natural fibres have been used as a means to enhance the mechanical and hygrothermal performance,

‘pseudo ductility’, and density [81], [86], [152]–[154] of composites. The effects of composition, configuration, fibre surface treatment, and fibre orientation have been investigated in previous studies to varying degrees. A work by Akil et al. [155], for instance, showed that the degradation of mechanical properties in jute fibre composites due to moisture absorption can be significantly reduced by the addition of glass fibre [155]. Furthermore, the moisture absorption behaviour in these hybrid composites was also seen to be dependent on the stacking sequence, with the best performance observed when the glass fibre is used as a barrier layer. The damping performance of synthetic fibre reinforced composites can also be improved by hybridisation with natural fibres, depending on the stacking sequence. Several studies have reported that adding natural fibre external layers onto glass and carbon fibre laminates can significantly improve their damping performance [156]–[158]. Assarar et al. [156] observed that for flax-carbon hybrids with exterior flax layers the damping performance increased with increasing flax fibre content. Fairlie and Njuguna [157] also reported that adding two external flax fibre layers improved the damping performance of carbon fibre composites by 94%.

These past works regarding the performance of synthetic-natural fibre hybrid composites have primarily focussed on conventional laminates with slow production times and intermediate processes that are not viable for high production volumes in the automotive industry. Therefore, the study in this chapter aims to investigate the performance of carbon-jute fibre reinforced hybrid SMC composites, as a novel investigation of high-performance and more ecofriendly hybrid materials for high-volume automotive applications. The tensile, flexural, and damping properties of the new hybrid composites are evaluated and compared against reference carbon and jute fibre SMCs, considering the effects of stacking sequence and hybridization ratio. The

weighted Cost Performance Ratios (CPRs) of the tested properties are also used as evaluation criteria for the value of such hybrid composites.

5.2 Materials and methods

The hybrid and non-hybrid SMC composites used in the current study have been prepared from T700SC carbon fibre and needle-punched non-woven jute fibre mat in Derakane 782 vinyl ester resin, at a nominal fibre volume fraction of 30%. Carbon fibre layers were prepared using the process outlined in Section 4.2 on a 250x250 mm area, then compacted under 10 MPa pressure to fill a volume of 400 x 400 x 1 mm at room temperature. The non-woven jute mats (needle-punched from approximately 50 mm length fibres with an average areal mass of 500 g/m^2) were cut to the mould size (400 x 400 mm) and sandwiched between two resin layers spread on a plastic film.

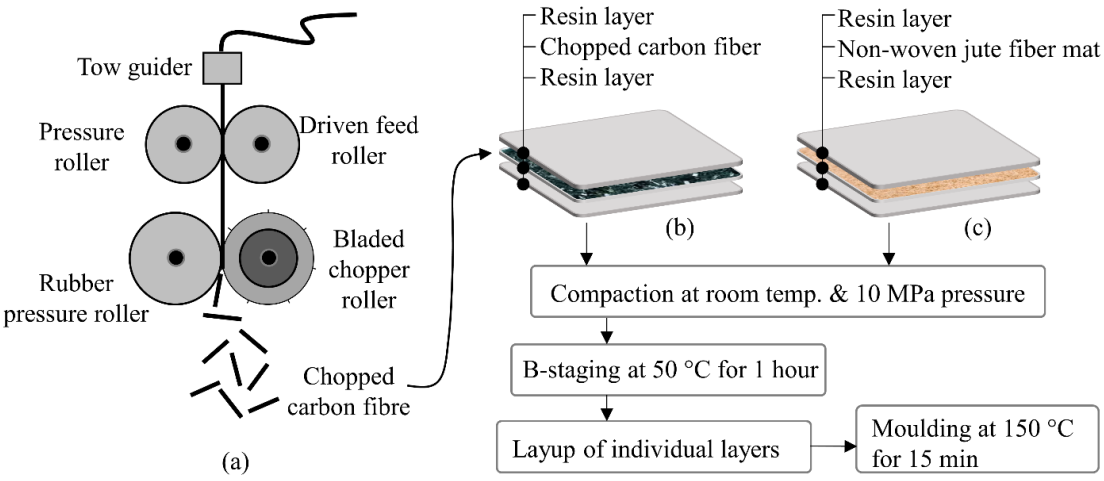

Figure 5-1：Schematic of chopped carbon fibre and non-woven jute mat preforming and moulding process; (a) deposition of chopped carbon fibre tow from chopper gun mounted on six-axis robot arm, (b) alternating layers of chopped carbon fibre and liquid resin and (c) non-woven jute fibre mat sandwiched between two resin layers.

To help through thickness resin infiltration, these charges were then compacted under 10 MPa pressure at room temperature for 5 minutes before B-staging. The final flat plaques of 400 x 400 x 4 mm were manufactured by stacking four of the B-staged layers together in a heated press mould. A schematic of the preforming and moulding process in shown in Figure 5-1.

Five different panels were prepared in order to evaluate the effect of hybridization configuration and ratio on the tensile, flexural, and damping performance of hybrid and non-hybrid SMCs. The layup of these SMCs and the hybridization ratio (volume of carbon fibre compared to the total volume of fibre, V_{CF}/V_{TF}) is shown in Figure 5-2 and Table 5-1.

Figure 5-2: Layup configuration of the various SMC panels.

Table 5-1: Configuration and hybridization ratio of panels used.

Configuration	$[J]_4$	$[JC]_S$	$[CJ]_S$	[CJC]*	$[C]_4$
Hybridization ratio	0	0.43	0.44	0.72	1.00
Density (g/cm^3)	1.22	1.27	1.27	1.30	1.33

* Prepared from two 1.5 mm carbon skin layers about a single jute later, with a total thickness of 4 mm.

Note: Subscripts 4 and S indicate the number of layers and symmetry in the layup respectively.

5.3 Characterizations

To evaluate the mechanical performance of the different composites, tensile and flexural tests were performed according to ISO 527-4 and ISO 178 respectively, using samples taken from two orthogonal directions of the same plaques. Tensile coupons of 200 x 25 mm, with a gauge length of 100 mm, according to the procedure outlined in Section 4.3.3. Samples for the three-point flexural test were cut to 80 x 10 mm and tested with a span of around 64 mm (16 times longer than the average sample thickness), at a loading rate of 12 mm/min. Damping characterization was performed according to ASTM E756–05 using an impact hammer test with cantilever beam configuration. Samples of size 205 x 10 mm were prepared, with a 25 x 10 mm region clamped at one end with the remaining 180 mm length free. The vibration was excited using a PCB-086C03 impact hammer in the out-of-plane direction and the free-decay time-domain signal was recorded from an accelerometer attached at the free end of the specimen. Micrographs were also taken from a similar location of each plaque for evaluation of manufacturing induced defects and homogeneity. Scanning Electron Microscope (SEM) was also used to characterise the fracture surface of composites after failure. Figure 5-3 shows the cutting plan used to prepare tensile, bending, damping, and microscopy samples. Figure 5-4 shows the sample size and configuration used for damping experiment.

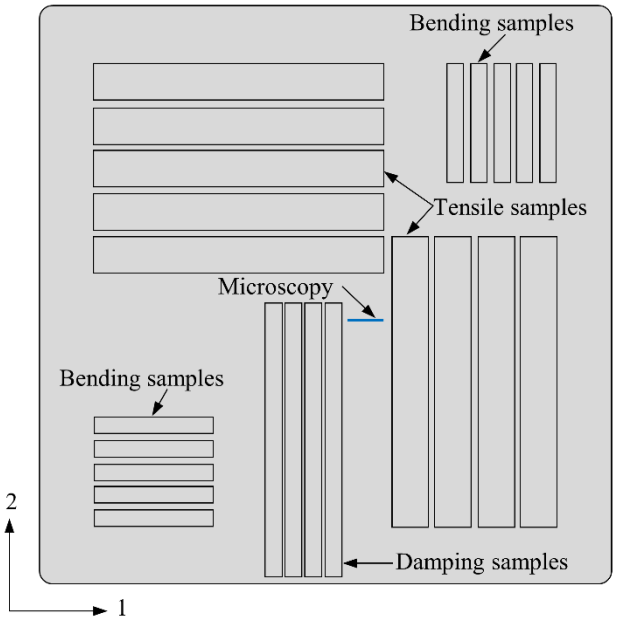

Figure 5-3: Tensile, flexural, and damping coupon cutting plan, and microscopy sample locations (all panels are 400 x 400 mm).

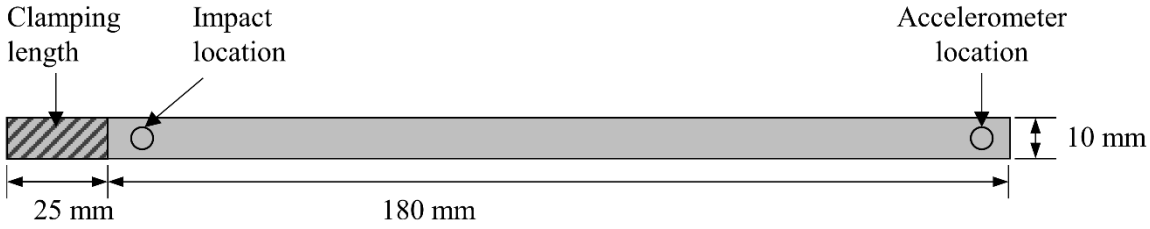

Figure 5-4: Experimental configuration of the damping test.

5.4 Result and discussion

5.4.1 Microscopy

Cross-sectional microscopy from four of the various SMC panels can be seen in Figure 5-5. From these images, the jute mat layers appear to produce a more random and uniform distribution of fibres with very few manufacturing defects. In both cases where carbon fibre layers were placed at the bottom of the mould (see Figure 5-5b and Figure 5-5c), there appear to be some voids; likely the result of entrapped air from the preforming stage. In both hybrid panels, the interface between the jute and carbon layers

is relatively irregular, due to local thickness variability in the jute fibre mat and the in-mound flow of the carbon fibre tows to accommodate the thickness variation.

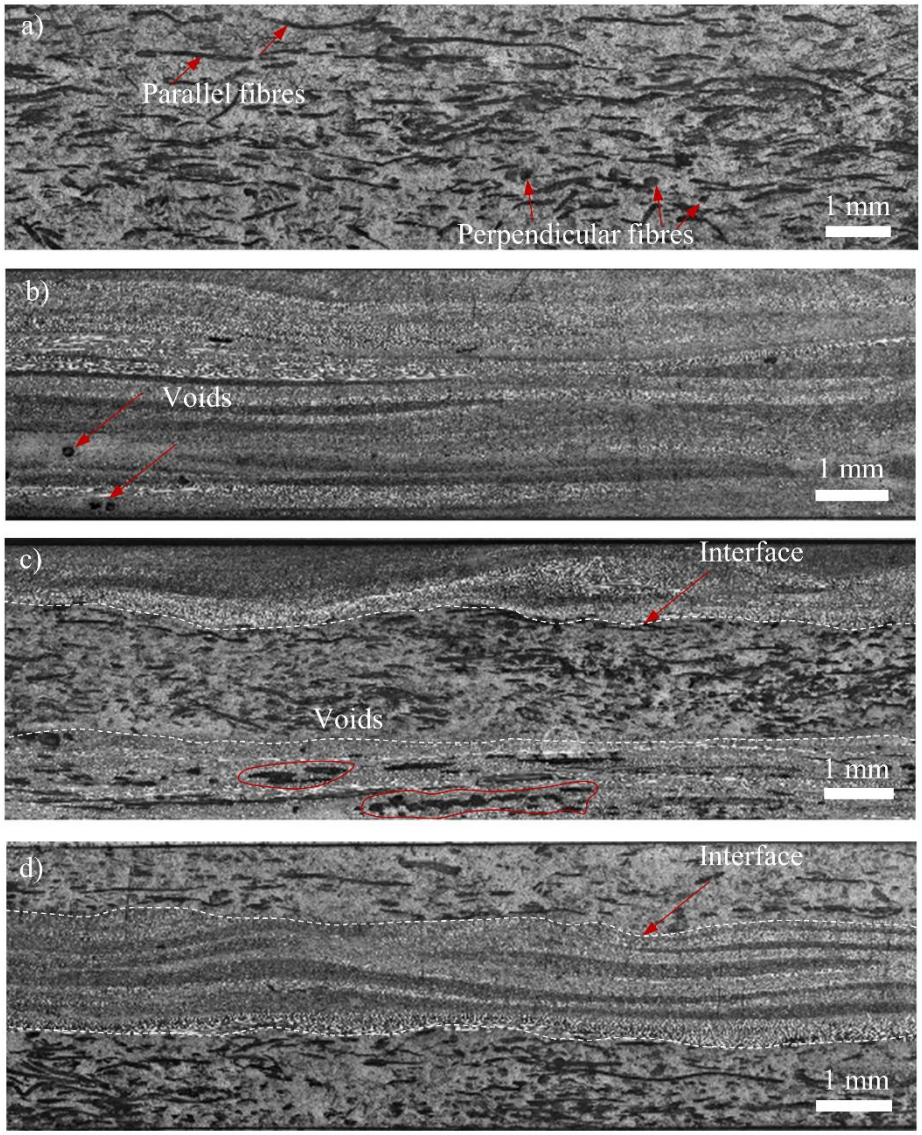

Figure 5-5: Micrographs showing the cross-section of samples: a) pure jute $[J]_4$, b) pure carbon $[C]_4$, c) carbon-skinned hybrid $[CJ]_S$ (also representative of the [CJC] hybrid), and d) jute-skinned hybrid $[JC]_S$ SMC composite panels.

5.4.2 Tensile properties

Figure 5-6 shows the tensile modulus and strength in each direction (1 and 2) for the hybrid and non-hybrid panels. A higher directional anisotropy in both tensile modulus

and strength (20% and 18% respectively) was observed in pure carbon samples, while the pure jute samples showed a lower anisotropy of 5% and 10% respectively. This high anisotropy in the pure carbon panels is due to a preferential alignment of the fibre tows as they were deposited from the chopping gun mounted on a moving robot arm. Moreover, greater variability was observed across the pure carbon samples, with relative standard deviations of 16% and 14% for modulus and strength respectively. Such material variability, as high as 20% [37], is a known issue for tow-based discontinuous carbon fibre composites. A narrower tow size [38], shorter fibre length [64], and induced filamentisation [74] can all be used to increase preform homogeneity and reduce material variability, but each require additional material costs or processing. On the other hand, the pure jute samples, based on the random mat reinforcement, showed greater consistency with relative standard deviations as low as 3% and 7% for modulus and strength respectively. The directional anisotropy and variability of the $[JC]_S$ and $[CJ]_S$ hybrid samples were evidently a compromise of the high-performance carbon and homogenous jute constituents.

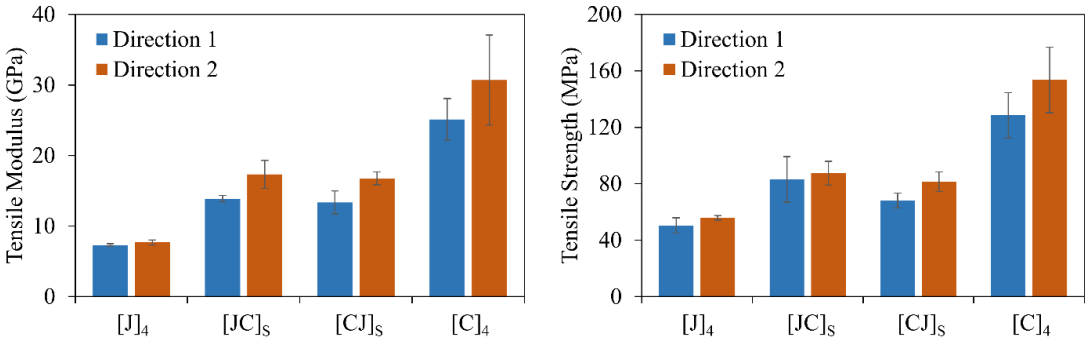

Figure 5-6: Tensile modulus and strength of different hybrid and non-hybrid SMCs plaques tested from two orthogonal directions.

Figure 5-7 shows the average tensile modulus and strength values of the different SMC composites, relative to their hybridization ratio (carbon fibre content over total fibre

content). As expected, the pure carbon fibre SMC resulted in the highest tensile modulus and strength, and jute fibre SMC the lowest. Moreover, although the carbon fibre content in the jute-skinned hybrid, $[JC]_S$, was about 4% lower that of the carbon-skinned hybrid, $[CJ]_S$; its tensile modulus and strength appeared slightly higher (4% and 14% higher respectively). This may be attributed to the blocking of the carbon layers within the composite core, and the appearance of more voids in the carbon-skinned hybrid. The lines of theoretical modulus and strength for the hybrids shown in Figure 5-7 were calculated from the pure carbon and pure jute values, using a simple linear rule of hybrid mixtures.

The modulus and strength of both hybrids fell slightly below the theoretical predictions relative to the fibre content, with the jute-skinned, $[JC]_S$, and carbon-skinned, $[CJ]_S$, hybrid strengths varying by as much as 6% and 19% respectively. A similar effect from hybridisation has been observed by Stevanović and Stecenko [159], [160] in the mechanical behaviour of carbon/glass hybrid composites [161]. Therefore, the theoretical prediction was considered as an upper bound for strength in most cases. All the hybrid and non-hybrid panels showed non-linear stress-strain behaviour with brittle failure at an average failure strain of 0.87%, 0.6%, 0.6%, and 0.51% for $[J]_4$, $[JC]_S$, $[CJ]_S$, and $[C]_4$ panels respectively. These failure strain values are much lower than the failure strain of their corresponding fibres, suggesting the presence of resin dominated failure.

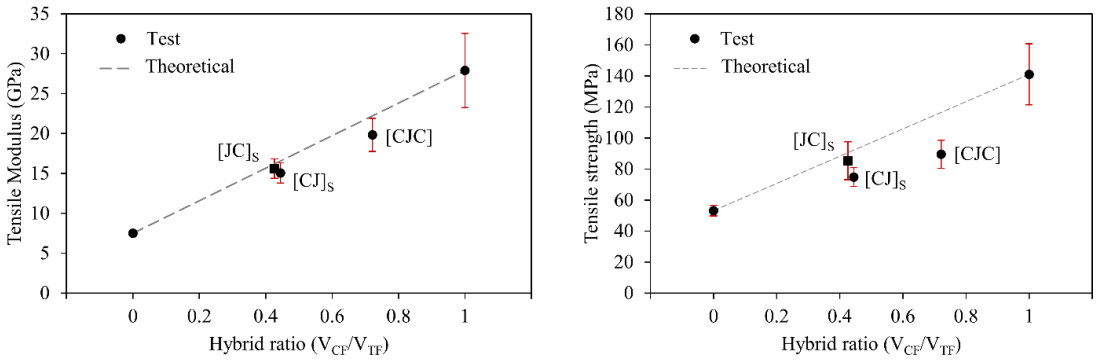

Figure 5-7：Effect of hybridization configuration and ratio on tensile modulus (left) and strength (right) of the hybrid SMCs.

Although the tensile properties of the hybrid configuration with carbon core layers was higher, using jute fibre layer as outer layer makes it prone to degradation due to environmental effects. Hence, the effect of hybridization ratio was studied using $[CJ]_S$ configuration with two intermediate hybrid ratios of 0.44 and 0.72. Figure 5-7 also shows the effect of hybridization ratio on the tensile modulus and strength of the hybrid SMCs. Although lower than the theoretically expected values, both tensile modulus and strength of the hybrid showed a linear increasing trend for an increasing carbon content in the hybrids. The deviations from the theoretical prediction were 9% and 19% in 0.44 hybrid ratio panel and 11% and 23% in 0.72 hybrid ratio for modulus and strength respectively. A relatively higher deviation in strength than in modulus and in higher hybrid ratio panels than lower was observed.

5.4.3 Flexural properties

Figure 5-8 shows the flexural modulus and strength of the different sample configurations tested from direction 1 and 2. Like the tensile results, the highest directional anisotropy was observed in the pure carbon SMC, with greater (35% and 27%) differences in flexural modulus and strength respectively. This was due to the fact that the flexural samples were taken from close to the edge of the plaque, where there

is greater preferential fibre alignment as a result of charge flow during the compaction stage [100]. The pure jute samples also showed higher flexural anisotropy than seen in tension, showing 22% and 24% differences in modulus and strength respectively. Variability was greatest among the carbon-skinned hybrid SMC, with relative standard deviations of 20% in modulus and 32% in strength. This is attributed to the thickness and interface irregularities seen in Figure 5-5c that give rise to locally weak sites, while the more homogeneous pure jute showed the lowest variability of 5% and 8% respectively.

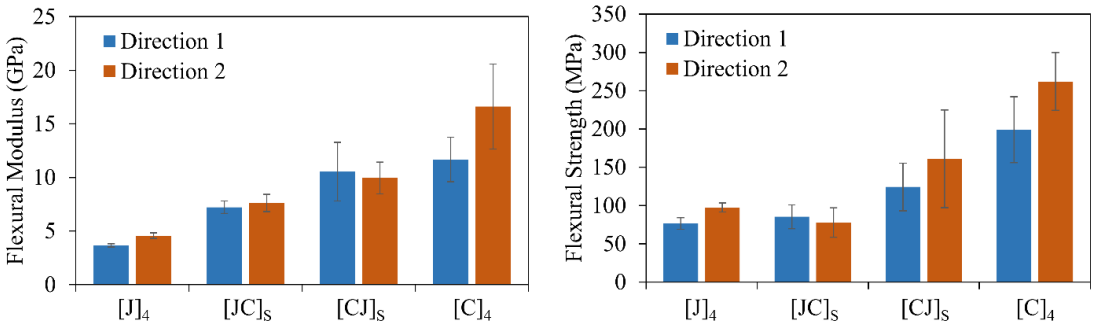

Figure 5-8：Flexural modulus and strength of different hybrid and non-hybrid SMCs plaques tested from two orthogonal directions.

The effect of hybridization on the flexural properties of the various panels is shown in Figure 5-9. The $[CJ]_S$ hybrid, where the stiffer and stronger carbon layers was used as outer skin layer, resulted in 38% and 75% improvement in flexural modulus and strength respectively over the $[JC]_S$ hybrid. With a hybrid ratio of 0.44, the flexural modulus and strength of the $[CJ]_S$ hybrid were 72% and 62% of the pure carbon fibre SMC values respectively. On the other hand, although the flexural modulus of the $[JC]_S$ hybrid was close to the theoretical value, its flexural strength was 45% lower and comparable to the pure jute fibre SMC. This is a result of the inefficient placement of the carbon layers in the centre of the layup, where the bending stresses are smallest, and

the weaker jute layers at the highly stressed outer surfaces where failure initiates. In general, greater variability (represented by the longer error bars) was observed in the flexural testing compared with tensile testing. Hence the bending properties appear to be more sensitive to the manufacturing defect and variabilities than the tensile properties.

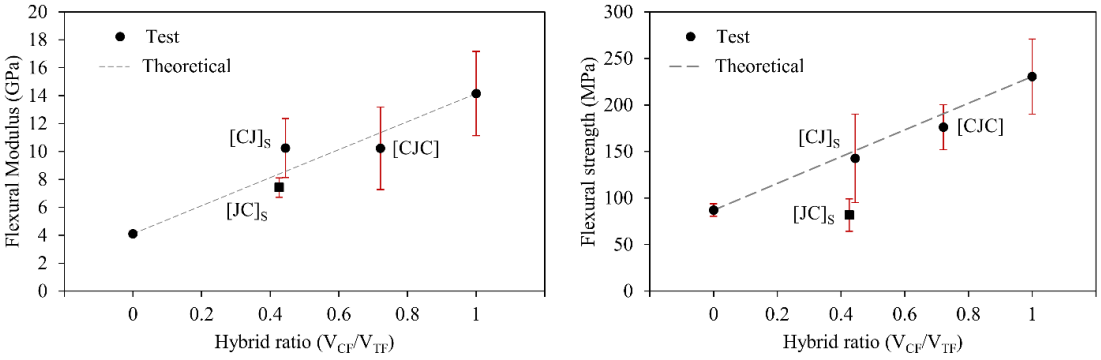

Figure 5-9：Effect of hybridization configuration and ratio on flexural modulus (left) and strength (right) of the hybrid SMCs.

Figure 5-9 also shows the effect of hybridization ratio on flexural properties of the hybrid panels. The $[CJ]_S$ hybrid with a hybridization ratio of 0.44 resulted in (20%) higher than the theoretically predicted value while that of 0.72 resulted in 10% lower flexural modulus. This was due to a relatively larger contribution of the thinner carbon layer in lower hybrid ratio panel than the higher in bending [159], [162]. Although no improvement in flexural modulus was observed for increasing carbon content, the flexural strength showed an increasing trend with 5% and 8% deviation from the theoretically predicted values for the 0.44 and 0.72 hybridization ratio composites respectively. In a similar study, the flexural modulus of hybrids was seen to increase up to a hybridization ratio of 0.5, attaining 90% of the maximum stiffness, while flexural strength was seen to increase over a wider range [160].

5.4.4 Damping properties

Since natural fibres generally offer better damping characteristics than synthetic fibres [158], the effect of hybrid configuration and hybrid ratio on the damping performance of composites has also been studied. Figure 5-10 shows the first mode damping ratio of the hybrid and non-hybrid composite panels in direction 2. The hybrid with external jute fibre layers performed as well as the pure jute composite (~13%), while the carbon-skinned (8.94%) hybrid performed as poorly as the pure carbon fibre SMC (7.86%). This is due to the dependence of the vibration energy dissipation on the external layers [156], [157]. Therefore, the $[JC]_S$ hybrid showed 49% higher damping performance over the $[CJ]_S$ hybrid despite their similar hybrid ratios. Similar observation have been previously reported for carbon-flax [156] and glass-flax [158] hybrid composites, where adding two external flax fibre layers increased the damping performance of hybrids to become comparable to a pure flax fibre composite.

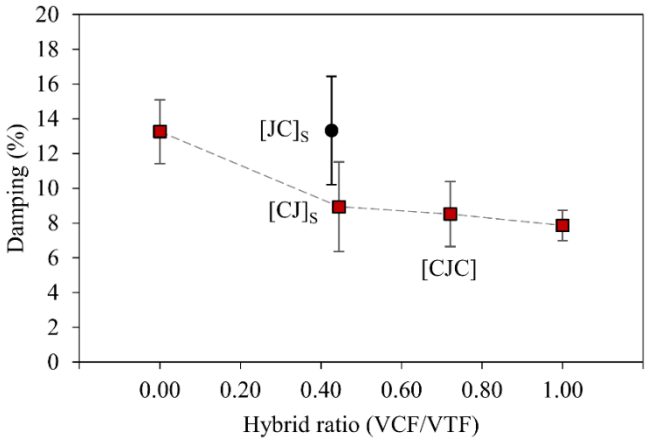

Figure 5-10：Effect of hybridization configuration and ratio on damping properties of the hybrid SMCs (the line indicates the relationship between carbon-skinned laminates with increasing carbon content).

A general reduction in the damping performance of carbon-skinned hybrids for increasing carbon content was also observed. Although the jute fibre content in the $[CJ]_S$ panel was double that of the [CJC] panel, the damping performance was only 5%

higher. Again, this confirms the dominance of the external layers for energy dissipation, where the carbon layer performance is relatively poor. This observation also agrees with the work of Assarar et al. [156], where carbon-flax hybrids with external carbon fibre layers resulted in only a 6% improvement in the damping performance over a pure carbon composite baseline.

5.4.5 Failure mechanism

Failure analysis of the composite fracture surfaces after tensile testing was conducted using a Scanning Electron Microscope (SEM), as shown in Figure 5-11. The fracture surface of the pure jute fibre composite (Figure 5-11a) showed poor interfacial bonding, as most of the fibres protruding from the fracture surface remained clean from any resin residue. Moreover, the gap between the protruding fibres and the surrounding matrix also reveals an inefficient fibre/matrix interface. However, significant fibre failure was also observed, due to the surface irregularity of the jute fibres and the mechanical interlocking from the needle punching process. Fibres oriented in the loading direction exhibited brittle failure, while those at angle showed fracture with micro-fibril splitting. Similarly, the absence of resin residue on the surface of the carbon fibres (notable in Figure 5-11b), was again an indicator of poor interfacial bonding, which lead to tow bundle delamination as the dominant failure mechanism. Such failure may also be attributed to the manufacturing process, as resin infiltration into the densely populated carbon fibre tows is a significant issue during SMC compression moulding: the tow itself has low permeability and the resin remains relatively viscous. The underlying resin rich regions also support this argument. In addition to this, stress concertation due to synchronized fibre ends in a bundle, as indicated in Figure 5-11c, also act as failure initiation site and give rise to fibre-matrix debonding [163]. The hybrid coupons also

exhibited a combination of these same jute and carbon fibre composite failure mechanisms, as shown in Figure 5-11c and d.

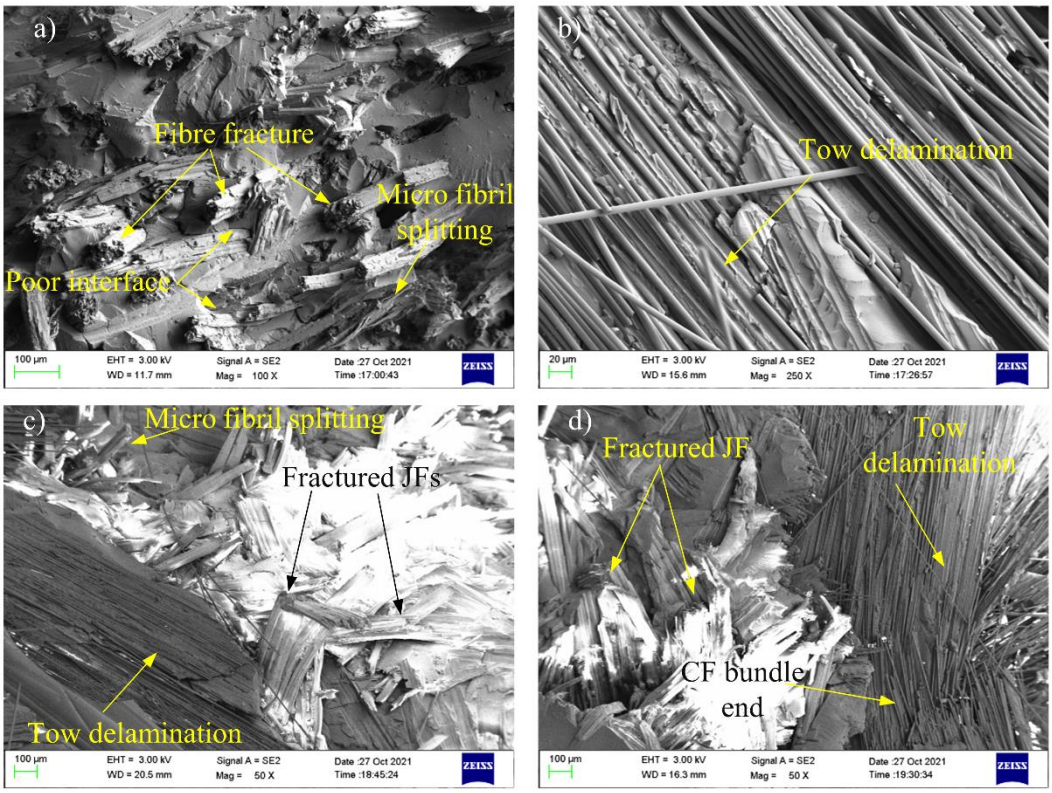

Figure 5-11：SEM images showing the fracture surface of a) $[J]_4$ b) $[C]_4$, c) $[CJ]_S$ and d) $[JC]_S$ SMC composites after tensile testing.

5.4.6 Cost-performance analysis

As important as the engineering properties are for material selection, cost, sustainability, and ease of processing may also be strong considerations. To further evaluate the carbon-jute hybrid SMC as an alternative to the plain carbon or jute fibre reinforced SMCs, the Cost-Performance Ratio (CPR) with respect to each of the properties tested has been analysed. The cost of each different SMC material has been calculated from the raw material cost [146], [164] to fabricate one kilogram of the composite. As the price of the materials is subject to change, a normalized cost with respect to lowest value material (jute fibre SMC) has been used to calculate the CPR values shown in

Table 5-2. As each material has its own strengths and weaknesses, an evenly weighted average of the CPR values has also been calculated for a better comparison across materials. According to the average CPR values, the pure jute fibre SMC $[J]_4$ would be the best value material (27.65). However, its poor fire resistance [165], [166], moisture resistance [167], [168], and mechanical performance makes it unfeasible for many structural applications. In terms of the hybrids, where the performance characteristics are evenly weighted, the carbon-skinned hybrid $[CJ]_s$ offers the better combination of properties (3.03) compared with the jute-skinned hybrid $[JC]_s$ (2.51), and pure carbon SMC (2.33). The higher carbon content [CJC] hybrid resulted in lower CPR value than $[CJ]_s$ due to higher increase in relative cost than the gains in mechanical performance.

Table 5-2: Cost-performance ratio of non-hybrid and hybrid SMCs.

Properties	$[J]_4$	$[JC]_S$	$[CJ]_S$	[CJC]	$[C]_4$
Tensile modulus (GPa)	7.50	15.60	15.06	19.84	27.90
Tensile strength (MPa)	53.15	85.29	74.79	89.54	141.03
Flexural modulus (GPa)	4.11	7.41	10.24	10.23	14.15
Flexural strength (MPa)	87.07	81.59	142.61	176.14	230.52
Damping (%)	13.26	13.33	8.94	8.52	7.86
Specific volume (cm^3/g)	1.32	1.28	1.28	0.77	1.23
Relative cost	1.00	13.57	13.86	22.05	30.24
Evenly weighted average CPR	*27.65*	*2.51*	*3.03*	*2.31*	*2.33*

5.5 Chapter conclusions

The effects of hybridization configuration and ratio on the mechanical and damping performance of carbon-jute fibre in vinyl ester resin SMC composites have been studied in this chapter. Two hybrid SMCs with $[CJ]_S$ and $[JC]_S$ configurations with similar hybrid ratios were manufactured and tested to evaluate the trade-offs in their tensile, flexural, and damping performances against plain carbon and jute benchmarks. Under tensile loading, the jute-skinned $[JC]_S$ hybrid SMC resulted in slightly higher tensile strength and modulus than the carbon-skinned $[CJ]_S$ hybrid due to the blocking effect of stacking the carbon fibre layers together. Conversely, the flexural modulus and strength properties of the $[CJ]_S$ hybrid were 38% and 75% higher than those of the $[JC]_S$ configuration respectively, as the stiffer and stronger carbon layers were used in the highly loaded skin sections. In damping, the $[JC]_S$ hybrid with jute fibre external layer performed similarly to the pure jute fibre SMC, resulting in almost 50% higher damping than the $[CJ]_S$ hybrid and pure carbon composites.

Moreover, the tensile modulus, strength, and flexural strength were seen to increase with increasing carbon content in the hybrids, while flexural modulus showed no improvement for the ratios considered. Also, no enhancement in the damping performance was seen for increasing jute fibre content in the carbon-skinned hybrids due to the dependence of the vibration energy dissipation on the external layers.

SEM analysis of the composites fracture surfaces showed poor fibre-matrix adhesion in all composites, with fibre fracture and tow delamination being the dominant failure modes in the jute and carbon reinforced layers respectively. An average cost-performance ratio (CPR) value of each of the tested properties was used to evaluate the hybrids, highlighting the potential value of the carbon-skinned hybrid. Thus, the hybridization of jute with carbon fibre SMCs demonstrated favourable improvements

in the mechanical performance, which represents a significant step towards realizing their utilization for high production volume structural and semi-structural components.

Chapter 6. Impact resistance and residual strength analysis

6.1 Introduction

Given the example of contradictory notch-sensitivity studies (outlined in Section 2.1), the complex material behaviour presents significant design challenge. Characterisation and optimisation works have been done in the past few decades regarding the in-plane quasi-static properties of advanced SMCs. However, their post-impact residual strength behaviour has received limited attention. As their application in automotive industry extends to closure panels, their susceptibility to impact damage (especially at low energy) increases, which can cause a significant strength reduction without being easily detected.

Early studies on the impact response of SMCs, showed an intermediate behaviour between that of a brittle and a ductile material, and failure behaviour that is influenced by the geometry/thickness, microstructure, and constituent material (fibre/matrix) type. For instance, Kau [169] demonstrated that the impact energy absorption of glass fibre-reinforced SMC decreased exponentially with a decrease in sample thickness. Lee et al. [170] also showed specimen thickness to be the most important parameter governing the energy dissipation capability of SMCs subject to low velocity impact (21 – 34J), and that the variation of initial impact velocities had little effect. However, Chaturvedi and Sierakowski [171] investigated the impact response of a glass fibre SMC over a greater range of energies (15 – 52J) and reported significant correlation between impact velocity/energy, damage size, and the residual tensile properties. Impactor size, mass, and shape have also been seen to influence the extent of induced damage and the corresponding failure mechanisms [170], [171]. Moreover, Trauth et al. [172] studied the impact response of SMCs from 1D and 2D flow, and showed that the microstructure,

i.e. fibre orientation, significantly influences the damage evolution and failure mechanism. The strength of the fibre matrix interface has also been reported to determine the impact resistivity of short carbon fibre epoxy composites [173].

In addition to the above studies on the impact response of SMCs, several other works have considered the post impact residual properties. Kravchenko et al. [174], for instance, investigated the effect of fibre length on the impact and compression after impact behaviour of carbon fibre SMCs made of prepreg chips, compared with quasi-isotropic continuous fibre laminates. The results showed the short fibre composites to have a larger damage area, greater reduction in the residual compressive strength, but greater energy absorption than SMCs with a longer fibre length or than continuous laminates. This was due to the increase in interfacial shear stress between the lower aspect ratio tow chips, which lead to greater energy absorption through delamination [175]. Such works suggest that SMC composites are more prone to impact induced damage [174], [176] than continuous fibre reinforced composites, and exhibit lower post-impact residual properties as a result. However other studies have reported contradictory results, and superior damage tolerance with SMCs [177]. Ogi et al. [178] also studied the impact damage and residual tensile strength of 0.3 mm thick carbon fibre SMCs subject to low energy impact (ranging from 1.1 – 3.5J). They observed a clear correlation between the extent of impact damage and residual tensile strength, depending mainly on impact damage depth. Although these studies independently considered the residual tensile and compressive properties of SMCs after low velocity impact, no comprehensive investigation is available to compare the different load cases.

6.2 Materials and methods

Carbon fibre SMCs were prepared from 25 mm, chopped, T700SC-12k carbon fibre tows in Derakane 782 vinyl ester resin using the same procedure outline in Section 4.2. Flat SMC panels of 400x400x4 mm were manufactured by cutting and centrally stacking the B-staged charge material at 25% mould coverage, prior to compression moulding. A total of six panels were prepared and six test samples were extracted from each panel by abrasive waterjet cutting. Figure 6-1 shows a representative fibre orientation distribution in the moulded plaques as a result of fibre orientation scanning (based on optical reflectance technique [179]) along with the sample cutting plan.

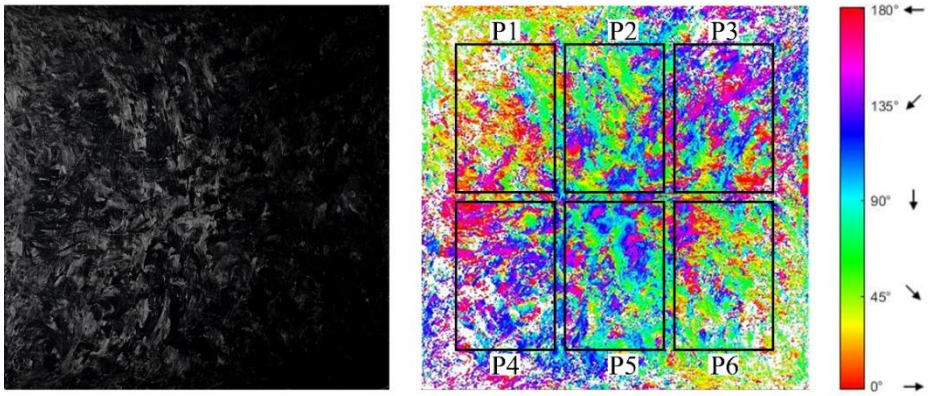

Figure 6-1: Raw image of the SMC panel (left) and representative fibre orientation distribution in the moulded plaques, along with sample cutting plan (right).

6.3 Experimental work

Low velocity impact tests were performed on 150x100 mm coupons according to the ASTM D7136 [180] standard on an Instron CEAST 9340 drop-weight impact tower with automated rebound-catch system. A hemispherical steel impactor of diameter 16 mm and mass 3.265 kg was dropped from heights of 234 mm and 468 mm, corresponding to 7.5J and 15J impact energies respectively. Impact force and velocity were digitally acquired from the force sensor and velocity gate connected to the

impactor. Five repeat tests were performed for each energy, on samples taken from three different panels to account manufacturing variability. Ultrasonic inspection was used to assess the size and extent of the damage. The dent depth on the impacted surface was also measured using a depth micrometre.

Compression After Impact (CAI) testing was performed in accordance with the ASTM D7137 [181] for the impact-damaged samples, along with a set of undamaged control samples. Samples were securely fixed within a CAI fixture and tested on a universal testing machine with 100 kN load cell at a loading rate of 1.3 mm/min to determine the residual compressive strength. After evaluating the impact damage size from ultrasonic C-scan and visual inspection, tension after impact (TAI) test samples were prepared by trimming 25 mm from each side of the sample width ensuring that the damage was fully contained in the remaining central 150 x 50 mm as shown in Figure 6-2. Then tensile testing was performed with a gauge length of 100 mm at a speed of 2 mm/min. A single camera (2D) Digital Image Correlation (DIC) system was used to assess the full-field surface strains during CAI and TAI tests.

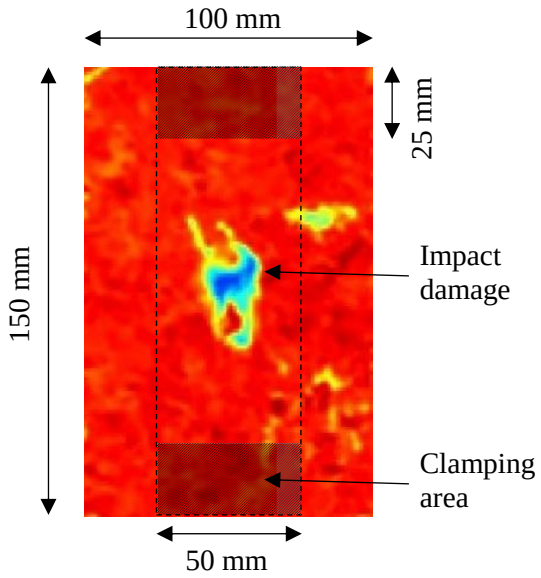

Figure 6-2: Tension after impact sample dimensions.

6.4 Results

6.4.1 Low velocity impact

Two sample groups, of five samples each, were tested at each incident energy for the subsequent tension and compression after impact tests. The representative force-history and force-displacement responses of the SMC panels under 7.5J and 15J impact energies are shown in Figure 6-3. Although some form of damage was detected at both energies, full perforation was not observed. At the lower 7.5J impact energy, damage occurred in the form of matrix cracking at the back surface and a permanent indentation was observed at the impacted location. The relatively smooth curves and near symmetric force-time response of the 7.5J impacted samples indicate that the damage had a negligible effect on the composite stiffness. The post-impact ultrasonic inspection (shown in Figure 6-5) was suggestive of only a network of small cracks around the impact site of the 7.5J samples, in addition to visible signs of minor breakthrough damage at the rear surface. Alternatively, the impact response of the 15J samples showed considerable fluctuations and an asymmetric force-time curve that are representative of greater damage initiation, internal matrix cracking, and delamination. These samples also showed visible fracture on the back surface of the specimens, but the more severe internal damage was also captured by the low amplitude regions of the C-scan images in Figure 6-5. Also, as can be seen from Figure 6-3 (left), the slope of the force-time curve of the 15J impacted sample is greater than that of the 7.5J impacted sample. This is due to the increased stiffness with increasing impact energy as a result of greater deflection and the associated membrane effect [182].

Table 6-1 also summarizes the low velocity impact response of the two sample groups used for TAI and CAI test. Both 7.5J CAI and TAI groups showed very consistent

impact response behaviour, with less than 1% difference in the mean contact force, absorbed energy, and peak displacement. On average 47% of the incident energy is absorbed in the 7.5J impacted samples due to friction and viscoelastic effects in addition to the aforementioned minor damage. Alternatively, the 15J sample groups generally showed greater variability (8-12%) in these parameters; likely due to the significant difference in mean thickness between the batches (3.57 mm for CAI and 3.98 mm for TAI). Observations of decreasing impact resistance with decreasing sample thickness, as similarly seen here, has been established in related work [170]. Due to the greater damage occurrence in the 15J impacted samples, a higher percentage of the impact energy (67%) was also absorbed. From ultrasonic C-scans, this also resulted in a 27% smaller mean damage area for the thicker 15J TAI sample group (365.59 ± 132.15 mm2) than that of the 15J CAI sample group (503.24 ± 61.86 mm2). Additionally, the overall mean damage area from all 7.5J impacted samples was 64% smaller than that of the 15J samples. Furthermore, as can be seen from Table 6-1, the 15J CAI group exhibited greater (63% higher) permanent deformation than the 7.5J sample group, while for the TAI sample groups this difference in dent depth was only 34% (likely due to the thickness effect). As damage progression prolongs the impact event, sample groups with greater damage also showed higher contact duration in general.

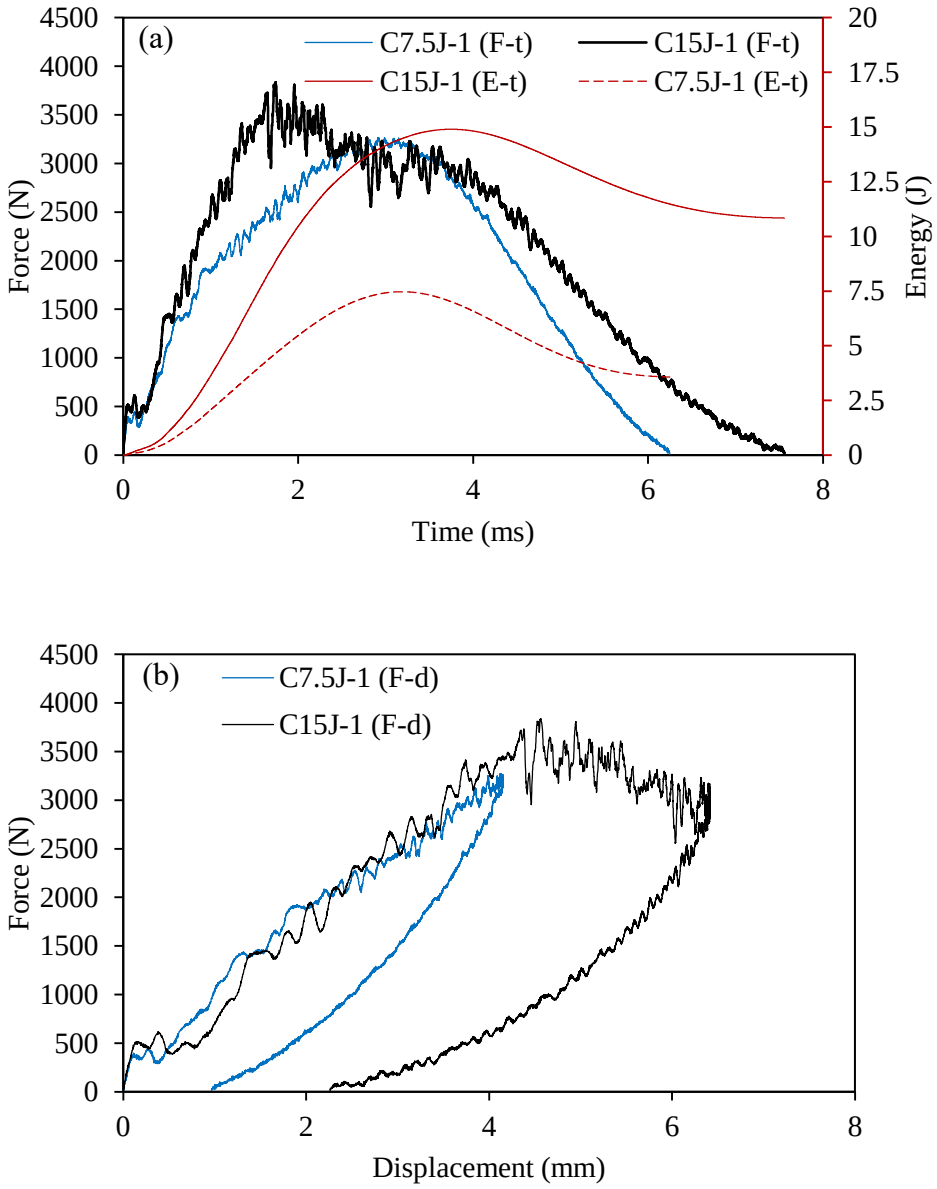

Figure 6-3: Representative force and energy history curves (a) and force-displacement curves of 7.5J and 15J samples (taken from CAI groups).

Table 6-1: Summary of low velocity impact test results for CAI and TAI sample groups (values in brackets indicate the standard deviation of measured parameters)

Sample group		***Thickness, mm***	***Contact force, N***	***Impact velocity, m/s***	***Rebound velocity, m/s***	***Absorbed energy, J***	***Peak displacement, mm***	***Contact duration, ms***	***Dent depth, mm***
CAI	Control	3.56 (0.07)	N/A	N/A	N/A	N/A	N/A	N/A	N/A
	7.5J	3.85 (0.07)	3269.72 (91.94)	2.12 (0.00)	1.55 (0.07)	4.31(0.22)	4.31 (0.22)	6.40 (0.28)	0.20 (0.06)
	15J	3.57 (0.12)	3670.94 (233.07)	3.01 (0.01)	1.53 (0.02)	7.05 (0.47)	7.05 (0.47)	7.97 (0.46)	0.54 (0.32)
TAI	Control	3.88 (0.08)	N/A	N/A	N/A	N/A	N/A	N/A	N/A
	7.5J	3.75 (0.05)	3307.64 (291.89)	2.12 (0.00)	1.86 (0.15)	4.27 (0.37)	4.27 (0.37)	6.37 (0.59)	0.18 (0.04)
	15J	3.98 (0.15)	4576.93(502.94)	3.01 (0.00)	1.56 (0.1)	5.73 (0.23)	5.73 (0.23)	6.27 (0.50)	0.35 (0.10)

6.4.2 Compression after impact

The residual compressive strengths of the SMC panels are shown in Figure 6-4 (left) as a function of impact energy. Four pristine samples were also tested as a reference, which all failed outside the central gauge region. Such “other” failure results serve as a minimum baseline strength under these loading conditions, but may not be representative of the true compressive strength of the panels. Similarly, three of the five 7.5J impacted samples and one of the five 15J impacted samples also failed away from the impact site, and have therefore not failed as a result of the impact damage. The full failure classification and results can be seen in Figure 6-4 (left) and Table 6-2. Quantitatively, there appears to be no significant reduction in the compressive strength of the 7.5J impacted samples, with all valid and invalid tests failing at similar loads to the pristine samples. However, the occurrence of failure initiation through the impacted regions of two samples suggests there may still be a stress concentration and knockdown from the true compressive strength that was simply not measurable with the current testing configuration. For the 15J impacted samples though, a mean 25% reduction of the residual compressive strength was recorded for the four tests with valid failure modes (28% if the invalid test is included). Considering the impact response behaviour of individual samples from Table 6-1 against the CAI results in Figure 6-4 (left), there does not appear to be any correlation between the results. Although plotting the CAI strength against the impact dent depth does reveal 15J samples with greater permanent deformation to have lower residual strength, even when accounting for the sample that failed outside of the central damage region.

The post impact ultrasonic C-scans and full-field strain responses of representative 7.5J and 15J impacted CAI samples can be seen in Figure 6-5. Surface strains were measured using DIC and are presented at the moments immediately before and after final failure.

The image results for samples C7.5J-2 and C15J-3 in Figure 6-5 are representative of all samples with valid failure modes (through the damage region), while samples C7.5J-3 and C15J-2 are examples of invalid failures. The failure of sample C15J-2 in particular initiated from the conjunction of a manufacturing defect (signified by a surface pock mark and a low attenuation region in the C-scan) and another high strain region propagating from the unconstrained left bottom edge.

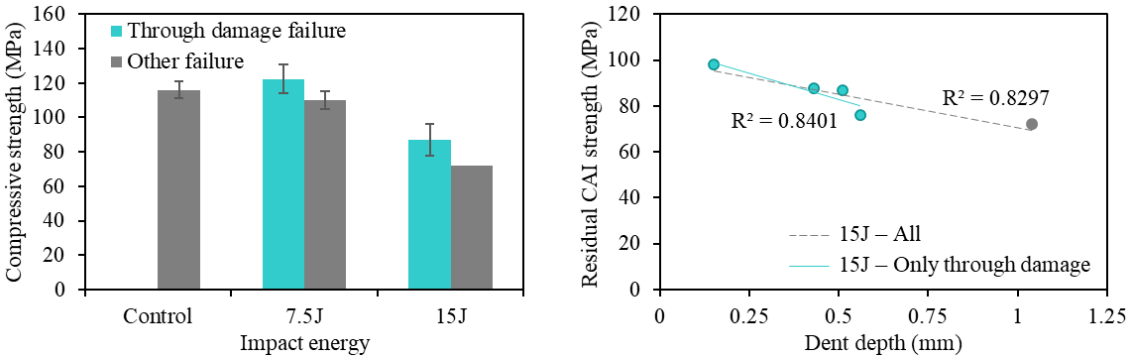

Figure 6-4: Residual compressive strength as a function of impact energy (left) and residual CAI strength of 15J impacted samples with dent depth (right).

Table 6-2: Summary of sample failure location and failure modes in CAI test according to ASTM D7137 [181].

Failure type, failure area, failure location	***Control***	***7.5J impacted***	***15J impacted***
Lateral, at/through damage, middle	-	2	4
Lateral, gauge/away from damage, middle	2	2	1
End crushing, at end/edge, top	2	1	-

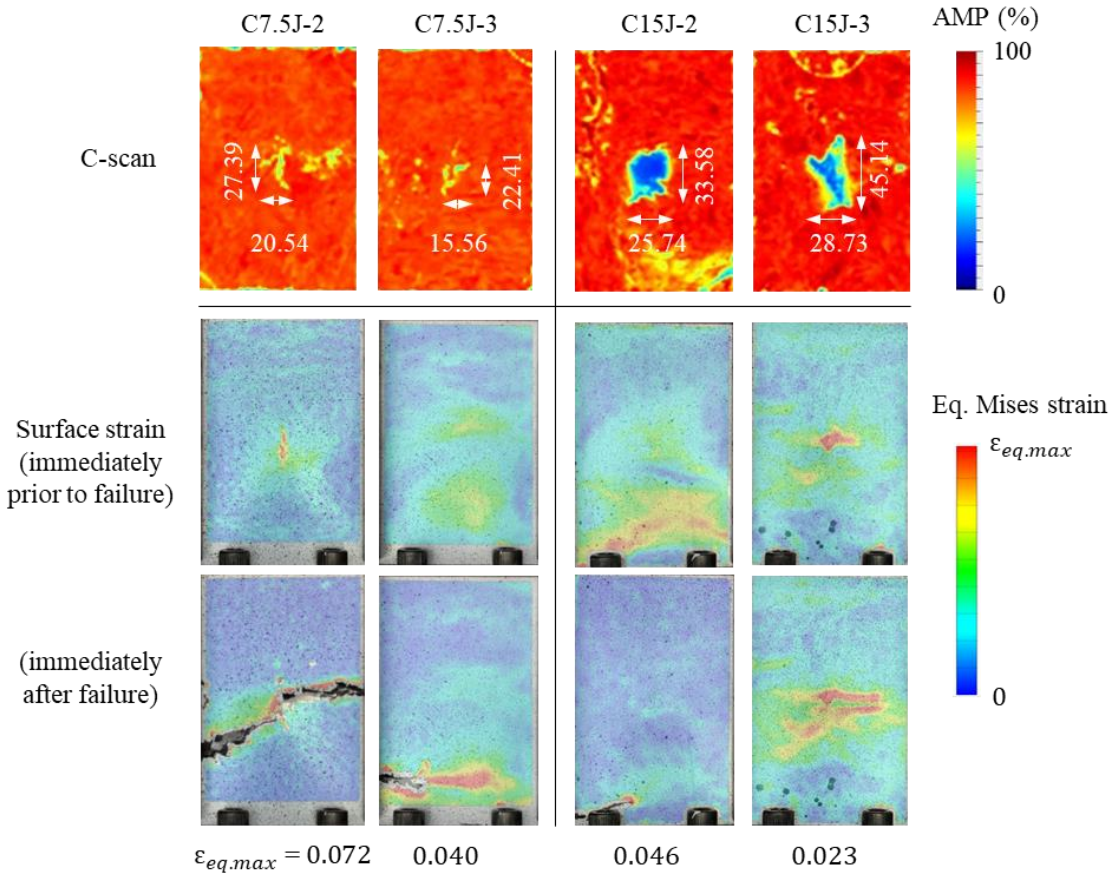

Figure 6-5: Representative C-scan and the corresponding CAI full-field surface strain immediately prior and post final failure in 7.5J and 15J impacted samples.

6.4.3 Tension after impact

The residual TAI strength can be seen in Figure 6-6 for each of the sample batches at different impact energies. Similarly, four pristine samples were tested in tension as a benchmark, all with valid failure modes (i.e. away from the clamping region). Here, the 7.5J impacted specimens also showed no observable strength reduction in tension compared with the control group. All samples failed in the gauge region with three through-damage failures. On the other hand, the 15J impacted samples showed a 16% tensile strength degradation from the baseline. Studies on the notch-sensitivity behaviour of discontinuous fibre composites showed that the onset of notch-sensitivity

depends on the notch diameter, which translates to the extent of damage in the case of damage tolerance. This onset threshold can be calculated using crack-bridging method which uses the materials elastic stiffness, E, strength, σ*, and fracture energy, GC. For the SMC composite in this study (E=24.21 GPa, σ*=173.45 MPa and GC =45.80 kJ/m2)[42], the onset diameter for notch sensitivity shall be more than 36.86 mm. The equivalent circular diameter of damage area measured for 15J impacted TAI samples of 21.57 is significantly lower than the onset diameter. The 16% reduction observed in this study may therefore also be affected by the directional orientation of the impact damage area as shown in Figure 6-7. The extent of damage from post impact ultrasonic inspection and full-field surface strain response right before and after failure for representative 7.5J and 15J samples are shown in Figure 6-7.

Although some size effect due to manufacturing (thickness) variability was identified in the impact response of samples, the SMC plaques showed greater performance in tension than in compression, consistently for all sample groups. Unlike the CAI results, or other reported literature [178], no clear correlation was observed between the individual dent depth of each specimen and the corresponding residual tensile strength.

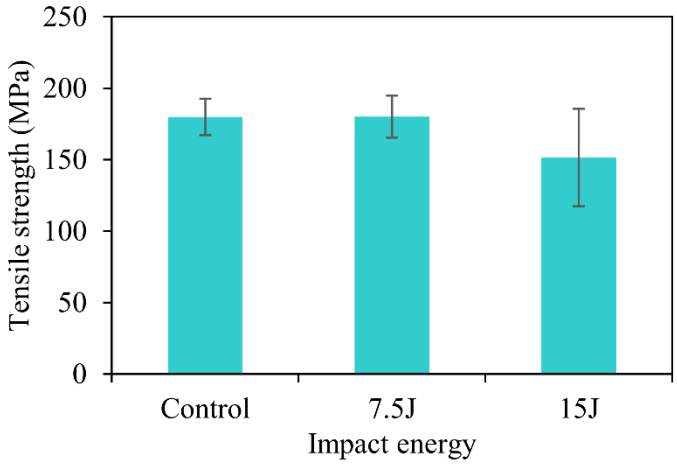

Figure 6-6: Residual tensile strength as a function of impact energy.

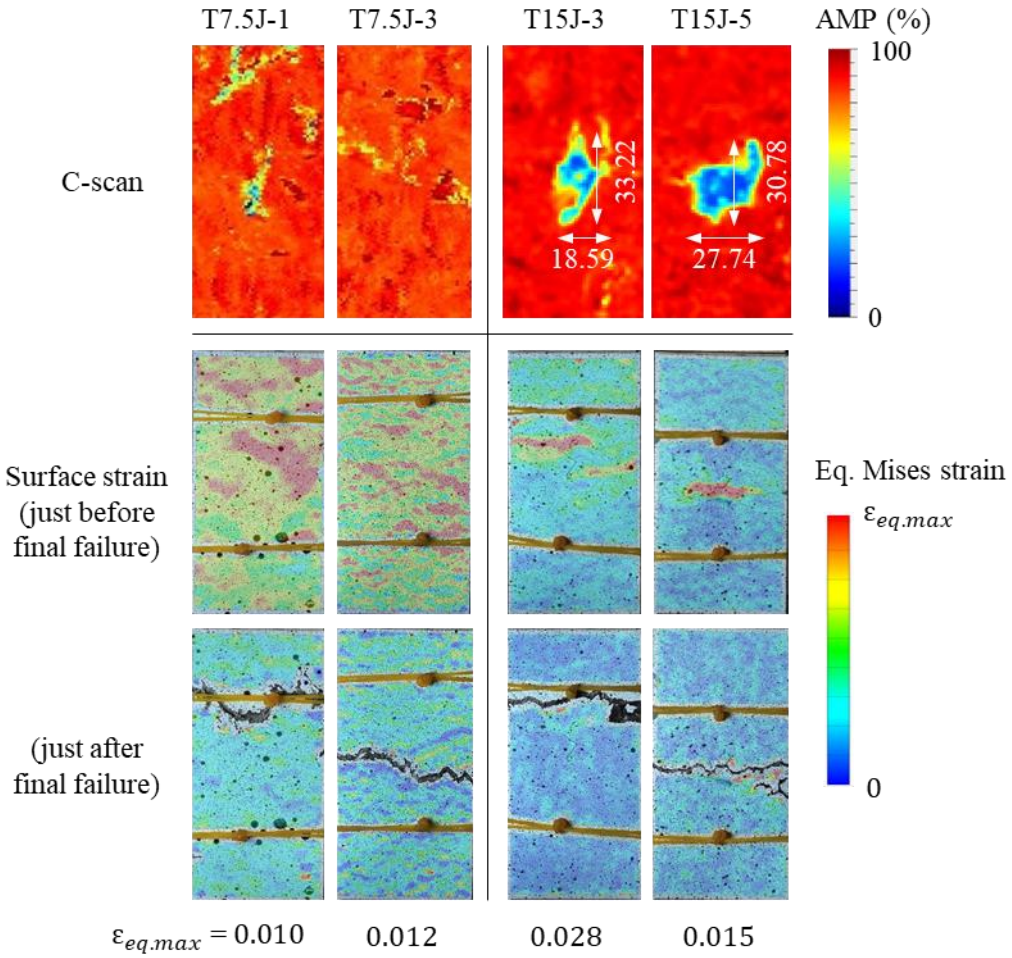

Figure 6-7: Representative C-scan and the corresponding TAI full-field surface strain immediately prior and post final failure in 7.5J and 15J impacted samples.

6.5 Chapter conclusions

In this chapter, the low velocity impact response and residual compressive and tensile strength of SMC composites was investigated. Ultrasonic C-scan and full-field DIC surface strain measurements were used to assess the extent of low velocity impact damage and its correlation with post-impact compression and tension failure initiation. At lower energy (7.5J) any damage was indiscernible from the inherent material variability, while significant damage areas and visible fibre breakthrough were observed at higher energy (15J). Furthermore, the impact response of the SMCs (i.e.

peak force, absorbed energy, damage size, and dent depth) showed significant sensitivity to specimen thickness. Lower energy (7.5J) impacted samples showed no measurable strength degradation in both compression and tension, while 25% and 16% reductions were observed respectively at higher impact energy (15J). This suggests that compression may be the more critical load case for post-impact testing of these composites. Moreover, the correlation between impact damage and post-impact failure initiation sites also appeared to be stronger in compression rather than in tension.

Chapter 7. Fibre alignment and charge flow

7.1 Introduction

The charge flow during compression moulding of SMCs allows easy manufacturing of complex shaped parts and integration of out-of-plane features. However, such flow also affects the local fibre orientation and fibre volume fraction in the manufactured part, ultimately affecting its mechanical performance. Many researchers have attempted to characterize the interaction between different moulding parameters and flow-induced phenomena, reporting complex interactions from fibre/matrix separation, warpage, and knit lines [183], [184].

The flow mechanism during the compression moulding of thermoset resin derived SMCs is characterized by preferential flow where there exists an unequal through-thickness flow velocity [185], [186]. This is due to the reduction of charge viscosity on the surfaces as the charge get in contact with the heated tool. Consequently, moulded plaques commonly show different through-thickness microstructures, with a core region sandwiched between two skin layers. Micro Computed Tomography (μCT) analysis of both glass [187] and carbon [95] fibre compression moulded SMCs showed that tows tend to fragment into individual fibres in the skin layers while the tows in the core may remain relatively intact with slightly deformed shapes. The reported thickness of such skin layers ranges between 5-200 μm [95], [187], [188], and these areas have shown lower fibre and void content than the core region due to through-thickness resin migration [187]. Homogenization of charge viscosity prior to compaction, and a high mould closure speed, were suggested to mitigate these preferential flow phenomena [186], [189]. However, these mitigation techniques can result in fibre matrix separation, as the low viscosity resin is prone to be squeezed out, resulting in significant volume

fraction variability (in some cases greater than 25%) between the initial coverage and flow regions [183], [190], [191].

Moreover, different fibre orientation states have been observed between the skin and core regions as a result of the viscosity gradient and shearing effect between the charge and mould surfaces [192], [193]. Alternatively, greater flow-induced fibre orientation has been observed on the back charge surface as it spends more time in contact with the hot mould surface before the mould closes [100]. Furthermore, locally varying fibre orientations can also develop as a result of in-mould charge flow in complex-shaped parts [193]. Understanding of flow-induced fibre reorientation is crucial as it governs the mechanical performance of the resulting part. Conventionally, optical micrographs are employed to determine the fibre orientation from the elliptical dimensions of fibre cross-sections [194]–[196]. Microtomography has also been used effectively to acquire fibre orientation and other microstructural details such as the fibre volume fraction and void content of SMC composites. However, the quality of image acquisition is subject to the relative contrast between constituents, while the sample size, image resolution, and data extraction are also somewhat limiting [197], making it less applicable for the characterization of larger industrial parts. Alternatively, Kracir et al. [198] used enlarged photographs of dyed glass fibre tracers to determine fibre orientation distributions, however this method is not applicable for opaque carbon fibres [30]. Recently, a non-destructive, image-based orientation analysis technique has shown considerable success for the measurement of in-plane fibre orientations and assessment of charge flow in carbon fibre SMC composite samples over a large area [100], [179].

In the study of SMC processing, in-mould charge flow has also been utilized as a means to preferentially align fibres in the loading direction and to tailor the mechanical performance by controlling the charge shape, size, and placement. For instance, Evans

et al. [30] used partial charge coverage and biased charge flow to introduce greater anisotropy in carbon fibre SMC composites as charge coverage reduced. A tensile stiffness and strength of 46 GPa and 408 MPa respectively were achieved in the flow direction from 50% charge coverage compared to the 100% coverage reference values of 36 GPa and 320 MPa. However, further decreasing the charge coverage (to 40%) resulted a reduction in tensile strength due to high out-of-plane fibre waviness. Similarly, high flow-induced anisotropy and in-plane tow distortion were observed in a related study on high-flow carbon fibre SMC composites [95].

In many of these previous works, mechanical testing from different sample orientations have commonly been used to evaluate the degree of fibre alignment and material anisotropy, due to the sample size limitations of conventional fibre orientation measurement techniques (i.e., microscopy and computed tomography). Simulation tools have also been used to predict flow-induced fibre orientations based on input processing parameters, but their accuracy depends on an assumption of the initial fibre orientations in the composite. Ultimately, there remains considerable research interest in the evolution of fibre reorientation as a result of charge flow.

The current work aims to experimentally investigate flow-induced fibre orientation in carbon fibre SMC composites. The effect of initial charge shape, size, and initial fibre orientation on the flow behaviour has been investigated by employing an image-based fibre orientation analysis technique before and after moulding. Furthermore, differences between the fibre orientations in the core and outer surfaces of the moulded plaques have also been examined. Mechanical testing of samples cut from two orthogonal directions of the different plaques has also been used to support the observations made from fibre orientation analysis.

7.2 Fibre orientation analysis

The fibre orientation of the preforms and moulded plaques from this study were measured using an optical technique [100], [179]. A total of 16 images were taken under different lighting conditions at regular angular offsets for each sample. Light source directions with the maximum peak fibre surface reflectance were then used to calculate the fibre orientation across the surface of the composite, producing a discrete frequency distribution that is a function of the number of images (different lighting orientations) used for the analysis.

In many studies, orientation tensors are often used for the tracking and description of fibre orientation in composite materials, due to their compact nature and computational efficiency. To achieve this, the spatial orientation state of the fibres can be generally expressed using a probability distribution function (ψ), with an assumption that fibres are uniform in length and spatial distribution. Continuous probability distribution functions are commonly used to approximate discrete measurements obtained experimentally for a subsequent closure approximation of the data set. The orientation state of individual fibres can be expressed by angles (φ, θ) corresponding to the in-plane and out-of-plane fibre orientation. Normal and Laplace or double exponential distributions have been used in previous studies [56], [74] for regular and highly aligned fibre orientation distributions respectively. However, these common distributions do not account the periodic nature of orientation measurements. In the current study, the experimentally obtained in-plane measurements were fitted using a von Mises distribution, which is an approximation of wrapped normal distribution around a circle, specially used for periodic data such as angular measurements. For instance, it is not reasonable to assume the mean direction of 10° and 170° to be 90°, as it should be 0° (or 180°). This circular statistics approach also offers more robust descriptive

parameters for the characteristics of the fibre orientation distribution. The probability density function of von Mises distribution is given by:

$$\psi(\Phi; \mu, \kappa) = \frac{exp(\kappa \cos(\Phi - \mu))}{2\pi I_0(\kappa)} \tag{7.1}$$

where μ and κ are location and concentration parameters respectively, and $I_0(\kappa)$ is the modified Bessel function of the first kind and order 0. A small concentration parameter, κ, will indicate a uniform distribution and when κ is large, it indicates a fibre distribution with a strong preferential alignment. Since the in-plane fibre orientations of angles Φ and (Φ+π) are essentially the same, the period of the probability density function in Equation 7.1 was modified from 2π (360°) to π (180°).

The out-of-plane fibre orientation distribution can also be obtained experimentally by taking micrographs of the sample at a filament level and the individual fibre orientations can be measured using image processing [37]. A trigonometric function of the form in Equation 7.2 has also been used in previous studies [37], [38] to describe the experimentally determined out-of-plane fibre orientation, where a and b are the normalization constant and shape parameter respectively.

$$f(\theta) = asin^{2(b-1)}\theta \tag{7.2}$$

The parameter 'b' approaches infinity for purely random fibres in the 1-2 plane and unity for 3D random fibres. In previous literature [37], 'b' was found to be approximately 26 for similar carbon fibre SMCs with different levels of induced filamentisation. However, using this approximate value for the current study, the resulting out-of-plane orientation is only expected to reduce the longitudinal modulus

of the SMC by 5%, compared with a purely 2D (in-plane) fibre distribution [74]. Therefore, in the current study, due to the significant fibre length (25-37.5 mm) relative to the mould cavity height (3 – 4 mm), the out-of-plane fibre orientation was assumed to be negligible, and a purely in-plane distribution was assumed.

Once the probability distribution function, $\psi(\theta, \Phi)$, has been defined, common orientation tensor components can then be calculated by performing a dyadic product of the Cartesian components (p_1, p_2, p_3) of a unit vector $\boldsymbol{p}$ that describes the fibre orientation, and subsequent integration over all possible directions. As the distribution function is even, only the even-order tensors are of interest. Therefore, the second and fourth order orientation tensor components can be calculated as:

$$a_{ij} = \int_0^{2\pi} \int_0^{\pi} p_i p_j \psi(\theta, \Phi)\, sin\theta d\theta d\Phi \tag{7.3a}$$

$$a_{ijkl} = \int_0^{2\pi} \int_0^{\pi} p_i p_j p_k p_l \psi(\theta, \Phi)\, sin\theta d\theta d\Phi \tag{7.3b}$$

One can also recover an approximate orientation distribution function from second and fourth order tensor components using the relationship:

$$\psi(p) = \frac{1}{4\pi} + \frac{15}{8\pi} b_{ij} f_{ij}(p) + \frac{315}{32\pi} b_{ijkl} f_{ijkl}(p) + \cdots \tag{7.4}$$

where b_{ij} and b_{ijkl} are the deviatoric versions of tensor components f_{ij} and f_{ijkl} are distribution functions as defined by Advani and Tucker [199]

Additionally, descriptive measures of directional statistics were used to quantitatively evaluate and compare the observed fibre orientation distribution of different panels and surfaces. Skewness (S) and circular Kurtosis (K), given in Equations 7.5 & 7.6, were used as a measure of the symmetry and peakiness of the fibre orientation distributions [200]. A skewness value close to 0 indicates a symmetric distribution, while its sign

indicates the direction of the skew. Similarly, a kurtosis value close to 0 indicates that the distribution exhibits a standard normal distribution shape, while positive kurtosis is reflective of a more peaked distribution (with significant fibre alignment) and negative kurtosis suggests a more uniform distribution.

$$S = \frac{1}{N}\sum_{i}^{N} \sin 2(\Phi_i - \bar{\Phi}) \tag{7.5}$$

$$K = \frac{1}{N}\sum_{i}^{N} \cos 2(\Phi_i - \bar{\Phi}) \tag{7.6}$$

7.3 Experimental methodology

7.3.1 Materials and methods

Two types of discontinuous carbon fibre SMC composites were prepared from regularly distributed and highly aligned T700SC 12k carbon fibre tows in vinyl ester resin, through a process described in Section 4.2. Preforms of the regularly distributed carbon fibre tow were prepared from similar processing parameters as in Section 4.2. The highly aligned preforms, on the other hand, were prepared using an alignment concentrator mounted on the fibre chopping device, with suitable adjustments to the traverse speed and path of the robot arm [56]. As a higher level of alignment can be achieved with longer fibre tows, a mixture of 37.5 and 25 mm fibre tows with a 3:1 ratio (limited by the chopping device design) were deposited on a 400 × 400 mm area.

Both types of preforms (regular and aligned) were then thermally B-staged, cut to the desired initial charge coverage size, and compression moulded. All panels were manufactured for a nominal fibre volume fraction of 30% and thickness of 3 and 4 mm for plaques of highly aligned and regularly distributed fibre tows respectively.

Six flat SMC plaques were manufactured from different initial charge coverages and degrees of preferential alignment as shown in Figure 7-1. Three square plaques were prepared from regularly distributed (R) tows, with 25, 50, and 100% initial charge coverages placed centrally in the mould, to study the effect of charge size on the mechanical performance of SMC composites. Three other panels, with the highly aligned (A) tow distributions, were manufactured to investigate the effects of radial 2D flow, and linear 1D flow with a longitudinal (A) or transverse (T) bias.

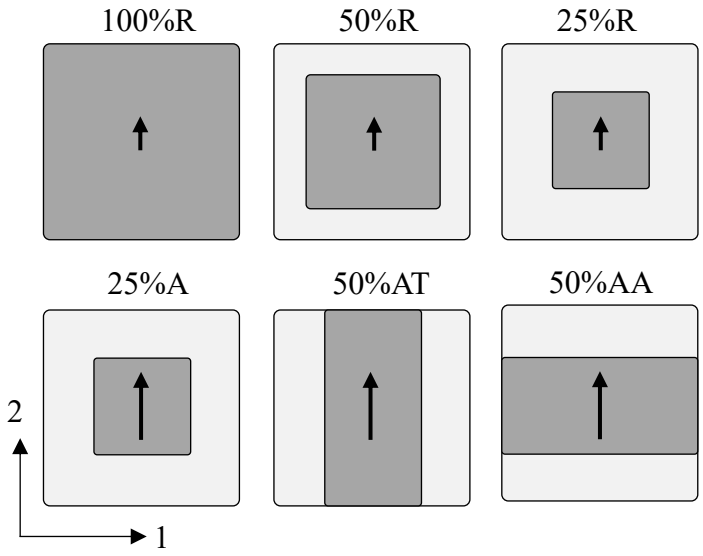

Figure 7-1: Schematic of initial charge placement of the six SMC panels: labels indicate percentage of initial charge coverage (25%, 50% or 100%), regular (R) or aligned (A) fibre distribution, and transverse (T) or longitudinal (A) flow direction relative to the preferential fibre direction (indicated by arrows).

7.3.2 Characterization

The fibre orientation of the preforms and moulded plaques (considering both the front and back surfaces) were measured using an image-based fibre orientation analysis technique implemented in MATLAB code [201]. The fibre orientation inside the core of one quadrant of the moulded plaques was also measured in the same way after

machining a quarter of the panel thickness from both the front and back surfaces. These sample sections were then fine polished to achieve a thickness variation of less than 2%. Figure 7-2 shows a photograph of a representative sample used for subsurface fibre orientation analysis after machining, along with the naming conventions that have been used for the different surfaces. Fibre orientation tensor components and statistical parameters were then used to evaluate the characteristics of flow-induced fibre orientation on the surface and subsurface pairs. The material anisotropy in the moulded plaques was evaluated by performing tensile testing on 200 × 25 mm coupons, with a gauge length of 100 mm, cut from two orthogonal directions. Testing was conducted according to the ISO 527-4 standard at a loading rate of 2 mm/min. Figure 7-3 shows the cutting plan used to prepare samples for mechanical testing and subsurface orientation analysis.

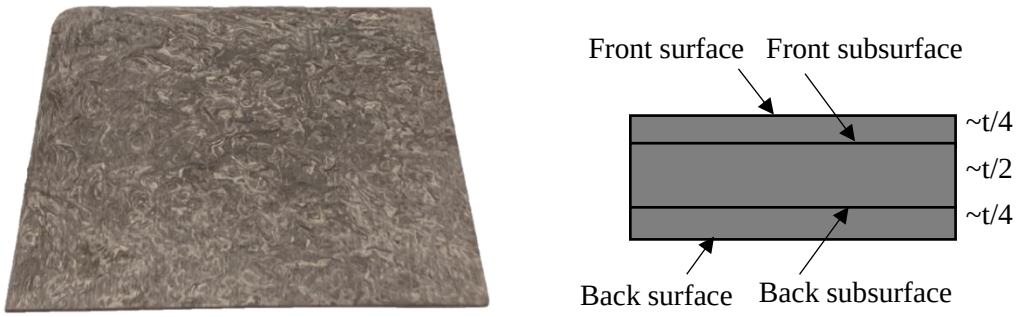

Figure 7-2: Photograph of representative sample used for subsurface fibre orientation analysis after machining (left) and surface naming convention (right).

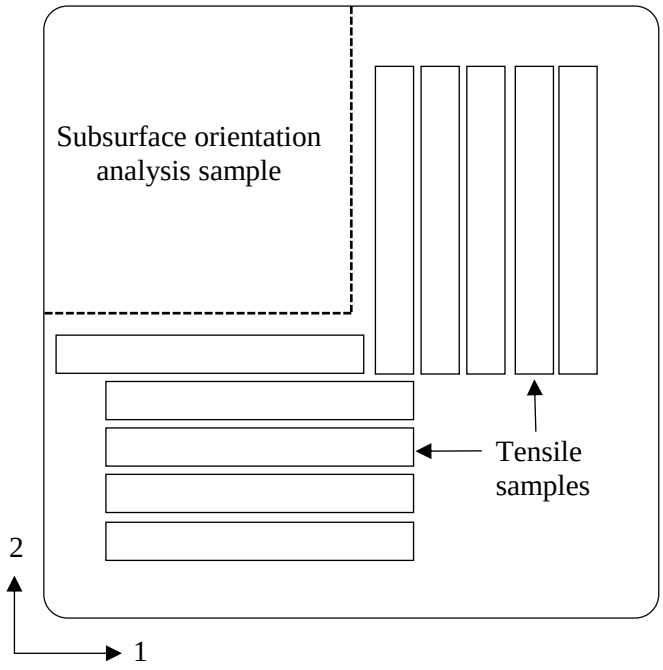

Figure 7-3: Tensile test coupon and subsurface orientation analysis sample cutting plan for all 400 × 400 mm panels.

7.4 Result and discussion

7.4.1 Effect of charge size

The effect of initial charge coverage on the fibre orientations and mechanical performance of SMC composites was studied using three panels moulded from regularly distributed 25 mm long fibre tows with 100%, 50%, and 25% initial charge coverage.

7.4.1.1 Surface fibre orientation analysis

The front surface fibre orientations of the regular panels, and the corresponding probability density functions (before and after moulding) can be seen in Figure 7-4. The tensor components calculated from closure approximation are shown in Table 7-1 along with descriptive measurement parameters from circular statistics. These statistical measurement parameters are particularly useful as they decouple the direction (location,

μ) and intensity (concentration, κ) of the fibre orientation bias, as well as providing more detailed information about the shape of the distribution (kurtosis, K, and skewness, S), which is not evident from tensor components alone. Furthermore, both second and fourth order tensor components are provided. Since fibres with out-of-plane orientation were assumed to insignificant and purely in-plane fibre distribution is considered, i.e., the principal axes lie in the plane of the material, the off-diagonal fourth order orientation tensor components (a_{1122} and a_{1212}) appeared equal as can be seen from the table as both represent the concentration of fibres intermediate between the principal axes. Hence, the fourth order components provide information on the correlation of fibres in 1- and 2-direction that second order do not. However, discussion on the result in this and following sections will be using second order components as the off-diagonal components are equal in all configurations. Overall, a relatively higher flow-induced fibre orientation was observed on the front surface than the bottom, which might be due to gelation of the resin on the back surface during mould closing which was better reflected with change in concentration parameter (22.8% vs. 2.3%, 28.4% vs. 11.3%, and 65.6% vs. 40.3% in 100%R, 50%R, and 25%R panels respectively).

In the 100% charge coverage case, the fibre tows mostly remain intact after forming, as seen in Figure 7-4, except near the corners where there may be minor flow due to uneven charge packing. Consequently, the inherent preferential alignment in the initial charge (as a result of the regular fibre chopping process), remained similar in the moulded plaque. This is demonstrated by the higher a_{22} tensor components or the more specific location parameter, μ, that remains around 90° before and after moulding.

In the 50%R panel, where there is considerably less flow, the fibre orientation distribution actually becomes slightly more aligned with the 90° direction after moulding. Although, an overall maximum of 3% change in a_{22} tensor component was

observed in 50%R panel due to the limited flow distance, the initial charge coverage areas exhibited a 9% and 4% increase in a_{22} components on the front and back surfaces respectively.

In the 25% coverage panel, 25%R, the tensor components in 2-direction of the front and 1-direction of the back surfaces before moulding appear slightly higher than the other directions. This was again due to the natural preferential alignment during deposition as the panel was moulded from four quarters of full coverage preform stacked orthogonally to balance charge pack thickness variability from the initial compaction process. However, this preferential alignment was reduced to nearly in-plane random distribution after moulding on both surfaces due to the significant reorientation of the fibres towards the radial flow direction, more noticeable outside the initial charge area, as has been well reported in previous study [100]. After moulding, the tensor components in preferential alignment direction of the front (a_{22}) and back (a_{11}) surfaces showed an 8% and 15% decrease respectively. The corresponding reductions in the initial charge coverage area were a lesser 2% and 13% respectively. The concentration parameter showed a greater reduction of 66% and 40% on the front and back surfaces respectively. Furthermore, all three panels produced from regularly distributed fibre tows showed moderate concentration parameters, with nearly standard normal distribution curves that are reflected by the very low kurtosis values. The skewness values for these distributions were also very low, showing little deviation from perfect symmetry ($S = 0$).

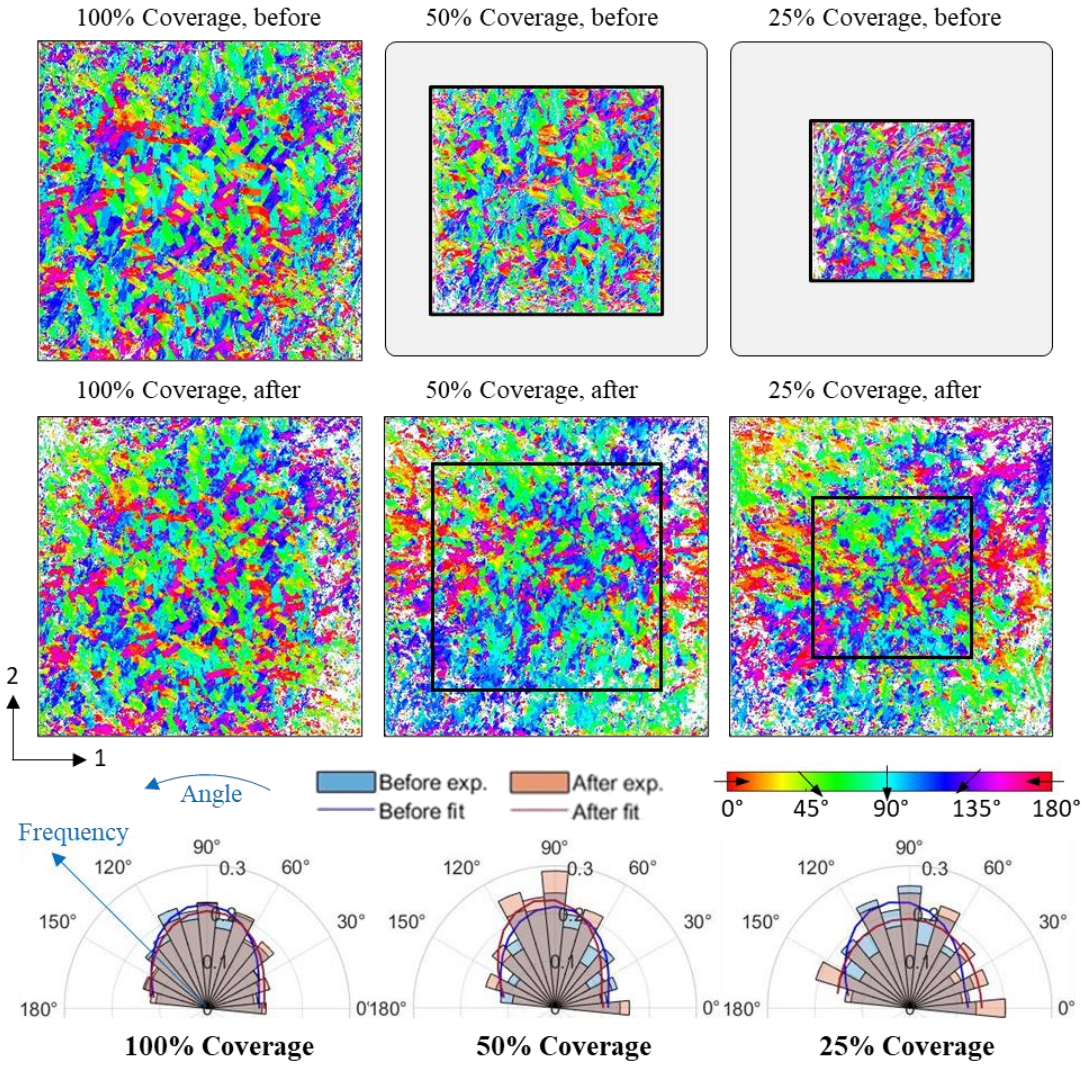

Figure 7-4: Front surface orientation analysis of panels manufactured from regularly distributed fibre tows with 100%, 50%, and 25% charge coverage, before and after moulding.

Table 7-1: Tensor components and statistical parameters for the front and back surfaces of panels manufactured from regularly distributed fibre tows with 100%, 50%, and 25% charge coverages, before and after moulding.

		100%R				***50%R***						***25%R***					
		Front surface		Front surface		Front surface			Back surface			Front surface			Back surface		
		Before	After	Before	After	Before	After	Initial	Before	After	Initial	Before	After	Initial	Before	After	Initial
Tensor comps.	a_{11}	0.416	0.434	0.417	0.422	0.421	0.403	0.369	0.379	0.385	0.354	0.428	0.474	0.439	0.548	0.467	0.474
	a_{22}	0.585	0.566	0.583	0.578	0.579	0.597	0.631	0.622	0.615	0.646	0.572	0.526	0.561	0.452	0.533	0.526
	a_{1111}	0.292	0.31	0.294	0.298	0.298	0.28	0.248	0.257	0.264	0.235	0.304	0.349	0.315	0.423	0.342	0.349
	a_{2222}	0.461	0.442	0.459	0.454	0.456	0.474	0.510	0.500	0.493	0.526	0.449	0.402	0.437	0.328	0.408	0.401
	a_{1122}	0.123	0.124	0.123	0.124	0.123	0.123	0.121	0.122	0.122	0.12	0.124	0.125	0.124	0.125	0.125	0.125
	a_{1212}	0.123	0.124	0.123	0.124	0.123	0.123	0.121	0.122	0.122	0.12	0.124	0.125	0.124	0.125	0.125	0.125
Statistical params.	μ	93.7°	89.4°	82.8°	76.9°	90.9°	97.6°	97.8°	80.5°	91.0°	89.0°	100.5°	96.1°	94.0°	16.0°	83.9°	90.4°
	κ	0.346	0.267	0.346	0.354	0.32	0.411	0.564	0.532	0.472	0.611	0.314	0.108	0.25	0.226	0.135	0.104
	S	0.003	-0.01	-0.008	0.016	0.017	-0.02	-0.01	0.035	-0.01	-0.01	-0.02	-0.03	0.001	0.011	0.051	0.007
	K	0.003	0.001	0.026	0.041	0.055	0.098	0.092	0.089	0.12	0.15	0.024	0.044	0.014	0.014	0.058	0.04

(μ – location parameter, κ – concentration parameter, S – skewness, K – kurtosis)

7.4.1.2 Mechanical performance

The tensile stiffness and strength of coupons tested from the two orthogonal directions of the three different moulded plaques, are presented in Figure 7-5. Here, the 100% and 50% charge coverage panels showed greater anisotropy in both stiffness and strength owing to the residual preferential alignment from fibre deposition, in good agreement with the observations from fibre orientation analysis. Similarly, the 25% charge coverage panel showed the least anisotropy in stiffness (5%), strength (26%), and fibre orientations as a result of the large regions of radial flow. The greater anisotropy in strength than stiffness could be due to the fact that stiffness is volume average property whereas strength is governed by critical defects in addition to slight preferential alignment observed in the moulded panel. Although no significant difference in the directional average tensile stiffness was observed across the different panels, the average strength of the 25% charge coverage panel was seen to be 14% higher than that of the 100% coverage panel. This improvement is expected to be a result of better fibre impregnation due to greater charge flow, as has been discussed in previous literature [100].

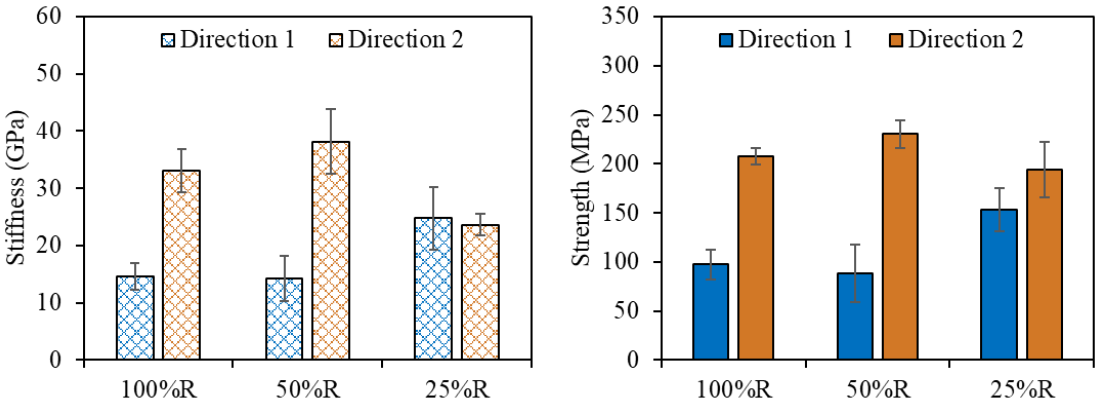

Figure 7-5: Directional tensile stiffness and strength of the SMC plaques manufactured from regularly distributed tows.

7.4.2 Effect of initial fibre alignment and flow direction

The effect of initial fibre alignment and flow direction on the extent of flow-induced fibre reorientation was studied using the remaining three panels, with greater initial fibre alignment and the 3:1 mixture of 37.5 mm and 25 mm fibre tows. These were moulded with a radial (25%A), linear longitudinal (50%AA), or linear transverse (50%AT) flow bias.

7.4.2.1 Surface fibre orientation analysis

Fibre orientation distributions from the front surface of the three panels manufactured from highly aligned initial charges, before and after moulding, are shown in Figure 7-6. In the 25%A panel, significant flow-induced fibre reorientation was observed after moulding. This is demonstrated by the 38% reduction in peak concentration, κ, or the 10% reduction in the a_{22} tensor component of the front surface seen in Table 7-2. Although charge flow was encouraged in all directions, the moulded panel retained a significant degree of the fibre preferential alignment as defined by the peak located at around 90°. Although not directly comparable due to thickness effect, compared to the 25%R panel moulded from shorter randomly distributed fibre tows, the 25%A panel moulded from highly aligned longer fibre tows showed lower flow-induced fibre reorientation. This is due to the greater resistance of longer fibres with high Reynolds number, i.e., a measure of the inertial forces in the fluid which is a function of fibre length, resist flow-induced fibre orientation and instead drift monotonically [30], [202].

The 50%AT panel appeared to show a very high degree of flow-induced fibre reorientation in the flow direction, where the initial strong longitudinal bias (κ = 0.965, μ = 83.4°) has been replaced by a slight bias in the opposite (transverse flow) direction

(κ = 0.190, μ = 170.1°) after moulding. As observed in other configurations, higher fibre reorientation was observed on the front surface with 36% reduction in a_{22} tensor component compared to the back surface with 29% reduction. Moreover, the initial charge coverage area showed a lower 26% reduction in a_{22}, retaining the initial fibre preferential alignment relatively, compared to the 39% reduction in the flow region on average between the front and back surfaces.

From Table 7-2, there is also a clear increase in both the distribution concentration parameter and kurtosis of the 50%AA orientation distribution, indicating a greater degree of overall alignment in the peak (96.8°) direction than any other panel. In this case a 2% increase in a22 was observed on the front surface while an inconsistent 10% reduction was observed on the back surface which may have been due to uneven charge pack. However, a similar trend in overall fibre alignment that is well characterised by the statistical parameters may not be captured by the tensor components if the orientation bias deviates further from the primary orthogonal directions. As seen in other configurations, a relatively lower fibre reorientation was observed in the initial charge coverage area. The fact that no meaningful improvement in preferential alignment, only 3% on average between front and back surfaces, was observed in the flow regions might also suggest the potential fibre agglomeration and entanglement increasing fibre to fibre friction in longer fibre panels [30]. By integrating the fitted orientation distribution function in Equation 7.3, 38.19% of the fibres were found to be oriented in ±15° to the preferential alignment 2-direction on average between front and back surfaces after moulding.

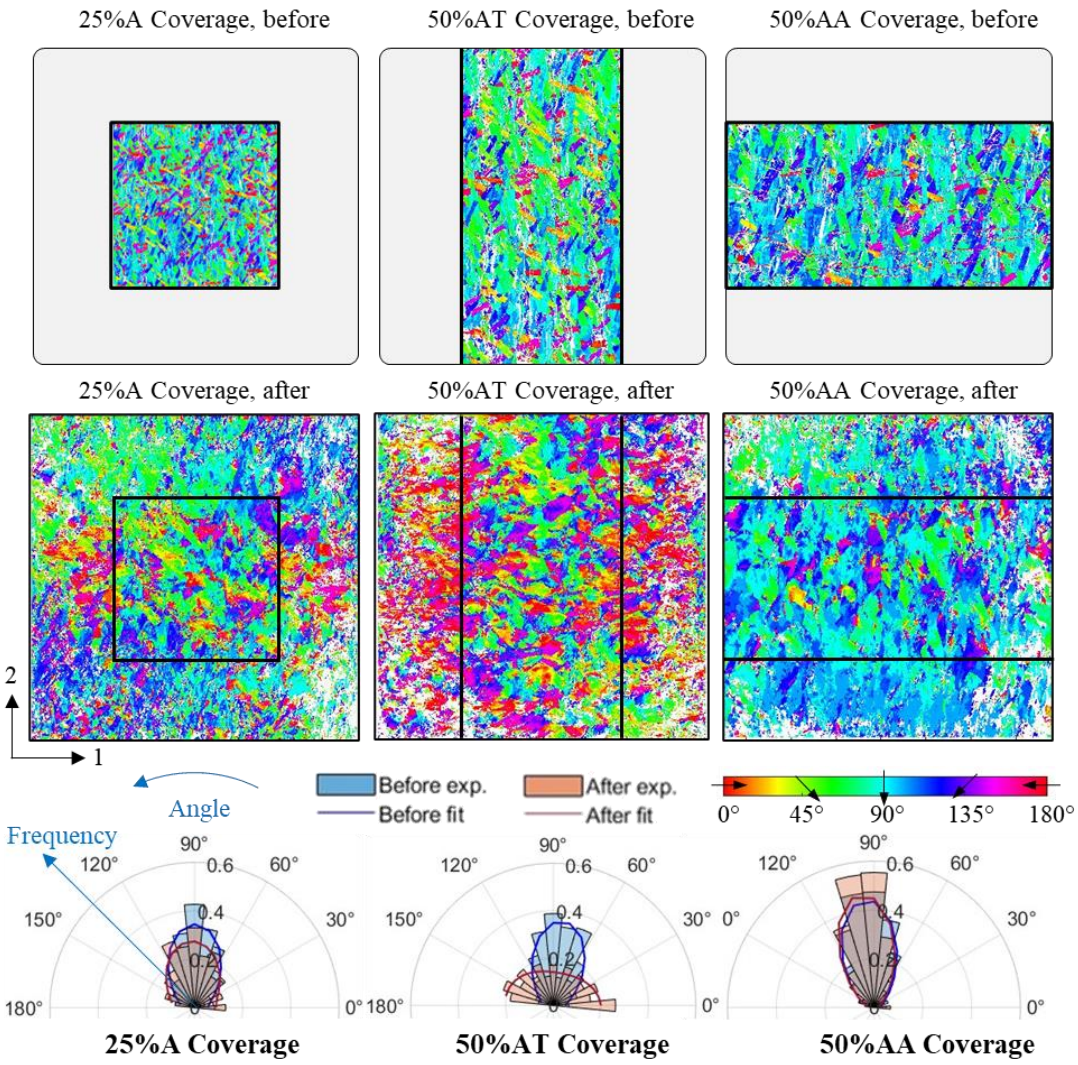

Figure 7-6: Front surface orientation analysis of panels manufactured from highly aligned fibre tows with various flow biases before and after moulding.

Table 7-2: Tensor components and statistical parameters for the front and back surfaces of panels manufactured from highly aligned fibre tows with biased 1D and 2D flows, before and after moulding.

		25%A						***50%AT***							
		Front surface			Back surface			Front surface				Back surface			
		Before	After	Initial	Before	After	Initial	Before	After	Initial	Flow*	Before	After	Initial	Flow*
Tensor comps.	a_{11}	0.295	0.367	0.371	0.255	0.344	0.325	0.289	0.544	0.508	0.581	0.3	0.502	0.449	0.555
	a_{22}	0.705	0.634	0.629	0.745	0.656	0.676	0.711	0.456	0.492	0.419	0.7	0.498	0.551	0.445
Statistical params.	μ	89.67	93	86.05	84.55	89.99	89.46	83.35	170.07	159.97	169.85	94.23	19.37	89.48	3.1
	κ	0.902	0.557	0.541	1.158	0.657	0.751	0.965	0.19	0.043	0.353	0.886	0.011	0.205	0.253
	S	-0.065	0.016	0.02	-0.055	-0.01	0.014	0.006	0.013	-0.02	0.035	0.009	-0.04	-0.01	-0.01
	K	0.153	0.084	-0.00	0.172	0.102	0.098	0.152	0.028	0.014	0.05	0.2	-0.01	0.007	0.062

(μ – location parameter, κ – concentration parameter, S – skewness, K – kurtosis)

Table 7-3: Tensor components and statistical parameters for the front and back surfaces of panels manufactured from highly aligned fibre tows with biased 1D and 2D flows, before and after moulding. (Continued)

		50%AA							
		Front surface				Back surface			
		Before	After	Initial	Flow*	Before	After	Initial	Flow*
Tensor comps.	a_{11}	0.219	0.207	0.196	0.216	0.204	0.269	0.283	0.248
	a_{22}	0.781	0.793	0.804	0.784	0.796	0.731	0.717	0.752
Statistical params.	μ	94.68	96.76	96.11	97.77	86.33	87.63	87.38	87.40
	κ	1.395	1.525	1.614	1.578	1.506	1.051	0.969	1.208
	S	-0.012	-0.03	-0.02	-0.05	-0.03	0.051	0.059	0.024
	K	0.258	0.328	0.305	0.389	0.32	0.304	0.257	0.371

7.4.2.2 Mechanical performance

The directional tensile stiffness and strength of the three panels manufactured from highly aligned initial charges are shown in Figure 7-7. In all three panels, higher tensile properties were observed in the direction of the initial fibre alignment. For the 25%A panel, the tensile stiffness and strength in direction 2 were both seen to be more than 3 times higher than those of direction 1, in agreement with the observation from fibre orientation analysis in the prior section.

However, in the case with transverse charge flow, 50%AT, the direction 2 dominant mechanical test results appeared to contradict the expectations based on the front surface orientation analysis in Table 7-2, where the peak distribution of fibres was instead biased towards direction 1. One explanation could be that the design of the panel cutting pattern (shown in Figure 7-3) did not capture the main fibre realignment and

flow regions within the gauge regions of the coupons. However, the more likely explanation is that the exterior surface orientation analysis may not be representative of a very different internal orientation distribution that dominates the performance. In spite of this contradiction though, the relative difference between the direction 1 and 2 mechanical properties for the 50%AT panel, were much smaller than those of the 25%A and 50%AA panels, and this observation is still well supported by the relative magnitudes of the concentration parameters, κ, and directional tensor components from the front surface fibre orientation analysis. Moreover, from samples taken from direction 2, those from initial charge coverage area showed 49% higher tensile stiffness on average than those from flow region. However, no reliable trend was observed in the tensile strength and sample location.

Lastly, in the panel where charge flow was aligned with the initial fibre alignment direction, 50%AA, the highest average directional stiffness (56.69 GPa) and strength (238.87 MPa) properties were obtained, compared with all other panels. Greater anisotropy was also observed, again agreeing well with the trends of the concentration parameters, κ, and directional tensor components from fibre orientation analysis in Table 7-2. Hence, using an aligned charge and encouraging flow in the same direction can be used effectively to maximise the directional mechanical performance of SMCs.

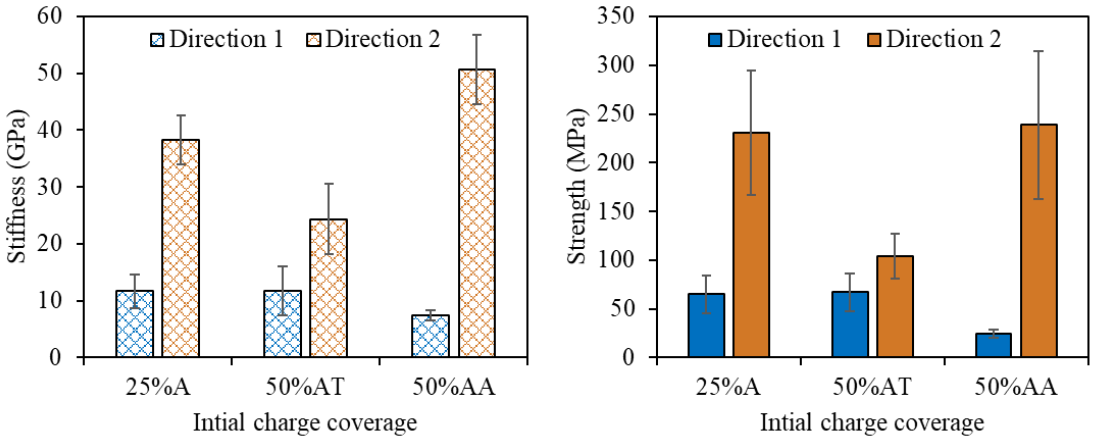

Figure 7-7: Directional tensile stiffness and strength of the SMC plaques manufactured from highly aligned initial charges.

7.4.3 Subsurface fibre orientation analysis

As presented in the previous sections, some notable discrepancies were observed between expectations (based on the surface fibre orientation distributions) and the mechanical test results. Additionally, previous work based on microtomography has reported significant differences between the surface (skin) and internal (core) fibre orientation distributions in short fibre reinforced composites [187]. Hence, further subsurface fibre orientation analysis was performed for this study, based on the upper-left quarter of several panels to better understand the internal fibre orientation distributions. The fibre orientation distributions from each of these quarter panel sections were then divided into a number of different regions of interest, as shown in Figure 7-8, for further analysis.

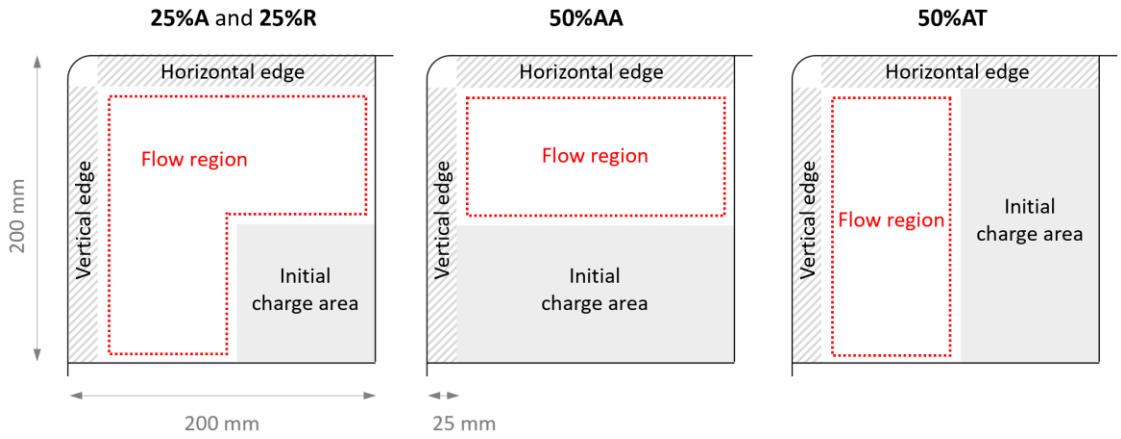

Figure 7-8: Division of upper-left moulded panel quarters into different regions of interest for surface and subsurface fibre orientation analysis.

7.4.3.1 Edge effects

In the panels moulded from a central square charge, with radial flow, the flow front evidently reaches the mould walls unevenly [203]. Subsequently, fibres tend to reorient themselves along the mould walls in the direction of the unfilled corners as the compression moulding progresses, resulting in the potential for significant edge effects. Such behaviour can be clearly seen in the 25%R panel, as shown in Figure 7-9. Here the probability density functions, in Figure 7-10, for the horizontal and vertical edges are compared with those of the flow regions for both the front surface and subsurface. These are also representative of similar results for the back surface and subsurface. Notably, the subsurface curves in Figure 7-10 exhibited clear peaks of fibre orientation parallel to the horizontal (0°) and vertical (90°) edges, significant deviations from the minor 45° peak resulting from flow aligned fibres in the flow region. Such effects were not so clear from the exterior surface analysis, where only a minor shift (towards 90°) in the distribution peak for the vertical edge was observed. Hence, the subsurface fibre orientation analysis appears to better identify edge effects

that may not be visible from the exterior surfaces. Edge effects were less apparent in the 25%A panel, likely due to the presence of longer fibre tows that exhibit a greater resistance to reorientation[30], [202]. The panels moulded from linear charge flow (50%AT and 50%AA), only exhibited disordered fibre orientations at the end-of-flow edges (perpendicular to the charge flow direction). Similar observations have been reported in past literature [30], [204], where significant in-plane and out-of-plane fibre waviness were observed within 25 mm of moulded plaque edge.

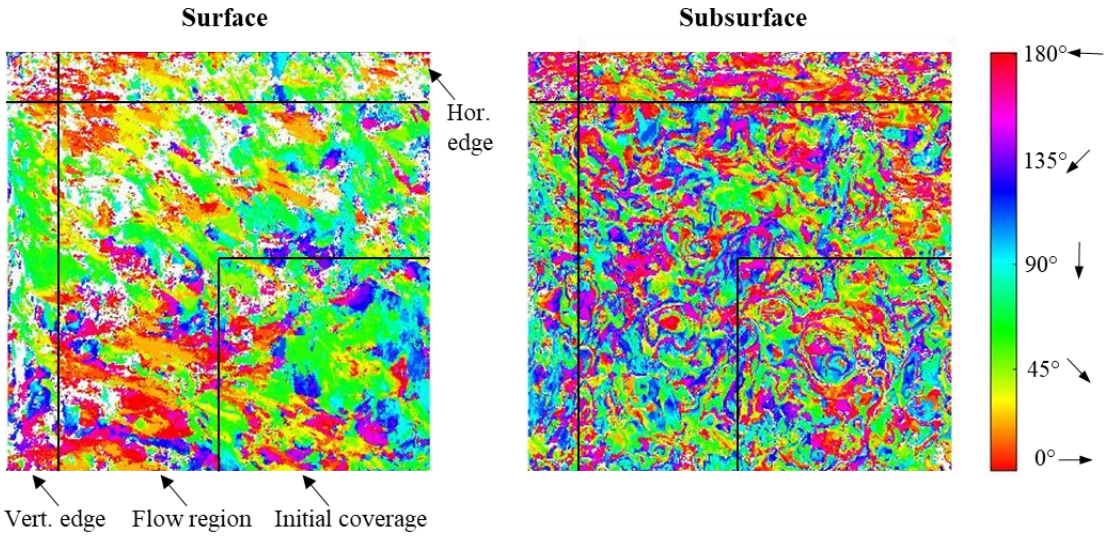

Figure 7-9: Edge effects observed from fibre orientation analysis of the 25%R front surface (left) and front subsurface (right).

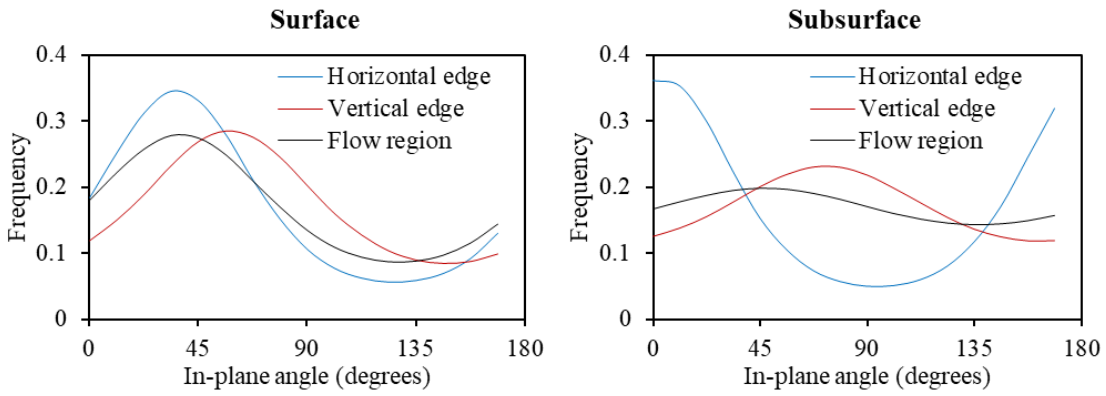

Figure 7-10: Probability density functions of the edge effects observed from the fibre orientation analysis of the 25%R front surface (left) and front subsurface (right) for different regions of the panel.

7.4.3.2 Radial (2D) flow moulding

A first look at the subsurface analysis results in Figure 7-11, suggests that the panel with greater initial alignment (25%A) has far fewer fibres in the 0° direction (red), and less prominent edge effects, than were observed for the 25%R panel in Figure 7-9. As both panels were manufactured from centrally-placed charges with an outward (radial) flow, the orientations in the upper left corner of both panels is predominantly biased towards the 235° (45°) direction. Focussing on the flow region alone (neglecting the edge and initial charge coverage regions), Figure 7-12 shows the fibre orientation probability density functions for the front and back, surfaces and subsurfaces, of both panels. Full details of the tensor components and statistical parameters for these subset regions are also outlined in Table 7-4. In general, the fibres at the exterior surfaces appear to be more sensitive to flow, with surface peaks located (μ) closer to the 45°

flow bias direction than the subsurface peaks. The subsurface probability density distributions appear to be more closely related to the initial state of the material. For example, subsurface distributions for the 25%R panel are more uniform (low concentration, κ) and subsurface peaks for the 25%A panel are located (μ) closer to 90°. In this case, such behaviour is not well captured by the second order tensor components in Table 7-4 alone because of the off-axis (45°) flow bias, emphasising the value of the statistical analysis parameters.

Ultimately, the initial alignment appears to have a more dominant effect on the internal orientations and performance of the moulded panel than the flow reorientation. For example, the relatively uniform subsurface orientation distributions for the 25%R panel provide a better explanation for the similar mechanical performance from orthotropic directions in Figure 7-5.

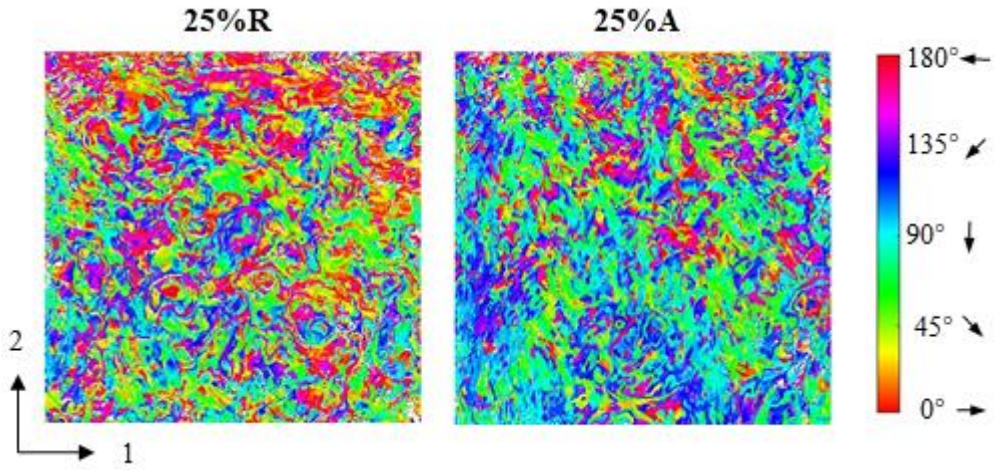

Figure 7-11: Fibre orientation distributions of the front subsurface of the 25%R (left) and 25%A (right) panels (from the upper left 200 × 200 mm section of the panels).

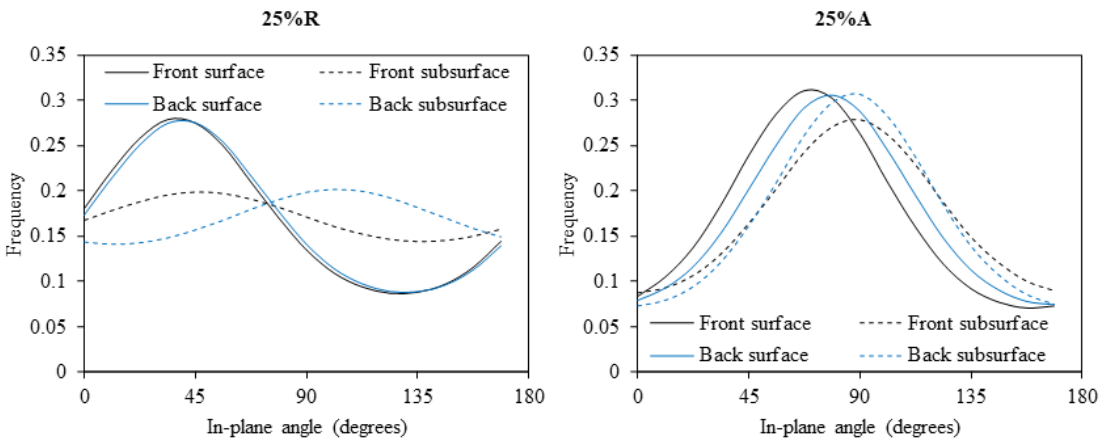

Figure 7-12: Probability density function curves for the in-plane fibre distributions taken from the surfaces and subsurfaces of the 25%R (left) and 25%A (right) panels.

Table 7-4: The calculated surface and subsurface orientation tensor components and statistical parameters for panels manufactured from radial charge flow (25%R and 25%A).

		25%R				***25%A***			
		Surface		Subsurface		Surface		Subsurface	
		Front	Back	Front	Back	Front	Back	Front	Back
Tensor components	a_{11}	0.535	0.525	0.497	0.460	0.365	0.347	0.362	0.332
	a_{22}	0.465	0.475	0.503	0.540	0.635	0.653	0.638	0.668
Statistical parameters	μ	37.8°	39.8°	46.9°	102.3°	70.3°	78.1°	87.9°	87.3°
	κ	0.585	0.575	0.161	0.177	0.743	0.710	0.578	0.719
	S	-0.041	-0.126	-0.015	-0.048	0.037	0.005	-0.024	-0.018
	K	-0.008	-0.129	-0.026	0.020	0.118	0.150	0.050	0.113

(μ – location parameter, κ – concentration parameter, S – skewness, K – kurtosis)

7.4.3.3 Linear (1D) flow moulding

The subsurface analysis of the aligned panels with transverse (50%AT) and longitudinal (50%AA) charge flow are shown in Figure 7-13. Although the front surface fibre orientation analysis in Section 7.4.2.1 showed considerable fibre reorientation in the flow direction, the subsurface analysis again displayed lesser fibre reorientation, with much of the initial preferential (90°) alignment retained in the subsurface probability density functions shown in Figure 7-14. As a result, the calculated tensor components from the initial preferential alignment direction, a_{22}, in Table 7-5 were 65% and 34% higher internally than at the exterior front and back surfaces respectively. This, in combination with the tensile performance observations in Section 7.4.2.2, suggests that there is greater flow-induced fibre reorientation at the exterior (skin) surfaces, while the subsurface (core) fibre orientations show much less deviation from their original state. Alternatively in the 50%AA panel, the surface (skin) and subsurface (core) orientation distributions shown in Figure 7-14 exhibit no significant differences, since the flow bias direction coincides with the initial alignment direction.

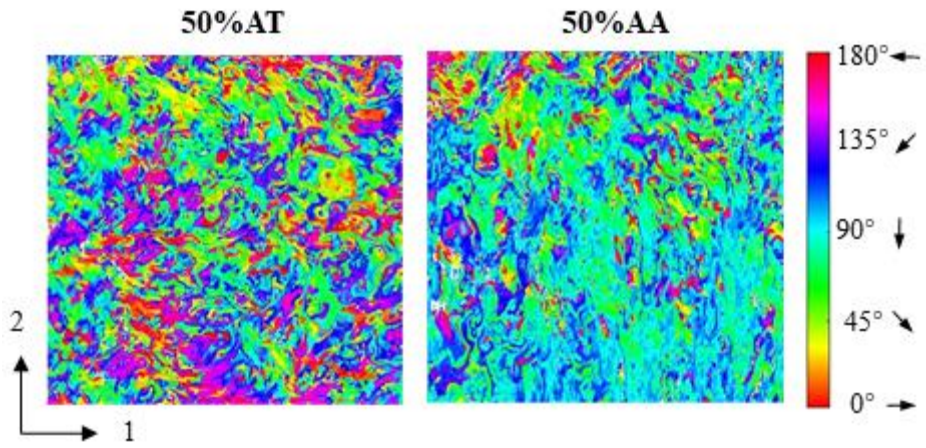

Figure 7-13: Fibre orientation distributions of the front subsurface of the 50%AT (left) and 50%AA (right) panels (from the upper left 200 × 200 mm section of the panels).

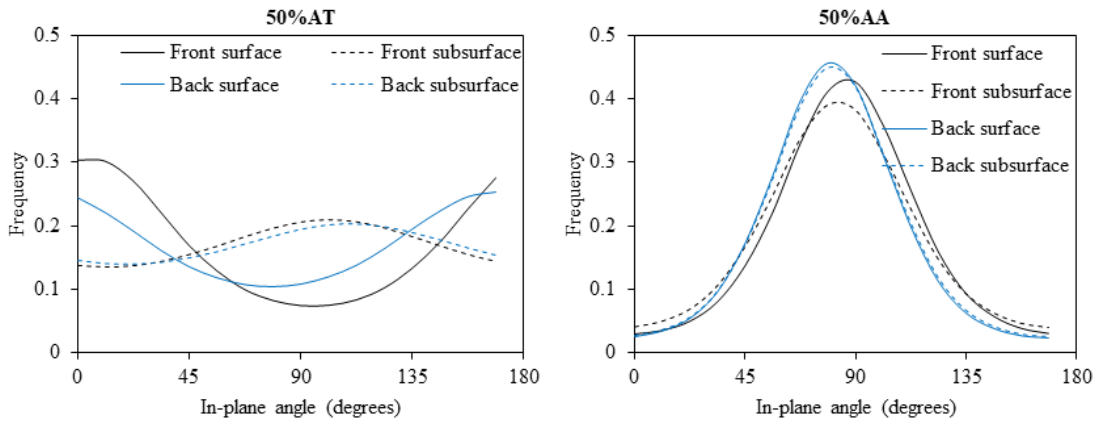

Figure 7-14: Probability density function curves for the in-plane fibre distributions taken from the surfaces and subsurfaces of the 50%AT (left) and 50%AA (right) panels.

Table 7-5: The calculated surface and subsurface orientation tensor components and statistical parameters for panels manufactured from linear charge flow (50%AT and 50%AA).

		50%AT				***50%AA***			
		Surface		Subsurface		Surface		Subsurface	
		Front	Back	Front	Back	Front	Back	Front	Back
Tensor components	a_{11}	0.667	0.600	0.449	0.463	0.226	0.221	0.258	0.225
	a_{22}	0.333	0.400	0.551	0.537	0.774	0.779	0.742	0.775
Statistical parameters	μ	5.0°	168.1°	101.4°	109.7°	86.1°	80.3°	82.9°	80.7°
	κ	0.720	0.446	0.224	0.192	1.336	1.480	1.157	1.440
	S	-0.067	0.055	-0.002	0.044	-0.011	0.058	0.030	0.022
	K	0.091	0.083	-0.093	-0.005	0.324	0.374	0.175	0.323

(μ – location parameter, κ – concentration parameter, S – skewness, K – kurtosis)

7.5 Chapter conclusions

In this chapter, the effects of initial charge coverage and preferential alignment on flow-induced fibre reorientation in carbon fibre SMC composites has been investigated experimentally using an image-based fibre orientation analysis technique and directional tensile testing. Flat panels were moulded from different configurations of initial charge coverage and preferential alignment at 30% fibre volume fraction. Greater charge flow, from the 25% initial charge coverage case, showed a significant improvement (up to 14%) in tensile strength and reduced anisotropy compared with the limited flow (100% coverage) case. Biases in the initial longitudinal alignment of fibres, and the corresponding effect on mechanical performance, were also significantly

altered by controlling and forcing particular directions of linear flow. In the case of aligning the flow direction with the initial orientation bias, directional stiffness and strength properties were maximised (56.69 GPa and 238.87 MPa respectively). Based on fibre orientation analysis of the exterior panel surfaces, as expected, the greatest fibre reorientation was seen in the areas of greatest mould flow. However, further subsurface (core) fibre orientation analysis also revealed significant edge effects and a stronger internal correlation with the initial orientation bias (and tensile anisotropy) than the flow-induced orientation phenomena observed at the exterior (skin) surfaces. Additionally, the application of circular statistical parameters has proven to be a useful alternative to tensor component analysis for the description of fibre orientation distributions, as it decouples the intensity and direction of any biases and shows greater sensitivity to any changes.

Chapter 8. Thesis conclusions

Discontinuous carbon fibre composites are becoming attractive options in automotive industries due to their high formability, lower cycle times (~5 minutes), and easy automation potential, thus providing cost efficient alternative. However, relatively lower mechanical performance compared to the conventional continuous fibre composites limits their application in demanding applications. The works in this thesis investigated different material, microstructural and process parameters on the mechanical performance of discontinuous fibre composites; to tailor and improve the achievable composite performance. Extensive experimental investigations have been carried out to characterise the influence of different parameters on the mechanical performance of this materials. In this chapter conclusions drawn from the current work towards improving discontinuous fibre composite properties are presented.

8.1 Size effects in carbon fibres

The tensile strength of carbon fibres is known to exhibit significant scattering resulting from inherent variability in flaw distribution during precursor treatment and handling processes. The number of critical flaws increase with the increase in volume, following Weibull distribution, resulting in reduced strength.

In this part of the work, the tensile strength of different grades of PAN- and pitch-based carbon fibres have been characterized. Laser diffraction-based measurement and SEM images were also used to study the correlation between geometric irregularity and tensile strength scattering. Some of the fibres studied showed significant geometric irregularity, deviation from assumed circular cross section which was referred as intra-

fibre diameter variability. High inter-fibre, from each batch of fibres, diameter variability has also been observed in both PAN- (4-7%) and pitch-based (8-10%) fibres. Fibres with high intra-fibre variability showed higher tensile strength scattering, which therefore required higher number of repeats to get statistically representative results. This was attributed to the observed geometric irregularity as they result in stress concentration which act as failure initiation sites.

Issues associated with traditional single fibre testing such as fibre misalignment and the use of mean cross-sectional area instead of individual fibre area for determining the tensile strength were also seen to affect the estimated Weibull parameters. Parameters determined from traditional method showed high correction factors against the more reliable and automated testing used in this study, up to 24% deviations in Weibull modulus and 7% correction factor in gauge length. In general, higher strength and modulus fibres (both PAN- and pitch-based) showed higher Weibull modulus, implying lower defect populations compared to the lower performance fibres. The strength variability increases with fibre length due to more critical flaws, thus, Weibull modulus decreases with increasing fibre length. Therefore, higher strength reduction was observed with increasing fibre length in fibres with lower Weibull modulus. However, this does not imply that shorter fibre length result in higher composite performance as other influencing parameters should also be considered.

8.2 Discontinuous fibre composites from high performance carbon fibres

Subsequently, discontinuous fibre composites were manufactured and tested from high modulus and high strength carbon fibres to investigate the achievable performance in practical applications. Experimental studies showed that increasing composite modulus

was observed with increasing fibre modulus. However, composite strength showed inconsistent trend with fibre strength where composites with higher fibre to matrix modulus ratio showed greater discrepancy with analytical prediction. This was due to high concentration of interfacial and normal stresses in composites with higher fibre matrix modulus ration.

Furthermore, meso-scale size effect has also been studied using analytical model superimposing micro-scale size effects from single fibre testing. All five fibres studied, showed a peak tow strength between 1.5 mm and 2 mm, beyond which a reduction in strength was observed due to the associated size effect at fibre level. Hence, fibres with lower Weibull modulus showed greater reduction in tow tensile strength with increasing tow length. Moreover, increasing composite strength was observed with increasing fibre length, reaching a peak at different fibre length for the different fibres. Fibres with lower Weibull modulus achieved peak composite strength at lower length (~50) than fibres with higher Weibull modulus (120 mm). In general, fibre length of 50 – 75 mm is recommended for most fibres as higher tensile strength was achieved in this range.

8.3 Fibre hybridisation effect

Growing environmental concern regarding their source and high material cost are challenges to large scale application of carbon fibre composites. Hybridisation with natural fibres is one effective way to address the challenges while retaining the useful properties of both. In the current study, the mechanical performance of carbon-jute fibre hybrid composite has also been investigated as eco-friendly material for high volume applications. The results showed that the jute-skinned (carbon-core) hybrid composite

resulted in slightly higher tensile properties due to the blocking effects. However, the carbon-skinned hybrid showed a 38% and 75% higher flexural stiffness and strength respectively than the jute-skinned hybrid. The jute-skinned hybrid showed greater damping performance, almost 50% higher, than carbon-skinned hybrids due to superior damping performance of the outer jute layers. Moreover, no improvement in damping performance was observed with increasing the jute fibre content in carbon-skinned hybrids due to the dependence of vibration energy dissipation on the outer most layers.

As each material configuration showed strengths and weaknesses, an evenly weighted cost-performance ratio of the composites has been used to evaluate the hybrids against the plain carbon and jute SMC composites. The CPR evaluation showed the plain jute fibre composites to be the best alternative (CPR - 27.65). However, considering the poor fire retardance and moisture resistance characteristics of jute fibre makes it unfeasible for many structural applications. Hence, the carbon-skinned hybrid (CPR - 3.03) offers a better combination of the evaluated properties than the pure carbon and jute-skinned hybrid SMC composites.

8.4 Residual properties of carbon fibre SMC composites

Low velocity impact and residual tensile and compressive strength of carbon fibre SMC composites have also been studied to determine the impact resistance and critical post-impact load case. In general, the impact response of the composites such as peak force, absorbed energy, damage size and dent depth showed significant sensitivity to composite thickness. Damage induced from lower energy impact were indiscernible from material variability, however, at higher energy (15 J) visible cracks and fibre breakage were observed. Consequently, low energy impacted samples showed no post-

impact strength reduction, while higher energy impacted samples showed a 25% and 16% reduction in compression and tension respectively. Thus, implying compression properties are more critical post-impact load cases for carbon fibre SMC composites. The correlation between impact damage region and post-impact failure initiation sites appeared to be stronger in compression than in tension.

8.5 Flow-induced fibre orientation in carbon fibre SMCs

The effect of charge coverage on the extent of flow-induced fibre alignment of carbon fibre SMC. Flat composite plaques were moulded from different charge coverages placed centrally in the mould. In panels manufactured from partial charge coverage, significant flow-induced fibre orientation towards radial flow direction was observed. Panels moulded from lower (25%) coverage resulted in near uniform fibre orientation distribution while panels of higher charge coverage retained the initial preferential alignment from the deposition process. Hence, greater charge flow, from 25% coverage, showed a significant improvement (up to 14%) in tensile strength and reduced anisotropy compared with the 100% coverage case. This is likely due to improved fibre impregnation during charge flow in lower charge coverage panels.

Moreover, panels moulded from highly aligned longer fibre tows exhibited greater resistance to flow-induced fibre alignment, thus, retaining more of their initial preferential alignment. Consequently, directional tensile properties showed greater anisotropy. By aligning the flow direction with the initial orientation bias, directional stiffness and strength properties were maximised (56.69 GPa and 238.87 MPa respectively at 30% volume fraction). Further subsurface (core) fibre orientation analysis also revealed significant edge effects and a stronger internal correlation with

the initial orientation bias (and tensile anisotropy) than the flow-induced orientation phenomena observed at the exterior (skin) surfaces.

8.6 Future work

From the works carried out in this thesis, the following valuable insights have been gained for future work towards performance improvement of discontinuous fibre composites.

1. The work on high performance discontinuous fibre composites from high performance carbon fibres showed poor fibre impregnation, hence subpar composite quality due to the higher viscosity resin used. Hence future extension of the work includes the use of directed fibre compounding (DFC) process with low viscosity resin for improved composite quality. This also allows exploring other sources of inconsistent trend in composite strength for increasing for increasing fibre strength.
2. From the high-performance fibres studied in the current study, the highest discrepancy with prediction was observed in fibres with high geometric irregularity, which affect the interfacial behaviour and load transfer efficiency. Thus, future work also includes characterization of the interfacial behaviour of the high-performance fibres.
3. Other works could include the use of liquid coupling agent for resin modification that simultaneously improve the interfacial strength and fibre impregnation thereby reducing the resin viscosity.

Appendix.A. Publications

The following conferences and journal papers have been produced as a result of the works carried out in this PhD project.

Conferences

1. Nega, B.F., Pierce, R.S., and Yi, X., 2020. Towards high-performance discontinuous fibre composites manufactured by automated fibre preforming. Oral presentation at the 29th Annual Conference – Beijing Adhesion Society.
2. Nega, B., Pierce, R.S., Yi, X. and Liu, X., 2022. Low Velocity Impact and Residual Strength Analysis of Carbon Fibre SMC Composites. In 20th European Conference on Composite Materials (pp. 263-270).
3. Nega, B., Pierce, R.S., Hu, Q., Yi, X. and Liu, X., 2023. In-mould flow and fibre orientation analysis of carbon fibre SMC composites. In the 23rd International Conference on Composite Materials.

Journal papers

1. Nega, B.F., Pierce, R.S., Liu, L., Yi, X. and Liu, X., 2022. Fibre alignment and mechanical performance of carbon fibre Sheet Moulding Compounds under different preform compaction. Journal of Reinforced Plastics and Composites, 41(13-14), pp.517-525.
2. Nega, B.F., Pierce, R.S., Yi, X. and Liu, X., 2022. Characterization of Mechanical and Damping Properties of Carbon/Jute Fibre Hybrid SMC Composites. Applied Composite Materials, 29(4), pp.1637-1651.

3. Nega, B., Pierce, R.S., Yi, X. and Liu, X., 2023. Experimental analysis of flow-induced fibre orientation during compression moulding of carbon fibre SMCs. In Composites Part A (submitted, under review).
4. Nega, B., Pierce, R.S., Liu, X., Yi, X., Harper, L.T., Warrior, N.A. Tensile strength characterisation of high-performance PAN- and Pitch-based Carbon Fibres for Sheet Moulding Compound Applications. (in preparation)

References

[1] "The Paris Agreement, Paris," *United Nations Framew. Conv. Clim. Chang.*, 2016.

[2] World Health Organization (WHO), "Climate impacts." https://www.who.int/sustainable-development/transport/health-risks/climate-impacts/en/

[3] "More cars are now sold in China than in America," *Econ. https//www.economist.com/news/2009/10/23/motoring-ahead*, [Online]. Available: https://www.economist.com/news/2009/10/23/motoring-ahead

[4] B. Srivari, "China: The World's Largest Automobile Market," *https://nolasia.net/the-worlds-largest-automobile-market/*, [Online]. Available: https://nolasia.net/the-worlds-largest-automobile-market/

[5] H. Hui and B. Anup, "Passenger car fuel-efficiency , 2020 – 2025," *Int. Coucil Clean Transp.*, pp. 2020–2025, 2013.

[6] P. Mock, "Emission Standards for Passenger Cars and Light-Commercial Vehicles in the European Union," *ICCT Policy Updat.*, no. January 2019, 2019, [Online]. Available: http://www.europarl.europa.eu/news/en/press-room/20181218IPR22101/curbing-co2-

[7] A. O. Akii Ibhadode and R. S. Ebhojiaye, "A New Lightweight Material for Possible Engine Parts Manufacture," *Futur. Intern. Combust. Engines*, pp. 1–19, 2019, doi: 10.5772/intechopen.82268.

[8] P. Brady, “The road to lightweight performance,” *Reinf. Plast.*, vol. 52, no. 10, pp. 32–36, 2008, doi: 10.1016/S0034-3617(08)70373-4.

[9] C. Caffrey, K. Bolon, G. Kolwich, R. Johnston, and T. Shaw, “Cost-Effectiveness of a Lightweight Design for 2020-2025: An Assessment of a Light-Duty Pickup Truck,” *SAE Tech. Pap.*, vol. 2015-April, no. April, 2015, doi: 10.4271/2015-01-0559.

[10] R. Roth, J. Clark, and A. Kelkar, “Automobile bodies: Can aluminum be an economical alternative to steel?,” *Jom*, vol. 53, no. 8, pp. 28–32, 2001, doi: 10.1007/s11837-001-0131-7.

[11] J. Marks and C. Bayliss, “Aluminum-meeting the challenges of climate change,” *Jom*, vol. 62, no. 8. pp. 33–36, 2010. doi: 10.1007/s11837-010-0122-7.

[12] S. Das, “Life cycle assessment of carbon fiber-reinforced polymer composites,” *Int. J. Life Cycle Assess.*, vol. 16, no. 3, pp. 268–282, 2011, doi: 10.1007/s11367-011-0264-z.

[13] D. Brosius, “Carbon Fiber: The Automotive Material of the Twenty-First Century Starts Fulfilling the Promise,” *3rd Annu. Soc. Plast. Eng. Automot. Compos. Conf. Expo.*, pp. 1–7, 2003, [Online]. Available: http://speautomotive.com/SPEA_CD/SPEA2003/pdf/f01.pdf

[14] M. Pervaiz, S. Panthapulakkal, B. KC, M. Sain, and J. Tjong, “Emerging Trends in Automotive Lightweighting through Novel Composite Materials,”

Mater. Sci. Appl., vol. 07, no. 01, pp. 26–38, 2016, doi: 10.4236/msa.2016.71004.

[15] Huntsman, "Araldite® composite solutions provide fast curing where high productivity is required," *https://www.huntsman-transportation.com/automotive-composites/body-in-white.html*, [Online]. Available: https://www.huntsman-transportation.com/automotive-composites/body-in-white.html

[16] Dow Automotive Systems, "VORAFORCE™ 5300 ultra-fast cure composite epoxy system", [Online]. Available: http://msdssearch.dow.com/PublishedLiteratureDOWCOM/dh_093d/0901b8038093d4dd.pdf?filepath=automotive/pdfs/noreg/299-52107.pd&fromPage=GetDoc

[17] Hexion, "Technical Data Sheet Epoxy Resin, EPIKOTE™ Resin 05475 and EPIKURE™ Curing Agent 05500 and HELOXY™ Additive 112," vol. 44, no. 0, pp. 1–3, 2000.

[18] Plastics Today, "Cytec automotive solutions include hot compression-molded carbon fiber reinforced door inner structure," *Https://www.plasticstoday.com/content/cytec-automotive-solutions-include-hot-compression-molded-carbon-fiber-reinforced-door-inner/2536486423463*, [Online]. Available: https://www.plasticstoday.com/content/cytec-automotive-solutions-include-hot-compression-molded-carbon-fiber-reinforced-door-inner/2536486423463

[19] Hexcel, “HexPly® Snap-Cure,” *https://www.hexcel.com/Products/HexPly-Snap-Cure*.

[20] “CSP VICTALL Receives Prestigious JEC Innovation Award | Business Wire.” https://www.businesswire.com/news/home/20190919005475/en/ (accessed Jan. 24, 2020).

[21] “Ford Focus To Use Composite Door Module Carrier.” https://fordauthority.com/2019/10/ford-focus-to-use-composite-door-module-carrier/ (accessed Jan. 24, 2020).

[22] “China’s Kangde Composites and BAIC Motor sign carbon fiber auto parts production order | JEC Group.” http://www.jeccomposites.com/knowledge/international-composites-news/china’s-kangde-composites-and-baic-motor-sign-carbon-fiber (accessed Jan. 25, 2020).

[23] “Sierra CarbonPro Bed: Innovation & Durability | GMC Life.” https://www.gmc.com/gmc-life/news/carbonpro-delivers-innovation-durability (accessed Jan. 25, 2020).

[24] “Voith unveils fully digital production line for Audi A8 carbon fiber rear wall panel | JEC Group.” http://www.jeccomposites.com/knowledge/international-composites-news/voith-unveils-fully-digital-production-line-audi-a8-carbon (accessed Jan. 25, 2020).

[25] “BMW i3: CFRP Life Module Vehicle Structure - MarkLines Automotive Industry Portal.”

https://www.marklines.com/en/report_all/Munro001_201704#report_area_2 (accessed Jan. 25, 2020).

[26] D. H. J. A. Lukaszewicz, C. Ward, and K. D. Potter, “The engineering aspects of automated prepreg layup: History, present and future,” *Compos. Part B Eng.*, vol. 43, no. 3, pp. 997–1009, 2012, doi: 10.1016/j.compositesb.2011.12.003.

[27] P. Feraboli, E. Peitso, F. Deleo, T. Cleveland, and P. B. Stickler, “Characterization of prepreg-based discontinuous carbon fiber/epoxy systems,” *J. Reinf. Plast. Compos.*, vol. 28, no. 10, pp. 1191–1214, 2009, doi: 10.1177/0731684408088883.

[28] Z. Xiao, “Advancements in discontinuous carbon fibre composite technologies for high- volume manufacturing processes,” Doctoral dissertation, University of Nottingham, 2018.

[29] C. C. Qian, “Structural optimisation of Structural Optimisation of Discontinuous Carbon Fibre Composites,” PhD Thesis, University of Nottingham, 2014.

[30] A. D. Evans, C. C. Qian, T. A. Turner, L. T. Harper, and N. A. Warrior, “Flow characteristics of carbon fibre moulding compounds,” *Compos. Part A Appl. Sci. Manuf.*, vol. 90, pp. 1–12, 2016, doi: 10.1016/j.compositesa.2016.06.020.

[31] M. Bruderick, D. Denton, M. Shinedling, and M. Kiesel, “Applications of carbon fiber SMC for the Dodge Viper,” *Proc. Second S.P.E. Automot. Compos. Conf. Exhib.*, 2002.

[32] “ASTAR Carbon Fibre SMC for Multifunctional Spare Wheel Pan of Mercedes-AMG E-Class | LinkedIn.” https://www.linkedin.com/pulse/astar-carbon-fibre-smc-multifunctional-spare-wheel-pan-astar-s-a-/ (accessed Jan. 26, 2020).

[33] “Lamborghini Wins the Innovation Award at the JEC Composites 2016.” https://www.thenewsmarket.com/news/lamborghini-wins-the-innovation-award-at-the-jec-composites-2016/s/b1242657-a1b5-41b9-be5b-fe9217ba42b5 (accessed Jan. 26, 2020).

[34] “Forged Composite: Tech. Department - Car and Driver.” https://www.caranddriver.com/features/a15124795/forged-composite-tech-department/ (accessed Jan. 27, 2020).

[35] “Toyota using Mitsubishi Rayon’s carbon fiber SMC for hatch door frame of new Prius PHV - Green Car Congress.” https://www.greencarcongress.com/2017/04/20170424-mrc.html (accessed Jan. 27, 2020).

[36] R. N. Yancey, *Challenges, Opportunities, and Perspectives on Lightweight Composite Structures: Aerospace Versus Automotive*. Elsevier Ltd, 2016. doi: 10.1016/B978-1-78242-325-6.00002-5.

[37] L. T. Harper, “Discontinuous Carbon Fibre Composites for Automotive Applications,” PhD Thesis, University of Nottingham, 2006.

[38] L. T. Harper, T. A. Turner, N. A. Warrior, J. S. Dahl, and C. D. Rudd, “Characterisation of random carbon fibre composites from a directed fibre

preforming process: Analysis of microstructural parameters," *Compos. Part A Appl. Sci. Manuf.*, vol. 37, no. 11, pp. 2136–2147, 2006, doi: 10.1016/j.compositesa.2005.11.014.

[39] U. Vaidya, "Composites for Automotive, Truck and Mass Transit: Materials, Design, Manufacturing," p. 419, 2011, [Online]. Available: http://books.google.com/books?id=1IgDOTSha9MC&pgis=1

[40] P. Feraboli, T. Cleveland, M. Ciccu, P. Stickler, and L. DeOto, "Defect and damage analysis of advanced discontinuous carbon/epoxy composite materials," *Compos. Part A Appl. Sci. Manuf.*, vol. 41, no. 7, pp. 888–901, 2010, doi: 10.1016/j.compositesa.2010.03.002.

[41] G. Kirupanantham, "Characterisation of discontinuous carbon fibre preforms for automotive applications," PhD Thesis, University of Nottingham, 2013. doi: 10.1016/j.geoforum.2013.12.005.

[42] J. E. Lindhagen and L. A. Berglund, "Application of bridging-law concepts to short-fibre compositesPart 2: Notch sensitivity," *Compos. Sci. Technol.*, vol. 60, no. 6, pp. 885–893, 2000, doi: 10.1016/S0266-3538(99)00109-8.

[43] A. D. Evans, L. T. Harper, T. A. Turner, and N. A. Warrior, "Joint design of continuous/discontinuous hybrid carbon fibre composites," *ICCM Int. Conf. Compos. Mater.*, vol. 2017-Augus, no. April 2018, 2017.

[44] H. He and F. Gao, "Effect of Fiber Volume Fraction on the Flexural Properties of Unidirectional Carbon Fiber / Epoxy Composites," *Int. J. Polym. Anal.*

Charact., vol. 20, no. 2, pp. 180–189, 2015, doi: 10.1080/1023666X.2015.989076.

[45] S. Louis, "Strength of Short-Fiber Reinforced Composites," *Polym. Eng. Sci.*, vol. 12, no. 1, 1972.

[46] "Effective Moduli of Random Short Fiber Composite : A Probabilistic Study," vol. 23, no. 7, pp. 751–760, 2015, doi: 10.1177/0731684404032866.

[47] L. T. Harper, C. C. Qian, R. Luchoo, and N. A. Warrior, "3D geometric modelling of discontinuous fibre composites using a force-directed algorithm," *J. Compos. Mater.*, vol. 51, no. 17, pp. 2389–2406, 2017, doi: 10.1177/0021998316672722.

[48] R. Luchoo, L. T. Harper, M. D. Bond, N. A. Warrior, and A. Dodworth, "Net shape spray deposition for compression moulding of discontinuous fibre composites for high performance applications," *Plast. rubber Compos.*, vol. 39, no. 3–5, pp. 216–231, 2010, doi: 10.1179/174328910X12647080902493.

[49] A. Endruweit, L. T. Harper, T. A. Turner, N. A. Warrior, and A. C. Long, "Composites : Part A Random discontinuous carbon fibre preforms : Permeability modelling and resin injection simulation," vol. 39, pp. 1660–1669, 2008, doi: 10.1016/j.compositesa.2008.07.006.

[50] A. Endruweit, F. Gommer, and A. C. Long, "Composit es : Part A Stochastic analysis of fibre volume fraction and permeability in fibre bundles with random filament arrangement," *Compos. Part A*, vol. 49, pp. 109–118, 2013, doi: 10.1016/j.compositesa.2013.02.012.

[51] M. Such, C. Ward, and K. Potter, “Aligned Discontinuous Fibre Composites : A Short History,” vol. 3, no. 2014, pp. 155–168, 2020, doi: 10.12783/issn.2168-4286/2/3/4/Such.

[52] S. H. Sunny, Tom; Pickering, Kim L; Lim, “Alignment of Short Fibres : An Overview,” *Process. Fabr. Adv. Mater.*, pp. 616–625, 2017.

[53] H. Yu, K. D. Potter, and M. R. Wisnom, “A novel manufacturing method for aligned discontinuous fibre composites (High Performance-Discontinuous Fibre method),” vol. 65, pp. 175–185, 2014, doi: 10.1016/j.compositesa.2014.06.005.

[54] M. L. Ericson and L. A. Berglund, “Processing and mechanical properties of orientated preformed glass-mat-reinforced thermoplastics,” *Compos. S,* vol. 49, pp. 121–130, 1993.

[55] Murty N. Vyakarnam; Lawrence T. Drzal, “Composites Material of Aligned Discontinuous Fibers,” *U.S. Pat. No. 6,025,285.*, no. 19, 2000.

[56] L. T. Harper, T. A. Turner, J. R. B. Martin, and N. A. Warrior, “Fiber alignment in directed carbon fiber preforms - A feasibility study,” *J. Compos. Mater.*, vol. 43, no. 1, pp. 57–74, 2009, doi: 10.1177/0021998308098151.

[57] J. L. M. L. Longana, H. Yu, T. R. Pozegic, S. Huntley, T. Rendall, K. D. Potter, and and I. Hamerton, “Quasi-Isotropic and Pseudo-Ductile Highly Aligned Discontinuous Fibre Composites Manufactured with the HiPerDiF (High Performance Discontinuous Fibre) Technology,” vol. 12, 2019.

[58] L. S. Sutherland, R. A. Shenoi, and S. M. Lewis, “Size and scale effects in composites: I. Literature review,” *Compos. Sci. Technol.*, vol. 59, no. 2, pp. 209–220, 1999, doi: 10.1016/S0266-3538(98)00065-7.

[59] I. J. Beyerlein and S. L. Phoenix, “Statistics for the strength and size effects of microcomposites with four carbon fibers in epoxy resin,” *Compos. Sci. Technol.*, vol. 56, no. 75–92, 1996.

[60] T. H. Ning Pan, Shumin Zhao, “Relationship Between Scale Effect and Structure Levels in Fibrous Structures,” *Polym. Compos.*, vol. 21, no. 2, pp. 187–196, 2000.

[61] W. Weibull, “A Statistical Theory of the Strength of Materials. Generalstabens Litografiska Anstalts Förlag, Stockholm,” *Gen. litografiska anstalts förlag*, 1939.

[62] F. W. J. Van Hattum and C. A. Bernardo, “Model to predict the strength of short fiber composites,” *Polym. Compos.*, vol. 20, no. 4, pp. 524–533, 1999, doi: 10.1002/pc.10376.

[63] F. C. Campbell, *Structural Composite Materials*. ASM international.

[64] L. T. Harper, T. A. Turner, N. A. Warrior, and C. D. Rudd, “Characterisation of random carbon fibre composites from a directed fibre preforming process: The effect of fibre length,” *Compos. Part A Appl. Sci. Manuf.*, vol. 38, no. 3, pp. 755–770, 2005, doi: 10.1016/j.compositesa.2006.09.008.

[65] A.Kelly; W.R. Tyson, “Tensile Properties of Fibre-Reinforced Metals: Copper/Tungsten and Copper/Molybdenum,” *J. Mech. Phys. Solids*, vol. 13, pp. 329–350, 1965.

[66] H. L. Cox, “The elasticity and strength of paper and other fibrous materials,” *Br. J. Appl. Phys.*, vol. 3, no. 3, pp. 72–79, 1952, doi: 10.1088/0508-3443/3/3/302.

[67] A. H. Cottrell and P. R. S. L. A, “Strong Solids,” in *Mathematical and Physical Sciences 282, no. 1388*, 1964, pp. 2–9. doi: 10.1098/rspa.1964.0206.

[68] L. T. Harper, D. T. Burn, M. S. Johnson, and N. A. Warrior, “Long discontinuous carbon fibre/polypropylene composites for high volume structural applications,” PhD Thesis, University of Nottingham, 2018. doi: 10.1177/0021998317722204.

[69] K. S. Kumar, C. R. Nair, and K. N. Ninan., “Effect of fiber length and composition on mechanical properties of carbon fiber-reinforced polybenzoxazine,” *Polym. Adv. Technol.*, vol. 19, pp. 895–904, 2008.

[70] E. Masoumy; L. Kacir; J. L. Kardos, “Effect of Fiber-Aspect Ratio and Orientation on the Stress-Strain Behavior of Aligned, Short-FiberReinforced, Ductile Epoxy,” *Polym. Compos.*, vol. 4, no. 1, pp. 64–73, 1983.

[71] G. C. Jacob, J. M. Starbuck, J. F. Fellers, and S. Simunovic, “Effect of fiber volume fraction, fiber length and fiber tow size on the energy absorption of chopped carbon fiber-polymer composites,” *Polym. Compos.*, vol. 26, no. 3, pp. 293–305, 2005, doi: 10.1002/pc.20100.

[72] J. L. Thomason and M. A. Vlug, “Influence of fibre length and concentration on the properties of glass fibre-reinforced polypropylene: 4. Impact properties,” *Compos. Part A Appl. Sci. Manuf.*, vol. 28, no. 3, pp. 277–288, 1997, doi: 10.1016/S1359-835X(96)00127-3.

[73] F. Rezaei, R. Yunus, and N. A. Ibrahim, “Effect of fiber length on thermomechanical properties of short carbon fiber reinforced polypropylene composites,” *Mater. Des.*, vol. 30, no. 2, pp. 260–263, 2009, doi: 10.1016/j.matdes.2008.05.005.

[74] L. T. Harper, T. A. Turner, N. A. Warrior, and C. D. Rudd, “Characterisation of random carbon fibre composites from a directed fibre preforming process: The effect of tow filamentisation,” *Compos. Part A Appl. Sci. Manuf.*, vol. 38, no. 3, pp. 755–770, 2007, doi: 10.1016/j.compositesa.2006.09.008.

[75] M. R. Piggott, “Mesostructures and their mechanics in fibre composites,” *Adv. Compos. Mater. Off. J. Japan Soc. Compos. Mater.*, vol. 6, no. 1, pp. 75–81, 1996, doi: 10.1163/156855196x00211.

[76] J. M. Starbuck and L. B. Cataquiz, “Evaluation of large tow-size carbon fiber for reducing the cost of CNG storage tanks,” *SAE Tech. Pap.*, no. 724, 2000, doi: 10.4271/2000-01-1526.

[77] A. Endruweit, L. T. Harper, T. A. Turner, N. A. Warrior, and A. C. Long, “Random Discontinuous Carbon Fiber Preforms: Experimental Permeability Characterization and Local Modeling,” *Polym. Compos.*, vol. 31, no. 4, pp. 569–580, 2010, doi: 10.1002/pc.

[78] R. Harikrishnan, P. M. Mohite, and C. S. Upadhyay, “Generalized Weibull model-based statistical tensile strength of carbon fibres,” *Arch. Appl. Mech.*, vol. 88, no. 9, pp. 1617–1636, 2018, doi: 10.1007/s00419-018-1391-9.

[79] K. Naito, Y. Tanaka, J. Yang, and Y. Kagawa, “Tensile properties of ultrahigh strength PAN-based , ultrahigh modulus pitch-based and high ductility pitch-based carbon fibers,” *Carbon N. Y.*, vol. 46, no. 2, pp. 189–195, 2007, doi: 10.1016/j.carbon.2007.11.001.

[80] N. Saha, A. N. Banerjee, and B. C. Mitra, “Tensile behaviour of unidirectional laminates polyethylene-glass fibres/PMMA,” vol. 37, no. 4, pp. 699–701, 1996.

[81] S. Mishra, A. K. Mohanty, L. T. Drzal, M. Misra, and S. Parija, “Studies on mechanical performance of biofibre / glass reinforced polyester hybrid composites,” *Compos. Sci. Technol.*, vol. 63, no. 10, pp. 1377–1385, 2003, doi: 10.1016/S0266-3538(03)00084-8.

[82] R. J. Muhi, F. Najim, and M. F. S. F. De Moura, “The effect of hybridization on the GFRP behavior under high velocity impact,” *Compos. Part B*, vol. 40, no. 8, pp. 798–803, 2009, doi: 10.1016/j.compositesb.2009.08.002.

[83] Y. Swolfs, L. Gorbatikh, and I. Verpoest, “Fibre hybridisation in polymer composites: A review,” *Compos. Part A Appl. Sci. Manuf.*, vol. 67, pp. 181–200, 2014, doi: 10.1016/j.compositesa.2014.08.027.

[84] P. W. Manders and M. G. Bader, “The strength of hybrid glass/carbon fibre composites Part 2 A statistical model,” *J. Mater. Sci.*, vol. 16, pp. 2246–2256, 1981.

[85] H. Yu, M. L. Longana, M. Jalalvand, M. R. Wisnom, and K. D. Potter, "Pseudo-ductility in intermingled carbon/glass hybrid composites with highly aligned discontinuous fibres," *Compos. Part A Appl. Sci. Manuf.*, vol. 73, pp. 35–44, 2015, doi: 10.1016/j.compositesa.2015.02.014.

[86] M. Cabrera-rı and N. Leo, "An Economical Way of Using Carbon Fibers in Sheet Molding Compound Compression Molding for Automotive Applications," *Polym. Compos.*, vol. 37, no. 1, pp. 915–924, 2016, doi: 10.1002/pc.

[87] S. N. A. Safri, M. T. H. Sultan, M. Jawaid, and K. Jayakrishna, "Impact behaviour of hybrid composites for structural applications: A review," *Compos. Part B Eng.*, vol. 133, pp. 112–121, 2018, doi: 10.1016/j.compositesb.2017.09.008.

[88] K. L. Pickering, M. G. A. Efendy, and T. M. Le, "A review of recent developments in natural fibre composites and their mechanical performance," *Compos. Part A Appl. Sci. Manuf.*, vol. 83, pp. 98–112, 2016, doi: 10.1016/j.compositesa.2015.08.038.

[89] J. Yang, J. Xiao, J. Zeng, L. Bian, C. Peng, and F. Yang, "Matrix modification with silane coupling agent for carbon fiber reinforced epoxy composites," *Fibers Polym.*, vol. 14, no. 5, pp. 759–766, 2013, doi: 10.1007/s12221-013-0759-2.

[90] K. H. Wong, D. S. Mohammed, S. J. Pickering, and R. Brooks, "Effect of coupling agents on reinforcing potential of recycled carbon fibre for

polypropylene composite," *Compos. Sci. Technol.*, vol. 72, no. 7, pp. 835–844, 2012, doi: 10.1016/j.compscitech.2012.02.013.

[91] D. T. Burn, L. T. Harper, M. Johnson, N. A. Warrior, L. Yang, and J. Thomason, "The influence of coupling agent, fibre sizing and matrix degradation on the interfacial shear strength between carbon fibre and polypropylene," in *16th European Conference on Composite Materials*, 2014, no. June, pp. 22–26.

[92] D. T. Burn, "Long Discontinuous Carbon Fibre / Polypropylene Composites for High Volume Automotive Applications," PhD Thesis, University of Nottingham, 2016.

[93] A. Arbelaiz, B. Fernández, G. Cantero, R. Llano-Ponte, A. Valea, and I. Mondragon, "Mechanical properties of flax fibre/polypropylene composites. Influence of fibre/matrix modification and glass fibre hybridization," *Compos. Part A Appl. Sci. Manuf.*, vol. 36, no. 12, pp. 1637–1644, 2005, doi: 10.1016/j.compositesa.2005.03.021.

[94] Q. Zhang, X. Li, S. Liang, X. Zhao, G. Sui, and X. Yang, "A kind of liquid-like MWCNT reinforcements for T1000 carbon fibre filament winding composites," *Compos. Sci. Technol.*, vol. 131, pp. 89–97, 2016, doi: 10.1016/j.compscitech.2016.06.004.

[95] L. M. Martulli, L. Muyshondt, M. Kerschbaum, S. Pimenta, S. V. Lomov, and Y. Swolfs, "Carbon fibre sheet moulding compounds with high in-mould flow: Linking morphology to tensile and compressive properties," *Compos. Part A*

Appl. Sci. Manuf., vol. 126, no. August, p. 105600, 2019, doi: 10.1016/j.compositesa.2019.105600.

[96] C. Nony-Davadie, L. Peltier, Y. Chemisky, B. Surowiec, and F. Meraghni, "Mechanical characterization of anisotropy on a carbon fiber sheet molding compound composite under quasi-static and fatigue loading," *J. Compos. Mater.*, vol. 53, no. 11, pp. 1437–1457, 2019, doi: 10.1177/0021998318804612.

[97] S. C. Tseng and T. A. Osswald, "Prediction of Shrinkage and Warpage of Fiber Reinforced Thermoset Composite Parts," *J. Reinf. Plast. Compos.*, vol. 13, no. 8, pp. 698–721, 1994, doi: 10.1177/073168449401300803.

[98] H. Kikuchi and K. Koyama, "Warpage, anisotropy, and part thickness," *Polym. Eng. Sci.*, vol. 36, no. 10, pp. 1326–1335, 1996, doi: 10.1002/pen.10527.

[99] S. F. Kite *et al.*, "Effect of charge placement on fibre orientation, distortion and failure of a carbon fibre reinforced sheet moulding compound," *ECCM 2018 - 18th Eur. Conf. Compos. Mater.*, no. June, pp. 24–28, 2020.

[100] B. F. Nega, R. S. Pierce, L. Liu, X. Yi, and X. Liu, "Fibre alignment and mechanical performance of carbon fibre Sheet Moulding Compounds under different preform compaction," *J. Reinf. Plast. Compos.*, 2022, doi: 10.1177/07316844211066637.

[101] M. S. A. Rahaman, A. F. Ismail, and A. Mustafa, "A review of heat treatment on polyacrylonitrile fiber," *Polym. Degrad. Stab.*, vol. 92, no. 8, pp. 1421–1432, 2007, doi: 10.1016/j.polymdegradstab.2007.03.023.

[102] S. Soulis, G. Konstantopoulos, E. P. Koumoulos, and C. A. Charitidis, “Impact of alternative stabilization strategies for the production of PAN-based carbon fibers with high performance,” *Fibers*, vol. 8, no. 6, 2020, doi: 10.3390/FIB8060033.

[103] H. D. Wagner, “Statistical Concepts in the Study of Fracture Properties of Fibres and Composites,” *Compos. Mater. Ser.*, vol. 6, no. C, pp. 39–77, 1989, doi: 10.1016/B978-0-444-87286-9.50006-1.

[104] W. J. Padgett, S. D. Durham, and A. M. Mason, “Weibull Analysis of the Strength of Carbon Fibers Using Linear and Power Law Models for the Length Effect,” *J. Compos. Mater.*, vol. 29, no. 14, pp. 1873–1884, 1995, doi: 10.1177/002199839502901405.

[105] E. G. Stoner, D. D. Edie, and S. D. Durham, “An end-effect model for the single-filament tensile test,” *J. Mater. Sci.*, vol. 29, no. 24, pp. 6561–6574, 1994, doi: 10.1007/BF00354022.

[106] W. Weibull, *A statistical theory of strength of materials. Ingeniorsvetenscapsakademien*. Generalstabens litografiska anstalts förlag:Stockholm, 1939.

[107] A. H. Cottrell and P. R. S. L. A, “Strong Solids,” in *Proceedings of the Royal Society of London Series A. Mathematical and Physical Sciences 282, no. 1388*, 1964, pp. 2–9. doi: 10.1098/rspa.1964.0206.

[108] ASTM D4018, “Standard Test Methods for Properties of Continuous Filament Carbon and Graphite Fiber Tows,” 2011.

[109] J. Crabtree, D. Penumadu, and S. Young, “Tensile properties of carbon fiber: Single filament vs tow based testing,” *32nd Tech. Conf. Am. Soc. Compos. 2017*, vol. 3, pp. 1538–1549, 2017, doi: 10.12783/asc2017/15290.

[110] K. Naito, J. M. Yang, Y. Tanaka, and Y. Kagawa, “The effect of gauge length on tensile strength and Weibull modulus of polyacrylonitrile (PAN)- and pitch-based carbon fibers,” *J. Mater. Sci.*, vol. 47, no. 2, pp. 632–642, 2012, doi: 10.1007/s10853-011-5832-x.

[111] T. Okabe and N. Takeda, “Size effect on tensile strength of unidirectional CFRP composites experiment and simulation,” *Compos. Sci. Technol.*, vol. 62, no. 15, pp. 2053–2064, 2002, doi: 10.1016/S0266-3538(02)00146-X.

[112] G. Bogoeva-Gaceva, E. Mäder, L. Haüssler, and A. Dekanski, “Characterization of the surface and interphase of plasma-treated HM carbon fibres,” *Compos. Part A Appl. Sci. Manuf.*, vol. 28, no. 5, pp. 445–452, 1997, doi: 10.1016/S1359-835X(96)00143-1.

[113] W. Y. Jiangwei Yao, “Tensile Strength and Its Variation for PAN-Based Carbon Fibers. II. Calibration of the Variation from Testing,” *J. Appl. Polym. Sci.*, vol. 104, pp. 2625–2632, 2007, doi: 10.1002/app.

[114] U. Genschel and W. Q. Meeker, “A comparison of maximum likelihood and median-rank regression for Weibull estimation,” *Qual. Eng.*, vol. 22, no. 4, pp. 236–255, 2010, doi: 10.1080/08982112.2010.503447.

[115] ISO-11566, “Carbon fibre - Determination of the tensile properties of single-filament specimens,” 1996.

[116] F. Vautard, J. Dentzer, M. Nardin, J. Schultz, and B. Defoort, “Influence of surface defects on the tensile strength of carbon fibers,” *Appl. Surf. Sci.*, vol. 322, pp. 185–193, 2014, doi: 10.1016/j.apsusc.2014.10.066.

[117] Z. Xu *et al.*, “Surface characteristics of kidney and circular section carbon fibers and mechanical behavior of composites,” *Mater. Chem. Phys.*, vol. 106, no. 1, pp. 16–21, 2007, doi: 10.1016/j.matchemphys.2007.04.059.

[118] V. E. Gonsalves, “Determination of Denier and Strength of Single Filaments by Vibroscope and Heim Tensile Tester,” *Text. Res. J.*, vol. 17, no. 7, pp. 369–375, 1947, doi: 10.1177/004051754701700703.

[119] E. M. Moore, R. L. Shambaugh, and D. V. Papavassiliou, “Ensemble Laser Diffraction for Online Measurement of Fiber Diameter Distribution during the Melt Blowing Process,” *Int. Nonwovens J.*, vol. os-13, no. 2, pp. 1558925004os–13, 2004, doi: 10.1177/1558925004os-1300212.

[120] J. J. Huether and W. V. Liebig, “Investigations of the carbon fibre cross-sectional areas and their non-circularities by means of laser diffraction,” *IOP Conf. Ser. Mater. Sci. Eng.*, vol. 942, no. 1, 2020, doi: 10.1088/1757-899X/942/1/012034.

[121] F. W. J. Van Hattum, “A study of the Mechanical Properties of Vapour Grown Carbon Fibres and Carbon Fibre-Thermoplastic Composites,” Universidade do Minho - PhD Thesis, 1999. [Online]. Available: http://repositorium.sdum.uminho.pt/handle/1822/282

[122] Y. Li, “The effect of variability in the microstructure of tow-based discontinuous composites on their structural behaviour,” Doctoral Thesis - Imperial College London, 2018.

[123] Toraycma, “T700S data sheet,” *[Material Technical Data sheet]*. https://www.toraycma.com/wp-content/uploads/T700S-Technical-Data-Sheet-1.pdf.pdf (accessed Aug. 15, 2021).

[124] Grafil Inc., “PYROFIL™ TR50S 12K data sheet,” *[Material Technical Data sheet]*. https://www.rockwestcomposites.com/media/downloads/TR50S_12K-14002_Fiber.pdf (accessed Aug. 15, 2021).

[125] J. Aubry, “HexMC - Bridging the gap between prepreg and SMC,” *Reinf. Plast.*, vol. 45, no. 6, pp. 38–40, 2001, doi: 10.1016/S0034-3617(01)80207-1.

[126] W. Chen, Y. Yu, P. Li, C. Wang, T. Zhou, and X. Yang, “Effect of new epoxy matrix for T800 carbon fiber/epoxy filament wound composites,” *Compos. Sci. Technol.*, vol. 67, no. 11–12, pp. 2261–2270, 2007, doi: 10.1016/j.compscitech.2007.01.026.

[127] J. D. H. Hughes, “The carbon fibre/epoxy interface-A review,” *Compos. Sci. Technol.*, vol. 41, no. 1, pp. 13–45, 1991, doi: 10.1016/0266-3538(91)90050-Y.

[128] T. F. MacLaughlin and R. M. Barker, “Effect of modulus ratio on stress near a discontinuous fiber,” *Exp. Mech.*, vol. 12, no. 4, pp. 178–183, 1972, doi: 10.1007/bf02330270.

[129] and G. B. Rondeau, R., S.R. Reeve, “The effect of tows and filament groups on the properties of discontinuous fiber composites,” *44th Int. SAMPE Symp. Exhib.*, 1999.

[130] T. J. Reinhart, “The potential of oriented, discontinuous carbon fiber preforms for low cost high performance aerospace structures,” *SAMPE-ACCE-DOE Adv. Compos. Conf. Proceedings(USA)*, pp. 1–44, 1999.

[131] H. Krenchel, “Fibre reinforcement; theoretical and practical investigations of the elasticity and strength of fibre-reinforced materials,” Technical University of Denmark, 1964.

[132] P. T. Curtis, M. G. Bader, and J. E. Bailey, “The stiffness and strength of a polyamide thermoplastic reinforced with glass and carbon fibres,” *J. Mater. Sci.*, vol. 13, no. 2, pp. 377–390, 1978, doi: 10.1007/BF00647783.

[133] F. Gortner, A. Schüffler, J. Fischer-schuch, and P. Mitschang, “Use of bio-based and renewable materials for sheet molding compounds (SMC) – Mechanical properties and susceptibility to fungal decay,” *Compos. Part C Open Access*, vol. 7, p. 100242, 2022, doi: 10.1016/j.jcomc.2022.100242.

[134] N. A. W. Z. Xiao, L. T. Harper, A.D. Evans, T.A. Turner, “Characterisation of random carbon fibre composites from a directed fibre preforming process: The effects of moulding process and fibre type,” vol. 38, no. 3, pp. 755–770, 2007, doi: 10.1016/j.compositesa.2006.09.008.

[135] T. W. Clyne, “A simple development of the shear lag theory appropriate for composites with a relatively small modulus mismatch,” *Mater. Sci. Eng. A*, vol. 122, no. 2, pp. 183–192, 1989, doi: 10.1016/0921-5093(89)90629-1.

[136] R. J. Tapper, M. L. Longana, H. Yu, I. Hamerton, and K. D. Potter, “Development of a closed-loop recycling process for discontinuous carbon fibre polypropylene composites,” *Compos. Part B Eng.*, vol. 146, no. January, pp. 222–231, 2018, doi: 10.1016/j.compositesb.2018.03.048.

[137] J. Zhang, K. Chaisombat, S. He, and C. H. Wang, “Hybrid composite laminates reinforced with glass/carbon woven fabrics for lightweight load bearing structures,” *Mater. Des.*, vol. 36, pp. 75–80, 2012, doi: 10.1016/j.matdes.2011.11.006.

[138] W. Fung and M. Hardcastle, *Textiles in Automotive Engineering*. Woodhead Publishing Limited, 2001. doi: 10.1201/9781439822722.

[139] A. K. Bledzki, O. Faruk, and V. E. Sperber, “Cars from bio-fibres,” *Macromol. Mater. Eng.*, vol. 291, no. 5, pp. 449–457, 2006, doi: 10.1002/mame.200600113.

[140] M. H. Norhidayah, A. A. Hambali, Y. M. Yuhazri, M. Zolkarnain, Taufik, and H. Y. Saifuddin, “A review of current development in natural fiber composites in automotive applications,” *Appl. Mech. Mater.*, vol. 564, no. October, pp. 3–7, 2014, doi: 10.4028/www.scientific.net/AMM.564.3.

[141] J. Holbery and D. Houston, “Natural-fiber-reinforced polymer composites in automotive applications,” *Jom*, vol. 58, no. 11, pp. 80–86, 2006, doi: 10.1007/s11837-006-0234-2.

[142] A. Gholampour and T. Ozbakkaloglu, “A review of natural fiber composites: properties, modification and processing techniques, characterization, applications,” *J. Mater. Sci.*, vol. 55, no. 3, pp. 829–892, 2020, doi: 10.1007/s10853-019-03990-y.

[143] E. C. Lee, C. M. Flanigan, K. A. Williams, D. F. Mielewski, and D. Q. Houston, “Hemp Fiber Reinforced Sheet Molding Compounds for Automotive Applications,” *Ford Mot. Company, Dearborn*, pp. 1–12, 2016, [Online]. Available: http://www.temp.speautomotive.com/SPEA_CD/SPEA2005/pdf/h/h2.pdf

[144] M. J. Mochane *et al.*, “Recent progress on natural fiber hybrid composites for advanced applications: A review,” *Express Polym. Lett.*, vol. 13, no. 2, pp. 159–198, 2019, doi: 10.3144/expresspolymlett.2019.15.

[145] T. Gurunathan, S. Mohanty, and S. K. Nayak, “A review of the recent developments in biocomposites based on natural fibres and their application perspectives,” *Compos. Part A Appl. Sci. Manuf.*, vol. 77, pp. 1–25, 2015, doi: 10.1016/j.compositesa.2015.06.007.

[146] F. Ahmad, H. S. Choi, and M. K. Park, “A review: Natural fiber composites selection in view of mechanical, light weight, and economic properties,”

Macromol. Mater. Eng., vol. 300, no. 1, pp. 10–24, 2015, doi: 10.1002/mame.201400089.

[147] A. V. Kiruthika, "A review on physico-mechanical properties of bast fibre reinforced polymer composites," *J. Build. Eng.*, vol. 9, no. June 2016, pp. 91–99, 2017, doi: 10.1016/j.jobe.2016.12.003.

[148] G. Saikrishnan, K. R. Sumesh, P. Vijayanand, S. Madhu, S. Nagarajan, and G. Suganya Priyadharshini, "Investigation on the mechanical properties of ramie/kenaf fibers under various parameters using GRA and TOPSIS methods," *Polym. Compos.*, vol. 43, no. 1, pp. 130–143, 2022, doi: 10.1002/pc.26362.

[149] K. R. Sumesh *et al.*, "The influence of different parameters in tribological characteristics of pineapple/sisal/TiO2 filler incorporation," *J. Ind. Text.*, 2021, doi: 10.1177/15280837211022614.

[150] K. R. Sumesh, K. Kanthavel, and S. Vivek, "Mechanical/thermal/vibrational properties of sisal, banana and coir hybrid natural composites by the addition of bio synthesized aluminium oxide nano powder," *Mater. Res. Express*, vol. 6, no. 4, 2019, doi: 10.1088/2053-1591/aaff1a.

[151] U. Kureemun, M. Ravandi, L. Q. N. Tran, W. S. Teo, T. E. Tay, and H. P. Lee, "Effects of hybridization and hybrid fibre dispersion on the mechanical properties of woven flax-carbon epoxy at low carbon fibre volume fractions," *Compos. Part B Eng.*, vol. 134, pp. 28–38, 2018, doi: 10.1016/j.compositesb.2017.09.035.

[152] H. Yu, M. L. Longana, M. Jalalvand, M. R. Wisnom, and K. D. Potter, "Pseudo-ductility in intermingled carbon/glass hybrid composites with highly aligned discontinuous fibre," *Compos. Part A Appl. Sci. Manuf.*, vol. 73, pp. 35–44, 2015, doi: 10.1016/j.compositesa.2015.02.014.

[153] A. Afdzaluddin, M. A. Maleque, and M. Iqbal, "Synergistic effect on flexural properties of kenaf-glass hybrid composite," *Adv. Mater. Res.*, vol. 626, pp. 989–992, 2013, doi: 10.4028/www.scientific.net/AMR.626.989.

[154] I. T. Fulton, "The Effect of Layup and Pressure on Mechanical Properties of Fiberglass and Kenaf Fiber Composites," Masters Thesis, Mississippi State University, 2011.

[155] H. M. Akil, C. Santulli, F. Sarasini, J. Tirillò, and T. Valente, "Environmental effects on the mechanical behaviour of pultruded jute/glass fibre-reinforced polyester hybrid composites," *Compos. Sci. Technol.*, vol. 94, pp. 62–70, 2014, doi: 10.1016/j.compscitech.2014.01.017.

[156] M. Assarar, W. Zouari, H. Sabhi, R. Ayad, and J. M. Berthelot, "Evaluation of the damping of hybrid carbon-flax reinforced composites," *Compos. Struct.*, vol. 132, pp. 148–154, 2015, doi: 10.1016/j.compstruct.2015.05.016.

[157] G. Fairlie and J. Njuguna, "Damping properties of flax/carbon hybrid epoxy/fibre-reinforced composites for automotive semi-structural applications," *Fibers*, vol. 8, no. 10, pp. 1–15, 2020, doi: 10.3390/fib8100064.

[158] S. Prabhakaran, V. Krishnaraj, M. Senthil Kumar, and R. Zitoune, “Sound and vibration damping properties of flax fiber reinforced composites,” *Procedia Eng.*, vol. 97, pp. 573–581, 2014, doi: 10.1016/j.proeng.2014.12.285.

[159] M. M. Stevanović and T. B. Stecenko, “Mechanical behaviour of carbon and glass hybrid fibre reinforced polyester composites,” *J. Mater. Sci.*, vol. 27, no. 4, pp. 941–946, 1992.

[160] H. Wells and N. L. Hancox, “Stiffening and strengthening GRP beams with CFRP,” *Composites*, vol. 2, no. 3, pp. 147–151, 1971, doi: 10.1016/0010-4361(71)90950-5.

[161] P. W. Sonparote and S. C. Lakkad, “Mechanical properties of carbon/glass fibre reinforced hybrids,” *Fibre Sci. Technol.*, vol. 16, no. 4, pp. 309–312, 1982, doi: 10.1016/0015-0568(82)90051-3.

[162] A. F. Johnson and G. D. Sims, “Mechanical properties and design of sandwich materials,” *Composites*, vol. 17, no. 4, pp. 321–328, 1986, doi: 10.1016/0010-4361(86)90749-4.

[163] J. Tang *et al.*, “Hybrid composites of aligned discontinuous carbon fibers and self- reinforced polypropylene under tensile loading,” *Compos. Part A Appl. Sci. Manuf.*, vol. 123, no. February, pp. 97–107, 2019, doi: 10.1016/j.compositesa.2019.05.003.

[164] A. Lotfi, H. Li, D. V. Dao, and G. Prusty, “Natural fiber–reinforced composites: A review on material, manufacturing, and machinability,” *J.*

Thermoplast. Compos. Mater., vol. 34, no. 2, pp. 238–284, 2021, doi: 10.1177/0892705719844546.

[165] T. D. Hapuarachchi, G. Ren, M. Fan, P. J. Hogg, and T. Peijs, "Fire retardancy of natural fibre reinforced sheet moulding compound," *Appl. Compos. Mater.*, vol. 14, no. 4, pp. 251–264, 2007, doi: 10.1007/s10443-007-9044-0.

[166] Ryszard Kozłowskiy and Maria Władyka-Przybylak, "Flammability and fire resistance of composites reinforced by natural fiber," *Polym. Adv. Technol.*, vol. 19, pp. 446–453, 2008, doi: 10.1002/pat.1135.

[167] A. Stamboulis, C. A. Baillie, S. K. Garkhail, H. G. H. Van Melick, and T. Peijs, "Environmental durability of flax fibres and their composites based on polypropylene matrix," *Appl. Compos. Mater.*, vol. 7, no. 5–6, pp. 273–294, 2000, doi: 10.1023/A:1026581922221.

[168] H. N. Dhakal, Z. Y. Zhang, and M. O. W. Richardson, "Effect of water absorption on the mechanical properties of hemp fibre reinforced unsaturated polyester composites," *Compos. Sci. Technol.*, vol. 67, no. 7–8, pp. 1674–1683, 2007, doi: 10.1016/j.compscitech.2006.06.019.

[169] H. T. Kou, "A Study of the Impact Behavior of Chopped Fiber Reinforced Composite," *Polym. Compos.*, vol. 11, no. 5, pp. 253–264, 1990.

[170] S. Lee, J. Cheon, and Y. Im, "Experimental and numerical study of the impact behavior of SMC plates," *Compos. Struct.*, vol. 47, no. 1999, pp. 551–561, 2000.

[171] S. K. Chaturvedi and R. L. Sierakowski, “Effects of Impactor Size on Impact Damage-Growth and Residual Properties in an SMC-R50 Composite,” *J. Compos. Mater.*, vol. 19, no. 2, pp. 100–113, 1985, doi: 10.1177/002199838501900201.

[172] A. Trauth, M. Bondy, K. A. Weidenmann, and W. Altenhof, “Mechanical properties and damage evolution of a structural sheet molding compound based on a novel two step curing resin system,” *Mater. Des.*, vol. 143, pp. 224–237, 2018, doi: 10.1016/j.matdes.2018.02.002.

[173] M. Fazeli, X. Liu, and C. Rudd, “The effect of waterborne polyurethane coating on the mechanical properties of epoxy-based composite containing recycled carbon fibres,” *Surfaces and Interfaces*, vol. 29, no. December 2021, p. 101684, 2022, doi: 10.1016/j.surfin.2021.101684.

[174] S. G. Kravchenko, C. Volle, and O. G. Kravchenko, “An experimental investigation on low-velocity impact response and compression after impact of a stochastic, discontinuous prepreg tape composite,” *Compos. Part A Appl. Sci. Manuf.*, vol. 149, no. June, p. 106524, 2021, doi: 10.1016/j.compositesa.2021.106524.

[175] S. G. Kravchenko *et al.*, “Tensile properties of a stochastic prepreg platelet molded composite,” *Compos. Part A Appl. Sci. Manuf.*, vol. 124, no. July, p. 105507, 2019, doi: 10.1016/j.compositesa.2019.105507.

[176] C. Hong, J. Kim, G. Kim, and W. Ji, “Effect of stacking sequence on impact resistance performance of hybrid composites laminated with continuous and

discontinuous fiber-reinforced layers," *Funct. Compos. Struct.*, vol. 3, no. 2, 2021, doi: 10.1088/2631-6331/ac06be.

[177] S. Pimenta, A. Ahuja, and A. Y. Lau, "Damage tolerant tow-based discontinuous composites," *ICCM Int. Conf. Compos. Mater.*, vol. 2015-July, no. July, pp. 19–24, 2015.

[178] K. Ogi, J. W. Kim, K. Ono, and N. Uda, "Impact damage and residual tensile strength of a CF-SMC composite," *Adv. Compos. Mater.*, vol. 22, no. 1, pp. 29–47, 2013, doi: 10.1080/09243046.2013.764779.

[179] R. S. Pierce and X. Liu, "Exploiting the optical reflectance behaviour of carbon fibre composites for low-cost inspection and orientations analysis," *J. Reinf. Plast. Compos.*, vol. 39, no. 23–24, pp. 869–879, 2020, doi: 10.1177/0731684420934868.

[180] ASTM D7136/D7136M-12, "Standard Test Method for Measuring the Damage Resistance of a Fiber-Reinforced Polymer Matrix Composite to a Drop-Weight Impact Event," 2012. doi: 10.1520/D7136.

[181] ASTM D7137/D7137M − 17, "Standard Test Method for Compressive Residual Strength Properties of Damaged Polymer Matrix Composite Plates," 2007. doi: 10.1520/D7137.

[182] L. S. Sutherland and C. G. Soares, "Impact characterisation of low fibre-volume glass reinforced polyester circular laminated plates," *Int. J. Impact Eng.*, vol. 31, no. 1, pp. 1–23, 2005, doi: 10.1016/j.ijimpeng.2003.11.006.

[183] C. Kuhn, Y. Ton, O. Taeger, and T. A. Osswald, “Experimental study on fiber matrix separation during compression molding of fiber reinforced rib structures,” *Annu. Tech. Conf. - ANTEC, Conf. Proc.*, vol. 2018-May, no. May, 2018.

[184] P. Dumont, L. Orge, D. Favier, P. Pizette, and C. Venet, “Compression moulding of SMC : In situ experiments , modelling and simulation,” *Compos. Part A*, vol. 38, pp. 353–368, 2007, doi: 10.1016/j.compositesa.2006.03.010.

[185] C. C. Lee and C. L. Tucker, “Flow and heat transfer in compression mold filling,” *J. Nonnewton. Fluid Mech.*, vol. 24, no. 3, pp. 245–264, 1987, doi: 10.1016/0377-0257(87)80040-X.

[186] D. M. Corbridge, “Compression moulding of hybrid carbon fibre composites for structural applications. PhD thesis,” University of Nottingham, 2017. [Online]. Available: http://eprints.nottingham.ac.uk/49219/1/PHD thesis David Corbridge 4212605.pdf

[187] T. H. Le, P. J. J. Dumont, L. Orgéas, D. Favier, L. Salvo, and E. Boller, “X-ray phase contrast microtomography for the analysis of the fibrous microstructure of SMC composites,” *Compos. Part A Appl. Sci. Manuf.*, vol. 39, no. 1, pp. 91–103, 2008, doi: 10.1016/j.compositesa.2007.08.027.

[188] M. Hohberg, “Experimental investigation and process simulation of the compression molding process of Sheet Molding Compound (SMC) with local reinforcements,” PhD Thesis, Karlsruher Instituts für Technologie (KIT), 2018.

[189] M. R. Barone and D. A. Caulk, “Kinematics of flow in sheet molding compounds,” *Polym. Compos.*, vol. 6, no. 2, pp. 105–109, 1985, doi: 10.1002/pc.750060208.

[190] N. E. J. Olsson, T. S. Lundström, and K. Olofsson, “Compression moulding of SMC: Coupling between the flow and the local void contents,” *ICCM Int. Conf. Compos. Mater. London*, 2009.

[191] E. Schmachtenberg, K. Skrodolies, and D. Lippe, “Faser/matrix-entmischung während des fliesspressens von SMC,” *Zeitschrift Kunststofftechnik/Journal Plast. Technol.*, no. 6, 2005.

[192] Y. Li *et al.*, “Modeling and Simulation of Compression Molding Process for Sheet Molding Compound (SMC) of Chopped Carbon Fiber Composites,” *SAE Int. J. Mater. Manuf.*, vol. 10, no. 2, pp. 2–9, 2017, doi: 10.4271/2017-01-0228.

[193] J. Teuwsen, S. K. Hohn, and T. A. Osswald, “Direct fiber simulation of a compression molded ribbed structure made of a sheet molding compound with randomly oriented carbon/epoxy prepreg strands—a comparison of predicted fiber orientations with computed tomography analyses,” *J. Compos. Sci.*, vol. 4, no. 4, 2020, doi: 10.3390/jcs4040164.

[194] G. Fischer, “Measuring Spatial Orientation of Short Fiber,” *Polym. Compos.*, vol. 9, no. 4, 1988.

[195] S. Toll and P. O. Andersson, “Microstructural characterization of injection moulded composites using image analysis,” *Composites*, vol. 22, no. 4, pp. 298–306, 1991, doi: 10.1016/0010-4361(91)90006-3.

[196] N. D. Sharp, J. E. Goodsell, and A. J. Favaloro, “Measuring fiber orientation of elliptical fibers from optical microscopy,” *J. Compos. Sci.*, vol. 3, no. 1, 2019, doi: 10.3390/jcs3010023.

[197] S. C. Garcea, Y. Wang, and P. J. Withers, “X-ray computed tomography of polymer composites,” *Compos. Sci. Technol.*, vol. 156, pp. 305–319, 2018, doi: 10.1016/j.compscitech.2017.10.023.

[198] L. Kacir, M. Narkis, and O. Ishai., “Oriented short glass-fiber composites. I. Preparation and statistical analysis of aligned fiber mats,” *Polym. Eng. Sci.*, vol. 15, no. 7, pp. 525–531, 1975.

[199] S. G. Advani and C. L. Tucker, “The Use of Tensors to Describe and Predict Fiber Orientation in Short Fiber Composites,” *J. Rheol. (N. Y. N. Y).*, vol. 31, no. 8, pp. 751–784, 1987.

[200] A. Pewsey, “The large-sample joint distribution of key circular statistics,” *Metrika*, vol. 60, no. 1, pp. 25–32, 2004, doi: 10.1007/s001840300294.

[201] “MATLAB.” Natick, Massachusetts: The MathWorks Inc.; 2019.

[202] G. Subramanian and D. L. Koch, “Inertial effects on fibre motion in simple shear flow,” *J. Fluid Mech.*, vol. 535, pp. 383–414, 2005, doi: 10.1017/S0022112005004829.

[203] Y. Li *et al.*, “Modeling and Simulation of Compression Molding Process for Sheet Molding Compound (SMC) of Chopped Carbon Fiber Composites,” *SAE Int. J. Mater. Manuf.*, vol. 10, no. 2, 2017, doi: 10.4271/2017-01-0228.

[204] C. Qian, D. Norman, M. A. Williams, and K. Kendall, “Experimental and numerical characterisation of fibre orientation distributions in compression moulded carbon fibre SMC,” *Plast. Rubber Compos.*, pp. 1–9, 2022, doi: 10.1080/14658011.2022.2108984.